

EFFECT OF PRISMATIC ROUGHNESS ON
HYDRAULIC JUMP IN TRAPEZOIDAL CHANNELS

A THESIS SUBMITTED TO
THE GRADUATE SCHOOL OF NATURAL AND APPLIED SCIENCES
OF
MIDDLE EAST TECHNICAL UNIVERSITY

BY

TAYLAN ULAŞ EVCİMEN

IN PARTIAL FULFILLMENT OF THE REQUIREMENTS
FOR
THE DEGREE OF DOCTOR OF PHILOSOPHY
IN
CIVIL ENGINEERING

MAY 2012

Approval of the thesis;

EFFECT OF PRISMATIC ROUGHNESS ON HYDRAULIC JUMP IN TRAPEZOIDAL CHANNELS

submitted by **TAYLAN ULAŞ EVCİMEN** in partial fulfilment of the requirements for the degree of **Doctor of Philosophy in Civil Engineering Department, Middle East Technical University** by,

Prof. Dr. Canan Özgen

Dean, Graduate School of **Natural and Applied Sciences**

Prof. Dr. Güney Özcebe

Head of Department, **Civil Engineering**

Prof. Dr. Nuray Denli Tokyay

Supervisor, **Civil Engineering Dept., METU**

Examining Committee Members:

Prof. Dr. Mustafa Göğüş

Civil Engineering Dept., METU

Prof. Dr. Nuray Denli Tokyay

Civil Engineering Dept., METU

Emiratus Prof. Dr. Tülay Özbek

Prof. Dr. Nevzat Yıldırım

Civil Engineering Dept., Gazi University

Assoc. Prof. Dr. Ayşe Burcu Altan Sakarya

Civil Engineering Dept., METU

Date:

24.05.2012

I hereby declare that all information in this document has been obtained and presented in accordance with academic rules and ethical conduct. I also declare that, as required by these rules and conduct, I have fully cited and referenced all material and results that are not original to this work.

Name, Last name: Taylan Ulař EVCİMEN

Signature :

ABSTRACT

EFFECT OF PRISMATIC ROUGHNESS ON HYDRAULIC JUMP IN TRAPEZOIDAL CHANNELS

EVCİMEN, Taylan Ulaş

Ph.D., Department of Civil Engineering

Supervisor: Prof. Dr. Nuray TOKYAY

May 2012, 168 Pages

A study of the hydraulic jump on a trapezoidal prismatic channel and roughened beds is presented. Extensive measurements have been made regarding the characteristics of hydraulic jumps as sequent depths, wing fluctuations, energy dissipation and jump length on artificially roughened beds for Froude numbers between 4.16 and 14.58. Three different types of prismatic roughness elements and nine different roughness patterns were installed separately on channel bottom and side walls throughout the experiments to obtain rough surfaces. Strip roughness elements were built from fiberglass sheets and implemented perpendicular to the flow direction. To avoid cavitation, roughness elements were designed in that way that the crests of the elements are not protruding into the flow. The founded properties were compared with the available data in literature and with the properties of hydraulic jump occurred on smooth bed.

Keywords: Hydraulic Jump, Trapezoidal Channel, Wing Oscillations, Rough Beds.

ÖZ

PRİZMATİK PÜRÜZLÜLÜĞÜN TRAPEZ KANALLARDA HİDROLİK SIÇRAMA ÜZERİNE ETKİSİ

EVCİMEN, Taylan Ulaş

Doktora, İnşaat Mühendisliği Bölümü

Tez Yöneticisi: Prof. Dr. Nuray TOKYAY

Mayıs 2012, 168 Sayfa

Trapez kanalda ve pürüzlü taban şartlarında hidrolik sıçrama üzerine yapılan bir çalışma sunulmaktadır. Sıçrama sonrası oluşan akım derinliği, kanat dalgalanmaları, enerji sönümlenmesi ve sıçrama uzunluğu gibi hidrolik sıçramanın nitelikleriyle ilgili kapsamlı ölçümler yapay pürüzlü kanallarda sel rejiminde 4.16 ile 14.58 arasında değişen Froude sayılarında yapılmıştır. Deneyler boyunca pürüzlü yüzeyler, üç farklı tipte prizmatik pürüzlülük ve dokuz farklı pürüzlülük düzeninin kanal tabanı ve kanal duvarlarına ayrı olarak yerleştirilmesiyle elde edilmiştir. Şerit şeklindeki pürüzler fiberglastan imal edilmiş ve akış yönüne dik olarak yerleştirilmiştir. Kavitasyondan korunmak için pürüz yükseklikleri memba tabanının seviyesine göre düzenlenmiş, böylece pürüzlülük elemanlarının tepe noktalarının akımın içine girmemesi sağlanmıştır. Sonuçlar, mevcut çalışmalarda bulunan verilerle ve pürüzsüz tabanda oluşan hidrolik sıçramanın özellikleriyle karşılaştırılmıştır.

Anahtar Kelimeler: Hidrolik Sıçrama, Trapez Kanal, Kanat Dalgalanması, Pürüzlü Taban.

To My Father

To live like a tree single and free

And like woods, in brotherhoods

That is our yearning

ACKNOWLEDGEMENTS

This study has been carried out under the supervision of Prof. Dr. Nuray TOKYAY in the Hydraulics Laboratory of the Department of Civil Engineering at the Middle East Technical University. The study was supported by the METU Scientific Research Projects (BAP), Grant No: BAP-2007-03-03-04.

The author wish to express his deepest gratitude to his supervisor Prof. Dr Nuray TOKYAY, for her guidance, advice and encouragement in the course of preparation of the dissertation.

The supports of Nazmi Çoruh and Temel-Su International Engineering Services Inc. on this study are gratefully acknowledged.

The author would like to thank Assoc. Prof. Dr. Burcu ALTAN SAKARYA for her valuable comments, criticism and suggestions.

The great supports of Güneş GOLER, Dr. Ing. Ronald HASELSTEINER, Selçuk Han DÜLGEROĞLU, Murat KARINCA and Gülfer KESKİN are gratefully acknowledged.

Special thanks go to beautiful persons, who have passed away untimely; My mother Nuran EVCİMEN, and friends Erdem TÜRKŞEN and Şerif LEVENT; thought ethics, justice and how to a good person should be.

The author would also like to thank Hydromechanics Laboratory staff, especially Turgut Ural for his invaluable assistance and labor.

Finally, author would like to thank his family and, especially his wife Ayşe EVCİMEN for her encouragement, belief and patience, which gave the inspiration to author to complete this study.

TABLE OF CONTENTS

ABSTRACT	iv
ÖZ	v
TABLE OF CONTENTS	viii
LIST OF FIGURES	xi
LIST OF TABLES	xvi
NOMENCLATURE	xvii
CHAPTERS	
1. INTRODUCTION	1
2. THEORITICAL CONSIDERATIONS	5
2.1 Hydraulic Jump.....	5
2.2 Characteristics of Hydraulic Jump	7
2.2.1 Dimensional Analysis	8
2.2.2 The Sequent Depths	9
2.2.3 The Jump Location.....	12
2.2.4 Energy Dissipation.....	14
2.2.5 Aeration	16
2.2.6 Turbulence Characteristics	20
2.2.7 Jump Length	21
2.2.8 Classification of Jumps	25
2.3 Jump on Rough Beds	31
2.3.1 Literature Review.....	34
3. HYDRAULIC JUMP IN TRAPEZOIDAL CHANNELS	41
3.1 Dimensional Analysis.....	42
3.2 Literature Review	44
3.2.1 Flow Structure.....	45

3.2.2	Sequent Depths	49
3.2.3	Jump Length	53
3.2.4	Energy Dissipation	58
4.	EXPERIMENTAL SETUP	61
4.1	Dimensioning of Physical Model	61
4.2	Experimental Equipment	63
4.2.1	Hydraulic Jump Flume	66
4.2.2	Inlet Gate Design	67
4.2.3	Overshoot Gate and Free Fall	76
4.2.4	Downstream Basin	76
4.2.5	Roughness Setup	78
4.2.6	Portable Ultrasonic Flowmeter	83
4.2.7	Discharge Measurement Flume	83
4.2.8	Wave Monitor	85
4.3	Experimental procedure	86
4.3.1	Calibration of Tailwater Measurement System	87
4.3.2	Hydraulic Jump Formation	87
4.3.3	Measurement of Incoming Water Depth	87
4.3.4	Tailwater measurement	87
4.3.5	Length measurements	88
4.3.6	Wing Oscillations	90
5.	EXPERIMENTS, RESULTS AND DISCUSSION	93
5.1	Experiments on Smooth Trapezoidal Channel	93
5.1.1	Flow Features	95
5.1.2	The Sequent Depths	101
5.1.3	Efficiency of Energy Dissipation	105
5.1.4	Length of Jump	107
5.1.5	Wing Oscillations	109
5.2	Experiments on Rough Beds	110

5.2.1	The Sequent Depths	111
5.2.2	Depth Reduction Factor	117
5.2.3	Efficiency of Energy Dissipation	119
5.2.4	Gain in Energy Dissipation	123
5.2.5	Length of Jump	126
5.2.6	Wing Oscillations	130
5.3	Experiments on Rough Side Walls	133
5.3.1	The Sequent Depths	134
5.3.2	Efficiency of Energy Dissipation	136
5.3.3	Length of Jump	138
5.3.4	Wing Oscillations	139
6.	CONCLUSION AND RECOMMENDATIONS	143
	REFERENCES	147
APPENDICES		
	A: INLET GATE CALIBRATION	153
	B: LABCARD MANAGEMENT	156
	C: EXPERIMENTAL DATA	160
	VITA	168

LIST OF FIGURES

FIGURES

Figure 2-1: Hydraulic Jump.....	6
Figure 2-2: Specific Force and Specific Energy Curves for Hydraulic Jump	7
Figure 2-3: Definition Sketch for Hydraulic Jump	8
Figure 2-4: Integrated Boundary Shear Force (Rajaratnam (1965)).....	10
Figure 2-5: Effect of Tailwater Level on Jump Formation	13
Figure 2-6: Energy Loss along Hydraulic Jump	15
Figure 2-7: Relative Energy Loss in Hydraulic Jumps	15
Figure 2-8: Air Concentration Close the Bed in a Hydraulic Jump (Rajaratnam, 1962).....	17
Figure 2-9: Bulk Characteristics of Air Entrainment in Hydraulic Jump (Leutheusser et al., 1972)	18
Figure 2-10: Turbulence Kinetic Energy along Hydraulic Jump (Küçükali and Çokgör, 2006).....	21
Figure 2-11: Length of Jumps as Function of, F_1 , (USBR, 1955)	24
Figure 2-12: Undular Jump.....	27
Figure 2-13: Submerged Wave	28
Figure 2-14: Experimental Results of Smetana (Leliavsky, 1959).....	28
Figure 2-15: Hydraulic Jumps on Sloping Aprons (Khatsuria, 2005)	31
Figure 2-16: Geometrical Properties in the Study of Tani (1987)	33
Figure 2-17: Mean streamlines for (a) d-type roughness, (b) intermediate roughness, and (c) k-type roughness (Cui et al., 2003).....	34
Figure 3-1: Hydraulic Jump in Trapezoidal Channel.....	42
Figure 3-2: Variation of Wave Front with Froude Number for Trapezoidal Channel (Ali and Ridgway, 1977)	46
Figure 3-3: Parts of the Flow for Hydraulic Jump in Trapezoidal Channel	48
Figure 3-4: Analytical Curves for Sequent Depths (Silvester, 1964)	50

Figure 3-5: Design Chart for Upstream and Downstream Depth (Mohed and Sharp, 1971).....	51
Figure 3-6: Theoretical Chart for the Hydraulic Jump in Trapezoidal Channels	52
Figure 3-7: Sequent Depth Ratio for Various M. (Wanoschek and Hager, 1989)	53
Figure 3-8: Results of Tests on Rectangular and Trapezoidal Channels (Silvester, 1964).....	55
Figure 3-9: Variation of L_j/y_1 in Trapezoidal Channels	57
Figure 3-10: Theoretical Curves for Energy Loss (Silvester, 1964).....	59
Figure 3-11: Energy Loss of Hydraulic Jump in Different Channels	60
Figure 4-1: Experimental Model of the Present Study.....	63
Figure 4-2: Experimental Model and its Parts	65
Figure 4-3: Physical Dimensions of Experimental Model	66
Figure 4-4: Experimental Model – Isometric View	67
Figure 4-5: Three Different Inlet Types for Experimental Studies.....	68
Figure 4-6: Inlet section.....	70
Figure 4-7: Plexiglas Pieces to Improve Inlet Conditions.....	71
Figure 4-8: Dough at Sides to Improve Inlet Conditions	71
Figure 4-9: Calibration Study at Inlet Section.....	72
Figure 4-10: Normalized Flow Surface Profiles at Inlet	75
Figure 4-11: Overshoot gate at the end of upper flume	76
Figure 4-12: Downstream Basin	77
Figure 4-13: Application Detail of Strip Roughness at Aprons.....	78
Figure 4-14: Installation of Roughness Elements on Channel Bed	80
Figure 4-15: Widths of strip roughness elements (in cm)	81
Figure 4-16: Bed Roughness Patterns in the Study.....	82
Figure 4-17: Portable Ultrasonic Flowmeter	83
Figure 4-18: Discharge Calibration Curve	85
Figure 4-19: (a) Wave Probe (b) Wave Probe Monitor.....	86

Figure 4-20: The Parameter Screen of Ms-Dos Program, 470	86
Figure 4-21: Indefinite End of Hydraulic Jump ($F1 = 6.87$).....	89
Figure 4-22: Air pockets at Downstream Flow ($F1 = 6.87$).....	90
Figure 4-23: Wing Oscillations ($F1 = 5.34$).....	91
Figure 4-24: Unstable Wings for the Same Hydraulic Jump.....	92
Figure 5-1: Comparison of Theoretical and Experimental Specific Force.....	94
Figure 5-2: Comparison of Theoretical and Experimental Subcritical Depths	95
Figure 5-3: Oblique Jump and Returned Flow ($F1 = 6.87$).....	96
Figure 5-4: Oblique Jump, Returned Flow and Side Flows ($F1 = 6.87$).....	97
Figure 5-5: Side Flow Towards to Upstream ($F1 = 5.34$).....	98
Figure 5-6: Flow Directions at Surface ($F1 = 6.87$).....	99
Figure 5-7: Fluctuating Toe and End of Hydraulic Jump ($F1 = 5.34$).....	100
Figure 5-8: Indefinite Length of Hydraulic Jump ($F1 = 9.81$)	101
Figure 5-9: Sequent Depth Ratio on Smooth Beds	102
Figure 5-10: Comparison of Sequent Depth Ratio with Previous Studies	103
Figure 5-11: Hydraulic Jump Sequent Depths; Present study vs. Ali and Ridgway (1977)	104
Figure 5-12: Comparison of Efficiency with the Data in the Literature	105
Figure 5-13: Comparison of Efficiency with Previous Studies	107
Figure 5-14: comparison of Hydraulic Jump Lengths with Previous Studies	108
Figure 5-15: Normalized Wing Oscillations.....	110
Figure 5-16: Comparison of Sequent Depth Ratio for Rough Beds	111
Figure 5-17: Sequent Depth Ratio for Different Roughness Intensities	113
Figure 5-18: Sequent Depth Ratio for Different Pitch Ratios	115
Figure 5-19: Normalized Sequent Depth Ratio on Rough Beds.....	116
Figure 5-20: Normalized Sequent Depth Ratio for Different Pitch Ratios	117
Figure 5-21: Depth Reduction Factor on Rough Beds for Different Pitch Ratios	118

Figure 5-22: Depth Reduction Factor on Rough Beds for Different Intensities	119
Figure 5-23: Comparison of Efficiency with Previous Studies	120
Figure 5-24: Comparison of Efficiency with Previous Studies on Rough Beds	121
Figure 5-25: Efficiency on Rough Beds for Different Roughness Intensities	122
Figure 5-26: Efficiency on Rough Beds for Different Pitch Ratios.....	123
Figure 5-27: Gain in Energy Dissipation on Rough Beds.....	124
Figure 5-28: Gain in Energy Dissipation on Rough Beds for Different I Values	125
Figure 5-29: Gain in energy Dissipation on Rough Beds for Different Pitch Ratios.....	125
Figure 5-30: Normalized Aeration Length on Rough Beds	126
Figure 5-31: Normalized Aeration Length on Rough Beds for Different Intensities.....	127
Figure 5-32: Normalized Aeration Length on Rough Beds for Different Pitch Ratios.....	128
Figure 5-33: Efficiency vs. Normalized Aeration Length for Different Pitch Ratios.....	129
Figure 5-34: Normalized Wing Oscillations on Rough Beds.....	131
Figure 5-35: Normalized Wing Oscillations for Different Roughness Intensities	131
Figure 5-36: Normalized Wing Oscillations for Different Pitch Ratios	132
Figure 5-37: The Effect of Side Roughness on Hydraulic Jump	133
Figure 5-38: Comparison of Sequent Depth Ratio for Rough Walls	134
Figure 5-39: Normalized Sequent Depths for Rough Walls.....	135
Figure 5-40: Sequent Depth Ratio of Different Wall Roughness Intensities .	135
Figure 5-41: Sequent Depth Ratio of Different Wall Roughness Pitch Ratios	136

Figure 5-42: Comparison of Efficiency with Previous Studies on Rough Side Walls.....	137
Figure 5-43: Normalized Aeration Length on Rough Side Walls	139
Figure 5-44: Normalized Wing Oscillations on Rough Side Walls.....	140
Figure 5-45: Dimensionless Wing Oscillations on Rough Side Walls for Different Roughness Intensities.....	141
Figure 5-46: Normalized Wing Oscillations on Rough Side Walls for Different Pitch Ratios.....	142
Figure A-1: Flow Surface Profile for G1	153
Figure A-2: Flow Surface Profile for G2	154
Figure A-3: Flow Surface Profile for G3	154
Figure A-4: Flow Surface Profile for G3	155
Figure A-5: Flow Surface Profile for G4	155

LIST OF TABLES

TABLES

Table 2-1: Classical Hydraulic Jump Length, Peterka (1958).....	24
Table 4-1: Experimental Model Dimensions of Previous Studies.....	62
Table 4-2: Measured Flow Depths along Inlet Section for G1, G2 and G4	73
Table 4-3: Normalized Flow Depths along Inlet Section for G1, G2 and G4..	73
Table 4-4: Measured Flow Depths along Inlet Section For G3	74
Table 4-5: Normalized Flow Depths along Inlet Section for G3.....	74
Table 4-6: Geometrical Properties of Roughness Setup	82
Table 5-1: Experiments on Smooth Trapezoidal Channel	94
Table C-1: Experiments on Smooth Channel	160
Table C-2: Experiments on Rough Beds	161
Table C-3: Experiments on Rough Walls.....	164

NOMENCLATURE

Symbols

a	Gate opening, [L]
a_v	The void ratio, [-]
b	Channel bed width of a prismatic channel, [L]
C_b	air concentration in the bottom layers, [-]
C_c	Contraction coefficient of Vena contracta, [-]
C_{MAX}	The maximum void fraction
d_h	The dimension to define channel height.
D	The diameter of the circular conduit in the experiments of Silvester (1964), [L]
D	$= (y_2^T - y_2) / y_2^T$, Sequent depth reduction factor, [-]
D_H	Hydraulic depth, [L]
E_1	Specific energy of supercritical flow, [L]
E_2	Specific energy of subcritical flow, [L]
E_L	Specific energy loss along hydraulic jump, [L]
E_L^*	Specific energy loss along hydraulic jump on smooth beds in rectangular Channels, [L]
F_τ	Integrated bed shear stress, [$F L^{-2}$]
F_{MAX}	The maximum bubble count rate
F_1	Froude number of supercritical flow, [-]
F_2	Froude number of subcritical flow, [-]
F_u	Modified upstream Froude number, [-]
g	Gravitational acceleration, [LT^{-2}]
G	$= (E_L - E_L^*) / E_L$, Gain in energy dissipation factor, [-]

G1	Gate opening of 1 cm [L]
G2	Gate opening of 2 cm [L]
G3	Gate opening of 3 cm [L]
G4	Gate opening of 4 cm [L]
h_r	The actual measured depth of an submerged jump, [L]
h_2	The hypothetical downstream depth of a submerged jump, [L]
H2	Gradually varied flow profile on horizontal bed, [-]
H3	Gradually varied flow profile on horizontal bed, [-]
I	Uniform Areal Roughness Intensity in plan view, [-]
J	Downstream turbulence-flux correction factor, [-]
k	Shape factor; b/my_1 ; [-]
ks	Height of roughness element in study Rajaratnam (1995) , [L]
K	Air concentration in the bottom layers
L	Length of roughness element, [L]
L_A	Aeration length of a hydraulic jump, [L]
L_E	Erosion length of a hydraulic jump, [L]
L_J	Length of a hydraulic jump, [L]
L_J^*	Length of a hydraulic jump on smooth beds in Rectangular Channel, [L]
L_O	Jump length definition of Ohtsu, [L]
L_M	The jump length definition, from toe to the section where the depth is maximum, [L]
L_R	Length of a roller, [L]
L_W	Length of wing oscillations, [L]
m	Cotangent of side wall of a trapezoidal channel, [-]
M	Shape factor; $1/k$; my_1/b ; [-]

p	Submergence ratio of a submerge jump
P_1	Pressure at upstream of a jump [FL^{-2}]
P_2	Pressure at downstream of a jump [FL^{-2}]
PR	The pitch ratio; w/z , [-]
T	Surface width of a channel
T_a	The fraction of the total duration of observation during which the hot-film probe sensed air, [-]
T_w	The time fraction for water contact of the probe; [-]
q	Discharge per unit width of the flow, [L^2T^{-1}]
Q	Volumetric discharge, [L^3T^{-1}]
Re	Reynolds Number
Re_1	Reynolds Number of supercritical stream, [-]
s	Wavelength of the corrugation, [-]
$S_{\underline{f}}$	Integrated dimensionless bed shear force per unit width, [L]
\bar{S}	Non dimensional bottom shear force, [-]
U_{max}	The maximum velocity inside the boundary layer, [L/T],
t	Height of corrugation, [L]
u'	The fluctuating velocity component along x direction, [L/T]
v'	The fluctuating velocity component along y direction, [L/T]
w'	The fluctuating velocity components along z direction, [L/T]
v_1	The average velocity of incoming supercritical flow, [L/T]
w	Distance between two roughness element, [L]
x	Space Parameter, [L]
x_1	Starting point of hydraulic jump, [L]
x_2	The last point where an air bubble touches the bed, [L]
x	Horizontal length scale, [L]

y	Vertical length scale, [L]
y_{CONT}	Flow depth at vena contracta, [L]
y_d	The tailwater level of a stilling basin
y_r	Depth of flow at the end of a roller in hydraulic jump, [L]
y_1	Depth of supercritical flow, [L],
y_2	Depth of subcritical flow on rough beds, [L]
y_2^*	Depth of subcritical flow on smooth beds in rectangular ch. [L]
y_2^T	Depth of supercritical flow on smooth beds in trapezoidal ch.[L]
Y	Sequent depth ratio, [L]
Y_H	Surface Profile parameter of Hager, [L]
z	Height of a roughness element, [L]
α	Oblique jump angle respect to channel axis, [-]
β_1	Momentum correction coefficient at the beginning of jump, [-]
β_2	Momentum correction coefficient at the end of jump, [-]
Γ	Shape factor of Silvester, [-]
γ	Unit Weight of water, [ML^{-3}]
ΔE	Difference of Specific Energies before Sluice Gate and after Hydraulic Jump Downstream of sluice gate [L]
ΔF	Difference of Specific Forces before Sluice Gate and after Hydraulic Jump Downstream of sluice gate [L^3]
δ	A thickness related with boundary layer height, [L]
δ_1	The boundary layer thickness, [L]
ϵ	Nondimensional integrated shear force of Rajaratnam (1965),[-]
η	Efficiency of energy dissipation

η_r	Surface profile parameter of Rajaratnam & Subramanya, [-]
ϕ	Roughness coefficient of Belanger Eq. by Carollo et al. (2007) , [-]
λ	The kinetic flow factor, F_1^2
λ_r	Surface profile parameter of Rajaratnam & Subramanya, [-]
μ	Dynamic viscosity of water, $[ML^{-1}T^{-1}]$
ρ	Mass density of water, $[ML^{-3}]$
σ	Shape factor of Silvester, [-]
σ_r	The submergence ratio, [-]
ψ	Energy deficiency factor of Ohtsu, [-]

CHAPTER 1

INTRODUCTION

The hydraulic jump is the sudden change of flow depth and state in open channel flow under certain conditions, where the existence of both upstream and downstream controls sets a conflict between upstream and downstream flow depths and flow states.

Hydraulic jump is also a natural energy dissipator by merit of the basic laws of nature. The nature of this phenomenon has been used in engineering field to dissipate excess energy of high velocity flow.

In hydraulic structures, such as spillways and sluice gates, downstream flow velocities are high and excess kinetic energy of water should be dissipated within a short distance to protect the base of the hydraulic structures. This is necessary for protecting the riverbed and banks from erosion and, to ensure that the dam and adjoining structures like powerhouse, canal, etc. are safe and not undermined by the high velocity flow.

The most common form of energy dissipator at the outlets of shaft/tunnel spillways is throwing the water a long distance as a free jet. However, when topographical, geological and economic conditions are not favorable, a hydraulic jump stilling basin is the only choice regardless of upstream discharge and energy. Hence in such cases, hydraulic jump is used as an energy dissipator.

Through the hydraulic jump, energy of flow field is transformed into turbulent energy. During this transformation intense mixing, air entrainment and rapid rise of depth occur. Due to those properties the hydraulic jump is also used for different purposes, such as to raise the water level, to mix chemicals in streams, to desalinate the sea water and to aerate streams which are polluted by biodegradable wastes.

The exact analytical solution of hydraulic jump has been proved for prismatic channel sections, and the basic conservation law behind this solution is the conservation of momentum. Furthermore, experiments made on "direct" jumps with high kineticity give good results in agreement with the exact analytical solutions. This is the reason why a lot of experimental studies have been conducted on the hydraulic jump. Experimental setup and experimental procedure of the study has been covered in Section IV.

Hydraulic jump stilling basins include horizontal and sloping aprons and basins equipped with energy dissipating appurtenances such as chute blocks, baffle piers, and dentated end sills. Regardless of the selected energy dissipation method, the dissipation of energy is through internal friction and turbulence or impact and diffusion of the high velocity flow in the mass of water. A well designed energy dissipator reduces up to 60% of the energy entering the basin depending on the Froude number of the flow. As resulting from intermittent cavitation, vibration, uplift, and hydrodynamic loading, hydraulic jump stilling basins are not recommended for heads exceeding about 100 m and Froude numbers greater than 10. Hydraulic characteristics of hydraulic jump have been covered in Section II.

Natural channels often have trapezoidal cross sections, and, man-made channels often have a trapezoidal or circular cross section. The main reason of selecting those geometries is based on economic comparison of sloped side lining of trapezoidal channel and vertical wall construction of rectangular

channel. However in practice, the sidewalls of a hydraulic jump stilling basin are vertical and current hydraulic jump stilling basins are normally rectangular in cross-section.

The reason of such a preference is explained by poor hydraulic performance of trapezoidal hydraulic jump stilling basins. USBR (1987) states that *“Model tests have shown, however, that the hydraulic-jump action in a trapezoidal basin is much less complete and less stable than it is in the rectangular basin. In a trapezoidal basin, the water in the triangular areas along the sides of the basin adjacent to the jump does not oppose the incoming high-velocity jet. The jump, which tends to occur vertically, cannot spread sufficiently to occupy the side areas. Consequently, the jump will form only in the central portion of the basin, while areas along the outside will be occupied by upstream-moving flows that ravel off the jump or come from the lower end of the basin. The eddy or horizontal roller action resulting from this phenomenon tends to interfere and interrupt the jump action to the extent that there is incomplete dissipation of the energy and severe scouring can occur beyond the basin.”* Present knowledge and literature review of hydraulic jump on trapezoidal channels are presented in Section III.

Change of flow pattern through rough boundaries is an interesting subject and it has been investigated in many fields from micro scale to macro scale i.e. from heat transfer to coastal engineering. The effect of rough boundaries on hydraulic jump properties has been investigated since the last quarter of 20th century. Rough or corrugated beds in stilling basins increases friction inside the jump and the hydraulic jump properties change significantly. In order to reduce the jump characteristics, obstacles can be also used, but that are subjected to cavitation problems. Hence, replacing blocks with rough beds decreases maintenance costs due to cavitation.

As previously mentioned, hydraulic performance of trapezoidal hydraulic jump stilling basins are poor. However, increasing the bottom friction by roughening

it might increase the hydraulic performance of trapezoidal hydraulic jump basins. Furthermore, since the construction of sloped side lining of trapezoidal channel is much more economical than vertical wall construction; significant amount of savings can be made for any hydraulic jump stilling basin.

The objective of this study is experimental investigation of the effect of wall roughness on hydraulic jump characteristics in trapezoidal channels. Experimental results are discussed in Section V.

CHAPTER 2

THEORITICAL CONSIDERATIONS

2.1 Hydraulic Jump

Hydraulic jump (Figure 2-1) is defined as in many ways by several authors. A local phenomenon by means of which flow passes in an abrupt manner from a rapid to a tranquil state (Bakhmateff, 1932); the abrupt change of flow depth in the direction of flow in an open channel flow under certain conditions, where flowing stream passes from supercritical flow to subcritical flow (Chow, 1959; Chaudry, 2008); transfer of flow abruptly from the supercritical to the subcritical condition through a feature (Handerson, 1966; Leutheusser et al., 1972); flow changes from a supercritical to a subcritical state abruptly through a phenomenon (French, 1987); in open channels, the transition from a rapid flow to a slow flow (Chanson, 2004); the rapid transformation of a supercritical open channel flow into a fluvial regime (Küçükali and Chanson, 2008).

The existence of both upstream and downstream controls may set a conflict between upstream and downstream flow states. A supercritical flow is produced by upstream control; adversely subcritical flow is produced by downstream control. When upstream control causes supercritical flow in its downstream, while the downstream control impose subcritical flow in its upstream on the reach of channel between an upstream and a downstream control, the flow has to pass from supercritical to subcritical state.

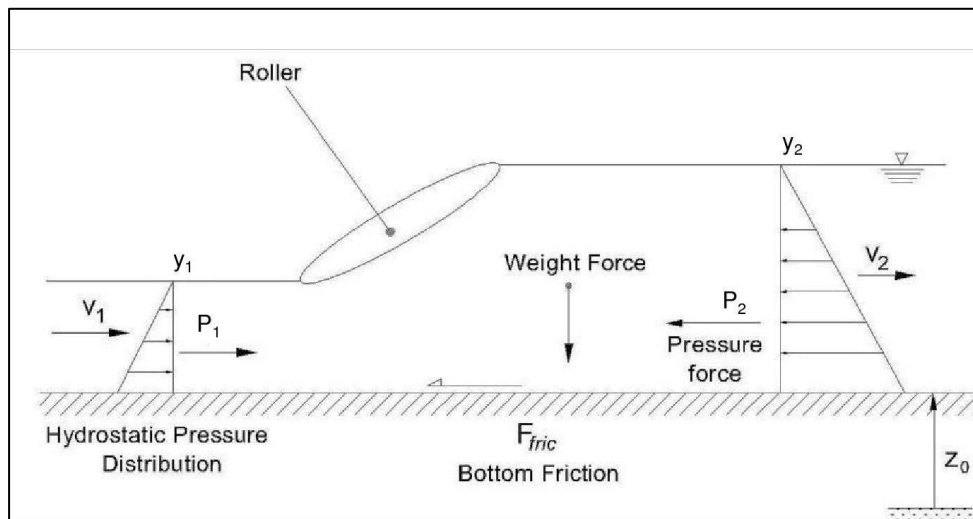


Figure 2-1: Hydraulic Jump

The change of flow state from supercritical to a subcritical state is accompanied by discontinuity in depth of flow, formation of a surface roller, visible air entrainment and two phase flow, significant turbulence (internal mixing), kinetic energy dissipation, generation of spray and sound; and generation of tailwater waves.

While Leonardo da Vinci (1452-1519) quotes the waves frequently observed on the surface of a field of ripe wheat, he was describing the hydraulic jump or standing wave as the first person in the history (Leliavsky, 1959). The inclination of the stalks caused by the wind creates the impression of a moving wave, whilst indeed there is no propulsive motion at all. The mean flow characteristics of the phenomenon have been studied extensively during the almost five centuries since the description of Leonardo da Vinci.

Italian Giorgio Bidone (1820) was the first one to conduct experiments on hydraulic jump through 1820's according to Şimşek (2006). According to Leliavsky (1959), J.B. Belanger (1828)¹ was the first one to have dealt with the

¹ J. B. Belanger, Essai sur la solution de quelques problèmes relatifs au mouvement permanent des eaux courantes (Paris, 1828), p. 31.

problem analytically began simply by using the Bernoulli equation by assuming that constant energy head ahead and behind the jump were the same. He compared the observation of M. Bidone (1820) with theoretical results and, explained the discrepancies up to 14% as resulting from accidental errors. Only later, when observations on jumps of greater height evidenced discrepancies of a more substantial character, was Belanger led to suggest the use of the momentum equation. (Bakhmateff, 1932).

Leliavsky (1959) stated that, Belanger's second method, that which is based on the momentum equation on rectangular channels, can be plotted in the same diagram, as in Figure 2-2. The curve has two lips, each represents the two characteristic types of flow, with a minimum at the same critical depth, y_{cr} .

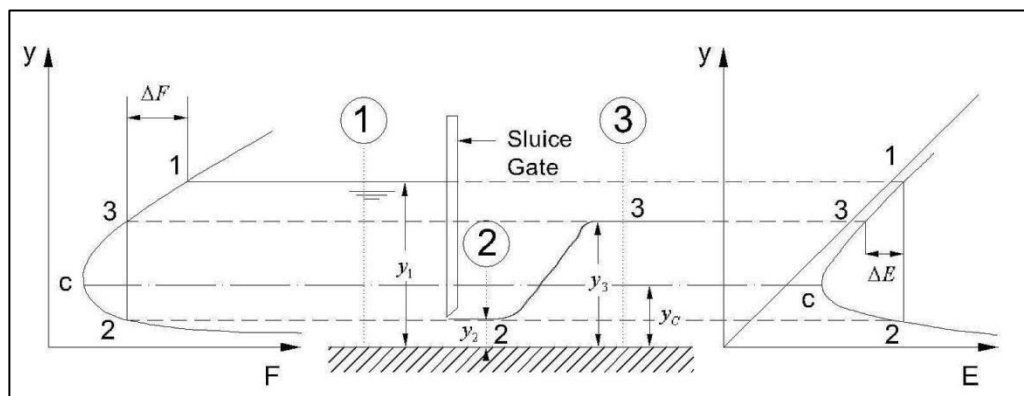


Figure 2-2: Specific Force and Specific Energy Curves for Hydraulic Jump

2.2 Characteristics of Hydraulic Jump

The basic characteristic of a hydraulic jump, such as the conjugate depth, location of jump, the energy loss in the jump, efficiency of jump, the length of the jump, the water surface profile of the jump, the velocity distribution of the jump will be given briefly in the following sections.

2.2.1 Dimensional Analysis

The hydraulic jump in a smooth, horizontal, wide prismatic rectangular open channel and approaching Froude Number, $v_1 / \sqrt{gy_1}$, $F_1 > 2$ is generally referred as classical jump (Bakhmateff, 1932; Peterka, 1958) and a lot of laboratory studies have been conducted on it. Hydraulic jump on a prismatic channel contains the variables shown in Figure 2-3.

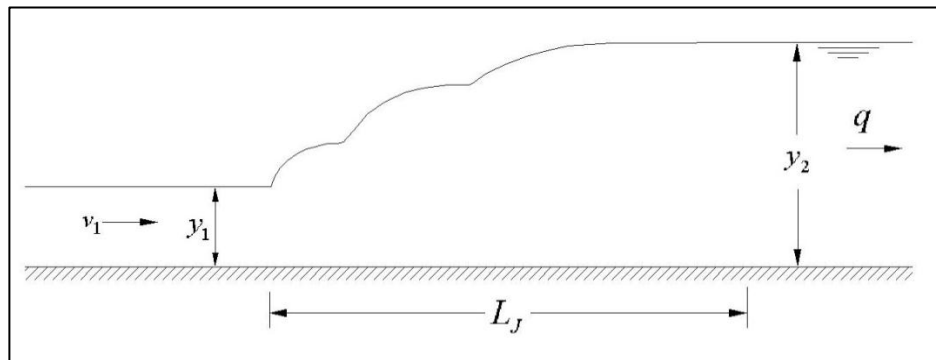


Figure 2-3: Definition Sketch for Hydraulic Jump

- where
- v_1 = the average velocity of incoming flow
 - y_1 = the incoming flow depth
 - y_2 = the tailwater depth
 - g = the acceleration of gravity
 - ρ = the mass density of water
 - μ = the dynamic viscosity of water
 - q = the unit discharge

The tailwater depth y_2 can be written as a function of following parameters;

$$y_2 = f(y_1, q, g, \rho, \mu) \quad (2.1)$$

To apply the Buckingham Pi Theorem to the problem, y_1 , q and ρ are selected as repeating variables, and the following dimensionless parameters may be found.

$$\frac{y_2}{y_1} = f\left(\frac{q^2}{g y_1^3}, \frac{\rho q}{\mu}\right) \quad (2.2)$$

The first term of the function is square of the incoming Froude number, F_1 , is a dimensionless number proportional to the square root of the ratio of the inertial forces over the weight of fluid. While a lot of researcher i.e. Peterka, (1958), Chow (1959) and Handerson (1966) used F_1 as dimensionless parameter, Leliavsky (1959) states that Bakhmeteff used kinetic flow factor λ , which is the square of F_1 instead of F_1 .

The second term of function represents Reynolds number, Re , can be neglected because the viscous forces are not significant with respect to the gravitational forces in open channel flow. Rajaratnam (1965) investigated pressure field, velocity field, and the boundary shear stress in hydraulic jumps as wall jet. He stated that, Reynolds number, Re , has not been found to influence the relations on boundary layer thickness and velocity distribution for the classical wall jets.

2.2.2 The Sequent Depths

One of the fundamental characteristic of the classical jump is the ratio of the sequent depths. According to Hager (1995), the sequent depths concept was accepted when Safranez published his results around 1930.

The momentum equation applied to a hydraulic jump on a horizontal basin in a rectangular channel can be reduced to Eq. 2.3, assuming that friction is negligible, the momentum correction coefficients β_1 and β_2 are equal to unity, and the pressure distribution is hydrostatic;

$$\frac{y_2}{y_1} + \left(\frac{y_2}{y_1}\right)^2 - 2F_1^2 = 0 \quad (2.3)$$

Solution of the equation yields, the well-known Belanger momentum equation.

$$\frac{y_2}{y_1} = \frac{1}{2} \left(-1 + \sqrt{1 + 8F_1^2} \right) \quad (2.4)$$

Rajaratnam (1965) attracted attention that Eq. (2.4) is essentially approximate because of the neglect of the boundary shear force and experimental observations often show that the observed values of y_2 are less than the values predicted by Eq. (2.4). He incorporated the integrated shear force and proposed another momentum equation, neglecting the turbulence contribution to the momentum and the effect of the variation of the velocity with the depth.

$$\left(\frac{y_2}{y_1} \right)^3 - \frac{y_2}{y_1} (1 - \epsilon + 2F_1^2) + 2F_1^2 = 0 \quad (2.5)$$

Where, ϵ is nondimensional integrated shear force, depends on F_1 , presented by Rajaratnam (1965) in Figure 2-4.

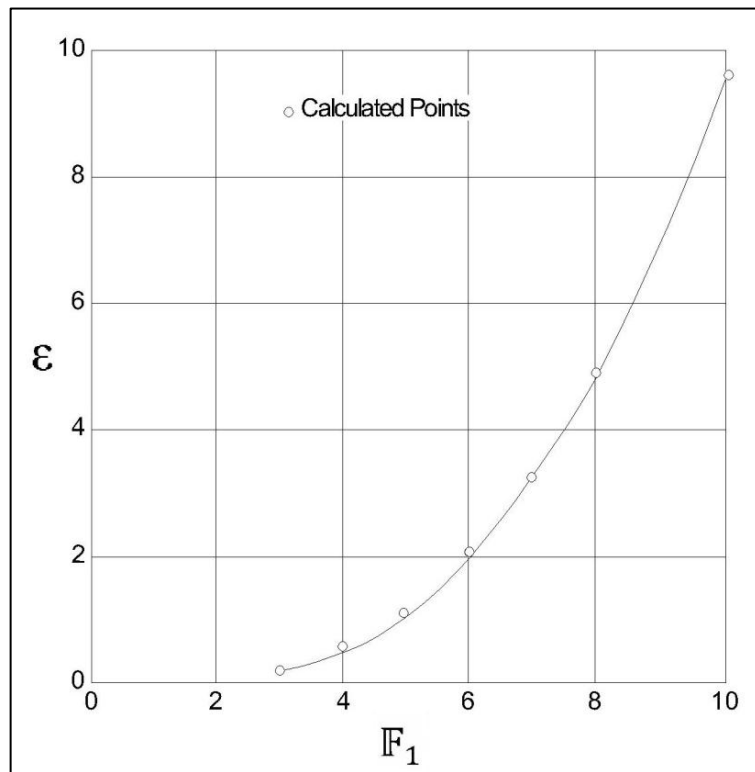


Figure 2-4: Integrated Boundary Shear Force (Rajaratnam (1965))

Ohtsu & Yasuda (1994) reported that the momentum equation proposed by Rajaratnam (1965), takes the friction into account and predicts the sequent depth ratio more accurately than Belanger equation.

Hager and Bremen (1989) indicated that, for flows in which the incoming flow depth y_1 is small, there exists a significant scale effect on sequent depth ratio.

Hager,(1995) proposed the following equation for the values of incoming Froude number, greater than 2.

$$\frac{y_2}{y_1} = \sqrt{2}F_1 - \frac{1}{2} \quad (2.6)$$

Ead & Rajaratnam (2002) stated that, for relatively large values of incoming Froude number, if $F_1 > 8.0$, instead of equation (2.4), for the purpose of quick estimation of the sequent depth ratio, the following equation could be used.

$$\frac{y_2}{y_1} = 1.41F_1 \quad (2.7)$$

As quoted by Hager and Bremen (1989), the equation presented by Harleman (1959) is suitable for the determination ratio of conjugate depths;

$$F_1^2 = \frac{1}{2} \frac{Y[(Y+1)(Y-1) + \bar{S}]}{\beta_1 Y - (\beta_2 + J)} \quad (2.8)$$

where β_1 = momentum correction coefficient at section 1
 β_2 = momentum correction coefficient at section 2
 J = downstream turbulence-flux correction factor,
 Y = the sequent depth ratio, y_2/y_1
 \bar{S} = dimensionless bottom shear force

The dimensionless bottom shear force \bar{S} is formulated as;

$$\bar{S} = 2 \frac{F_1^2}{v_1 R_1} \int_0^{L_j} \left(\frac{\partial \bar{u}}{\partial y} \right)_{y=0} dx \quad (2.9)$$

where, v_1 is the incoming velocity of the stream and R_1 is the Reynolds number of upstream and L_J is the length of the jump.

2.2.3 The Jump Location

From the designer's standpoint, hydraulic jump is a powerful energy dissipation mechanism and due to its erosive potential, is the centroid of scour. In order to take full advantage of the hydraulic jump in apron design, the erosive effect of jump should be confined to the limits of the heavily protected bed surface, hence intensive scour energy would not cause any harm to apron. This is why; hydraulic jump should be in a stilling basin with a fixed location.

Tailwater level plays a significant role in the formation of jump at a particular location. A curve between Q and the tailwater level, y_d is referred to as the tailwater rating curve. A curve between Q and y_2 is referred to as jump curve.

Leliavsky (1955) stated that, five different flow situations are possible depending on the realization of these two curves. These alternatives are shown in Figure 2-5, in which a full line demonstrates the tailwater curve and a dashed line is used for the jump curve. These five cases are;

(a) For all rates of discharges, the tailwater rating curve and the jump curve are the same and coincide. The required sequent depths are always satisfied independent from discharge and, hydraulic jumps occur at the same point. This is an ideal design situation for stilling basins and in nature can be observed rarely.

(b) The relevant sequent depth, y_2 , is always higher than tailwater depth, hence jump curve is always above the tailwater curve and, the jump moves downstream. To make certain jump formation on the apron, obstacles i.e. sills and blocks may be applied.

(c) The relevant sequent depth, y_2 , is always lower than tailwater depth, hence jump curve is always below the tailwater curve and, the jump moves upstream. Providing a drop in the channel bottom ensures formation of jump on apron. Tolerating the jump formation on a sloping apron is another design alternative.

(d) The relevant sequent depth, y_2 , is higher than tailwater depth at low rates of discharges and, below it for large discharges. The stilling basin should be designed so that the jump occurs on the basin on low discharges and on a sloping apron at high discharges.

(e) The relevant sequent depth, y_2 , is lower than tailwater depth at low rates of discharges and, above it for large discharges. The stilling basin should be designed so that the jump occurs on the basin at high discharges and on a sloping apron at low discharges. Case is completely opposite of the case (d).

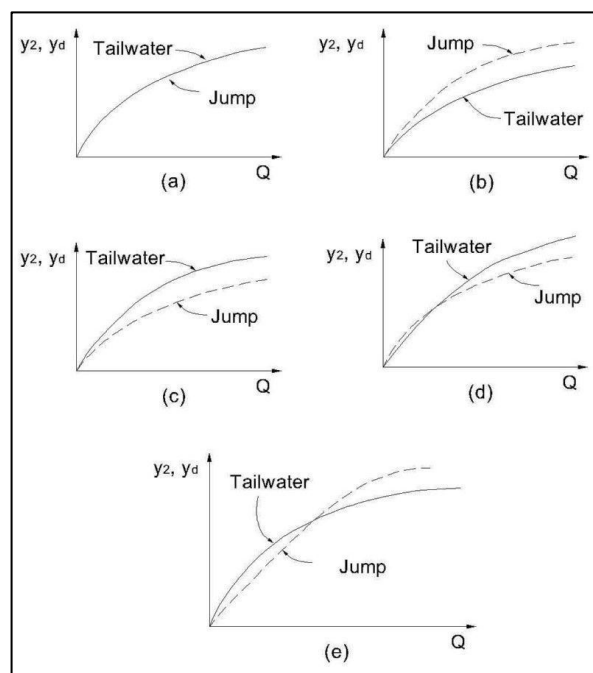


Figure 2-5: Effect of Tailwater Level on Jump Formation

The appurtenances which help controlling the location of a jump, are baffle blocks, sill (sharp or broad-crested weir), drop or rise in the channel bottom.

Application of the momentum equation and accurate design is difficult for these cases, due to non-uniform velocity distribution in the close vicinity of the applied appurtenances. This is the reason of conducting model studies and laboratory works for specific projects.

2.2.4 Energy Dissipation

Henderson (1966) stated that prior to late 19th century, designers tried to avoid hydraulic jumps whenever possible to minimize the risks of channel destruction. Since the beginning of the 20th century the application of reinforced concrete as high-resistance material, hydraulic jumps are used to dissipate flow energy downstream of supercritical flow structures, so hydraulic jumps are known for their energy dissipation performances.

Design engineers should be careful about the selection of features to satisfy the stability of jump. Hydraulic jump stilling basins are designed to induce a steady jump or a strong jump; the incoming super critical Froude Number, F_1 , should be above 4.5 in practice. The selection of a strong jump requires a careful analysis about the determination of the location of the hydraulic jump due to the risk of bed erosion.

A lot of model studies conducted to improve hydraulic jump stilling basins i.e. USBR (1955), Peterka, (1958).

The energy loss along the hydraulic jump is obtained by applying the principle of the conservation of energy. The energy loss in the jump is the difference between the total head at upstream and downstream of the jump. For a horizontal channel bottom, the difference in the specific energy upstream and downstream of the jump is equal to the energy loss. Turbulent mixing along the hydraulic jump causes energy loss of supercritical stream as in Figure 2-6 up to 85% (Chow, 1959) depending on the incoming Froude number.

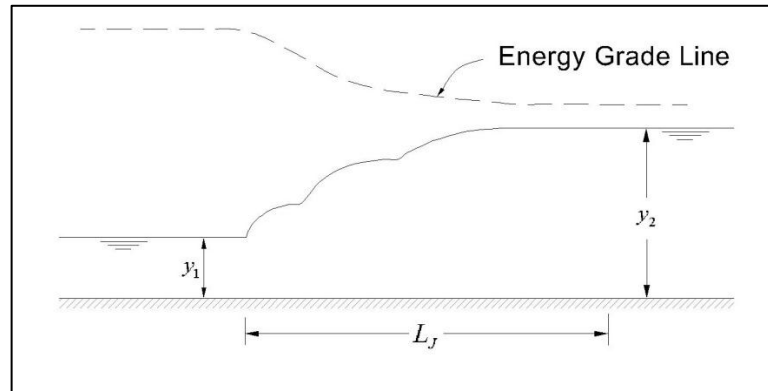


Figure 2-6: Energy Loss along Hydraulic Jump

The variation of the relative loss E_L / E_1 with the incoming Froude number, F_1 , has been constructed by recent researches and it is shown in Figure 2-7. Where, E_1 is the specific energy of supercritical flow and E_L is the energy dissipated through hydraulic jump. The head loss across the hydraulic jump is given by the equation (Chow, 1959).

$$E_L = \frac{(y_2 - y_1)^3}{4 y_1 y_2} \quad (2.10)$$

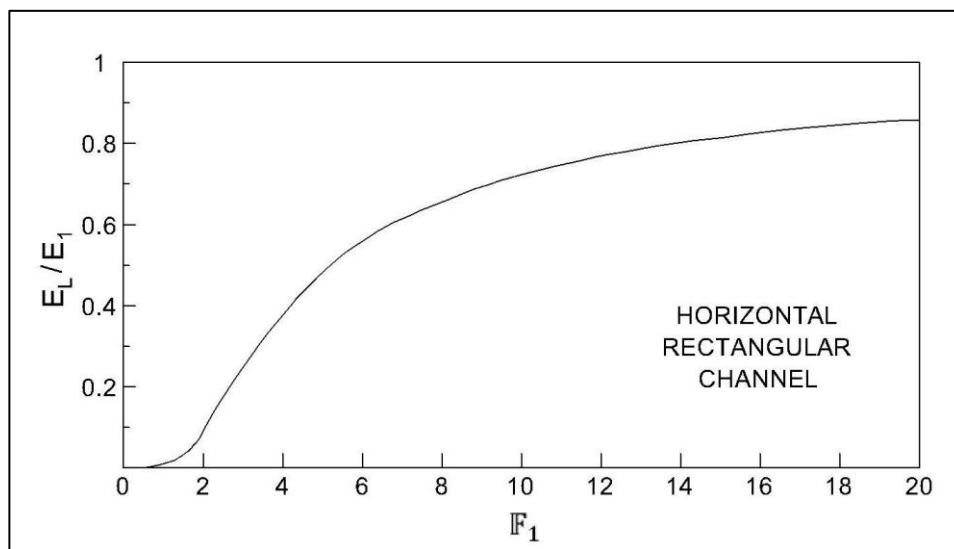


Figure 2-7: Relative Energy Loss in Hydraulic Jumps

(Reproduced from Chow, 1959)

The relative energy loss, E_L / E_1 is also called as the efficiency of the hydraulic jump $\eta = E_L / E_1$. Hager (1995) recommended the following equation to demonstrate the efficiency for classical hydraulic jumps when $F_1 > 2$.

$$\eta = \left(1 - \frac{\sqrt{2}}{F_1}\right)^2 \quad (2.11)$$

2.2.5 Aeration

The observed increase in mixing potential of jumps with fully developed inflow awakens the researcher's interest in hydraulic jumps as aeration devices and several investigators have studied the phenomenon of air entrainment through hydraulic jump. Aeration has some important applications related with the air-water mass transfer and oxygen transfer.

Küçükali and Chanson (2008) stated that void fractions measurements in hydraulic jumps were first conducted by Rajaratnam (1962). Rajaratnam (1962) showed that jumps with Froude Number higher than 6, large quantity of air entrain at the front of the jump close to the bed, characterized by intensive turbulence and large vortices. At the entrance section, air concentration is high, whereas the concentration drops rapidly at downstream sections (Figure 2-8). In Figure 2-8, C_b represents the the air concentration in the bottom layers.

Handerson (1966) stated that although air entrainment makes no difference to the tailwater level to be supplied downstream of the basin, its existence within the basin calls for a generous freeboard allowance.

Leutheusser et al. (1972) looked into void ratio, average bubble size, and statistical size distribution with hot-film probe, for $F_1 = 2.85$ for undeveloped and fully developed supercritical inflows. The void ratio, was defined as,

$$\alpha_V = \frac{T_a}{T_a + T_w} \quad (2.12)$$

where, T_a is the fraction of the total duration of observation during which the hot-film probe sensed air, and T_w is the corresponding time fraction for water contact of the probe.

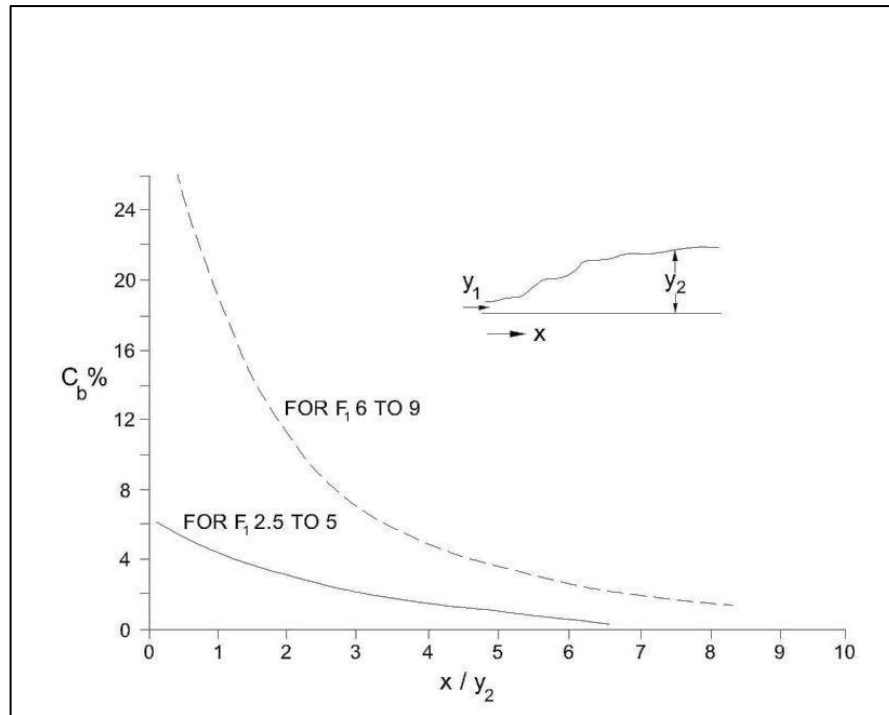


Figure 2-8: Air Concentration Close the Bed in a Hydraulic Jump (Rajaratnam, 1962)

Leutheusser et al. (1972) presented experimental results of bulk characteristics of air entrainment in hydraulic jump for undeveloped and fully developed flow conditions (Figure 2-9).

Hager (1995) stated that the aeration length L_a is longer than the length of jump and it can be used as a scaling parameter for classical hydraulic jump.

$$L_a = 3.5 y_2 \sqrt{(F_1 - 1.5)} \quad (2.13)$$

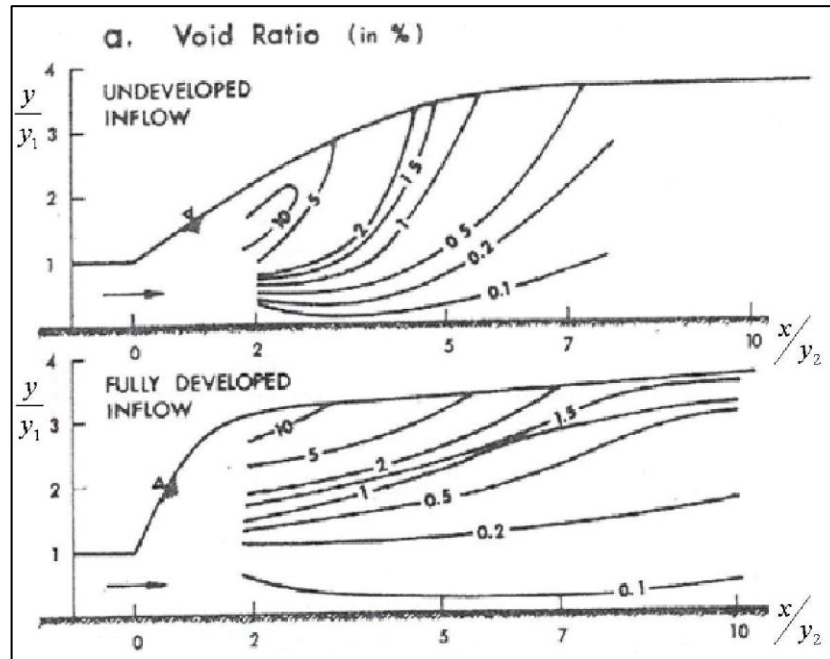


Figure 2-9: Bulk Characteristics of Air Entrainment in Hydraulic Jump
(Leutheusser et al., 1972)

Chanson (1996) states that air entrainment characteristics of hydraulic jumps are not completely understood. However, he quoted that Thandaswera (1974) showed that the air entrainment rate, the diffusion of air bubbles within the jump and the distributions of velocity, air concentration, and air bubble size are affected substantially by the initial free- surface aeration.

Afzal and Bushra (2002) analyzed the axial flow structure of turbulent hydraulic jump. They concluded that the longitudinal and transverse length scales of the mixing layer due to air-water interaction depend on both the supercritical Froude number and Reynolds number.

Khatsuria (2005) declared that the process of aeration and air bubble redistribution depends upon the inflow conditions of hydraulic jump. These conditions were described as: partially developed jump, fully developed jump, and pre-entrained jump. He also denoted that for hydraulic jumps with fully developed inflow conditions, the quantity of air entrained is comparatively larger than with the partially developed jumps. However, the partially developed jumps exhibit larger concentration of air in the bottom layers.

Khatsuria (2005) also reported that C_b is relevant to the mitigation of cavitation damage to the basin floor and appurtenances like chute blocks and baffle piers, against fluctuating pressure depressions.

For all the standard designs described above, it is recommended that no allowance for air entrainment need be made. This recommendation is based on experience which indicates that prototype stilling basins in which air entrainment is present perform at least as well as model basins, in which there is no air entrainment.

Küçükali and Çokgör (2006) investigated aeration performance of hydraulic jumps in terms of energy loss approach. A strong correlation was found between the aeration efficiency and head loss.

Küçükali and Chanson (2008) examined the air-water turbulent flow properties in hydraulic jumps with incoming Froude number range 4.76 to 8.50. It was stated that there is a linear relation between the normalized maximum free-surface fluctuation and the inflow Froude number. They also stated that maximum void fraction, C_{max} and maximum bubble count rate, F_{max} were functions of the inflow Froude number, F_1 , the inflow Reynolds number R_1 and of the streamwise position $(x - x_1)/y_1$. Where, x horizontal distance of the point of measurement from channel inlet, and x_1 is the distance of jump toe to inlet.

2.2.6 Turbulence Characteristics

The apparent loss of energy in a hydraulic jump is, conversion of velocity head into turbulent head. The sum of elevation, and pressure and velocity heads are transformed into turbulent energy first, and then into heat due to the viscous action of the fluid.

Leliavsky (1959) said that the hydraulic jump could be treated on the energy principle by adding a fourth term representing the energy of rotation in the vortices to Bernoulli equation, representing the principle of conservation of energy.

The most commonly used parameters for expressing turbulence are the fluctuations of velocity, pressure and force.

Hager (1995) stated that the loading of a floor beneath a hydraulic jump, and damage due to fatigue, structural resonance or cavitation depends significantly on the fluctuations of the turbulent pressure.

Khatsuria (2005) declared that to understand the origin and mechanism of damaging forces, i.e. vibration, cavitation, uplift and, all hydrodynamic loading forms, studying the turbulence structure of hydraulic jump is important.

Küçükali and Çokgör (2006) suggested that surface eddy's dominant role in the process of conservation of energy into turbulent head. It was found that (Figure 2-10) turbulence kinetic energy, K , (Eq. 2.14) decreases along hydraulic jump length.

$$K = (\overline{u'^2} + \overline{v'^2} + \overline{w'^2}) \quad (2.14)$$

Where, u', v', w' are the fluctuating velocity components along x, y, z directions, respectively.

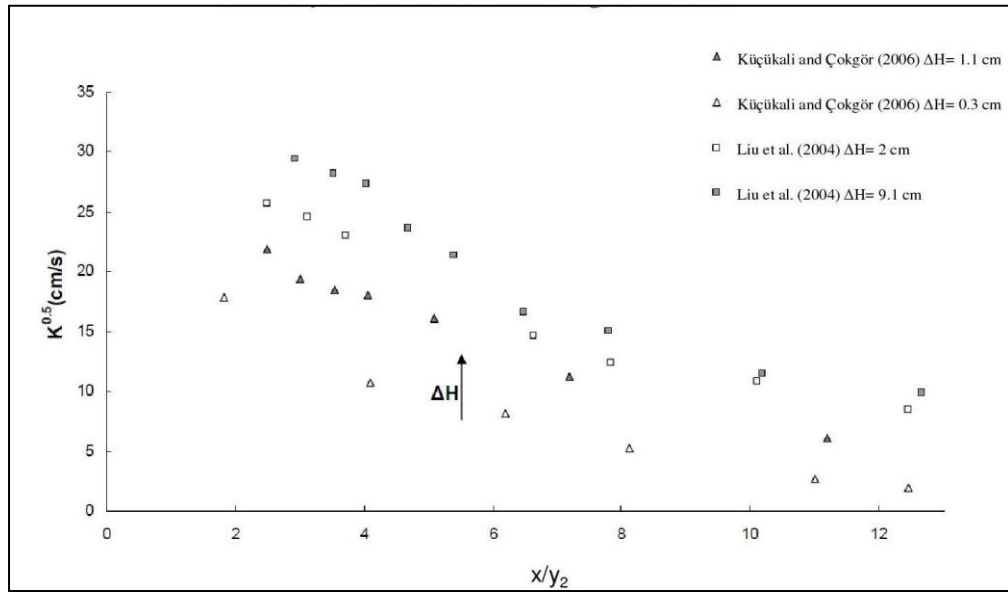


Figure 2-10: Turbulence Kinetic Energy along Hydraulic Jump (Küçükali and Çokgör, 2006)

2.2.7 Jump Length

From the engineering point of view, the hydraulic jump length is an important parameter; it determines the length of measures through the stilling basin against scouring and the height of the side walls. The shorter the hydraulic jump length, the more economical construction of stilling basin.

The length of hydraulic jump is usually considered as a purely empirical problem (Leliavsky, 1959). The analytical formulation for the length of the hydraulic jump is not possible; hence all knowledge about the length of jump is based on experimental studies.

Leliavsky (1959) quoted that Riegel and Beebe (1917) stated that, the length of the jump is approximately five times its height. This result was derived from the experiments they made for the Miami Conservancy District.

Bakhmateff, (1932) expressed that defining beginning or the end of the jump is not always simple and process of defining greatly depends on the type of the

jump and on other circumstances which surround the phenomenon. The highly turbulent flow surface, formation of roller and eddies; air entrainment and probable measurement errors are the main reasons, makes it difficult to mark the beginning and the end of a jump. Because of these reasons, various definitions have been forwarded such as:

L_m : The measured distance between the toe and the section of the maximum depth.

L_r : The surface roller length; the distance between the toe and the surface stagnation point, which separates the backward and forward flow.

L_e : The erosion length, the distance between the toe and the point, where bottom erosion disappears.

L_j : The length of a jump, in the literature it was measured according to two basic definitions;

- i. The end of a hydraulic jump is the horizontal distance between the toe of the jump to a section where the water surface elevation becomes essentially level.

Bakhmateff and Matzke (1936), Rajaratnam (1965), Rajaratnam and Subramanya (1968), Ohtsu and Yasuda (1994), Tokyay (2005), Şimşek (2006) have defined the end of the jump in this manner.

- ii. The end of a hydraulic jump is the distance from the toe of the jump to a point on the surface immediately downstream of the roller.

Chow(1959), Hughes and Flack(1984), USBR (1987), French (1987) conducted experiments in this frame.

It is difficult to determine the length of the jump according to first definition due to turbulence characteristics of a hydraulic jump and air entrainment as

mentioned before. Time averaged measurement of whole hydraulic jump profile may give consistent results.

Evcimen (2005) stated that the use of second definition is also insufficient because the jump does not finish just after roller and it has been shown that the flow depth at the end of the roller is somewhat less than the subcritical sequent depth. Different definitions of the length of the hydraulic jump cause some confusion in comparing the data of various studies.

U.S.B.R. (1955) investigated hydraulic jump lengths along six flumes and the relation between L_j/y_2 and upstream Froude number, was given in Figure 2-11. L_j/y_2 is practically constant when $F_1 > 5$ and expressed in Eq. (2.15). Dimensionless parameter L_j/y_2 depends on incoming Froude number when $F_1 < 5.0$.

$$L = 6.1 y_2 \quad (2.15)$$

Silvester (1964) conducted experiments in rectangular channel and correlated experimental data with the following expression,

$$\frac{L_j}{y_1} = 9.75(F_1 - 1)^{1.01} \quad (2.16)$$

Rajaratnam (1965) investigated the length of surface roller, L_r , length of the hydraulic jump, L_j , and the depth of flow at the end of roller, y_r as the case of plane turbulent wall jet. He compared the measured results with past studies and concluded that the results are very close to values presented by Peterka (1958) for practical purposes. He also stated that, it was found that y_r is always less than y_2 and that the ratio y_r/y_2 varies linearly with F_1 and given as

$$\frac{y_r}{y_2} = 0.834 + 0.012F_1 \quad (2.17)$$

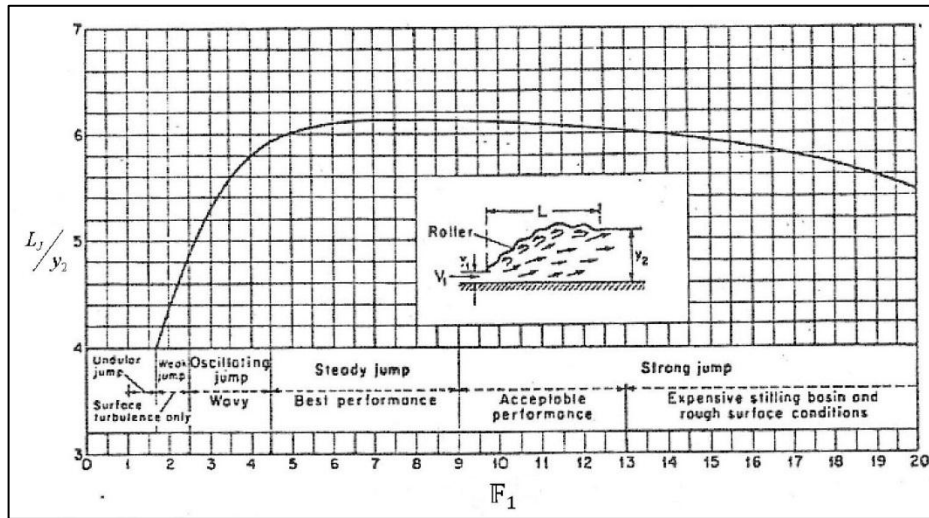


Figure 2-11: Length of Jumps as Function of, F_1 , (USBR, 1955)

Rajaratnam (1968) stated that although some investigators took the end of the surface roller itself as the end of the jump, it had been shown that the flow depth at the end of the roller was less than the subcritical sequent depth. For rectangular channels, the following relation was given.

$$\frac{L_j}{y_1} = 5.08F_1 - 7.82 \quad (2.18)$$

Peterka (1958) has presented a graph relating the length L_j/y_2 to F_1 , which can be summarized in (Table 2-1).

Table 2-1: Classical Hydraulic Jump Length, Peterka (1958)

Range of F_1	L_j / y_2
2.5-4.5	5-6
5-14	6-6.1
14-20	6-5.5

Experimental data have been summarized in a non-dimensional form relating the F_1 and L_j/y_1 or L_j/y_2 . According to Khatsuria (2005), approximately 40

formulae have been suggested defining L_j in terms of y_2 or y_1 ; ranging from 5 to 6 y_2 or 35 to 60 y_1 .

As quoted in Hager and Bremen(1989), Bretz(1987) examined length of the roller, L_r in experiments and suggested following equation;

$$\frac{L_r}{y_1} = 6.29 F_1 - 3.59 \quad (2.19)$$

Hager et al. (1990) proposed the following correlation for wide channels (i.e. $y_1/b < 0.10$), where b is the width of a rectangular channel.

$$\frac{L_r}{y_1} = 160 \tanh\left(\frac{F_1}{20}\right) - 1.2 \quad (2.20)$$

Hager (1991), developed the following equation for the length of the jump;

$$\frac{L_j}{y_1} = 220 \tanh\left(\frac{F_1 - 1}{22}\right) \quad (2.21)$$

Afzal and Bushra (2002) defined jump length in rectangular channels independent from incoming Froude number as,

$$\frac{L_j}{y_1} = 6.09 \left(1 - \frac{y_1}{y_2}\right) \quad (2.22)$$

2.2.8 Classification of Jumps

Hydraulic jumps can be classified according to the geometrical form, the incoming Froude number, or as a free, forced, or submerged jump.

It should be remembered that the Froude number ranges given below depend on local conditions and geometry, hence they are not exact. Hence the possibility of change of ranges must be considered in design considerations.

Direct and Undular Jumps

Bakhmateff (1932) classified hydraulic jumps into two forms as the direct form and the undular form. Hydraulic jumps were classified as direct jump if the upper stage is reached practically by one continuous rise of the surface. The direct jump features an underlying portion of expanding live stream covered by a surface roll within which the particles are engaged in circuitous movement and do not participate in the translator movement of the liquid from upstream to downstream. If the transition from the lower to the upper stage features a series of undulations of gradually diminishing size, such type of hydraulic jumps were classified as undular form.

Bakhmateff (1932) also indicated that the direct form is usually present in jumps accompanying flow through hydraulic structures whereas undular form is mostly observed in natural watercourses with moderately steep bottom slopes.

Leliavsky (1959) defined undular jumps such that the water surface is undulating with a very small ripple on the surface over considerable distances. He stated that the undular type occurs at relatively low "kineticity", i.e. when the ratio of kinetic to potential energies, in the critical section ahead of the wave, does not exceed a certain limit, $\lambda \leq 3$ and in tail-work design the undular type does not call for specific consideration.

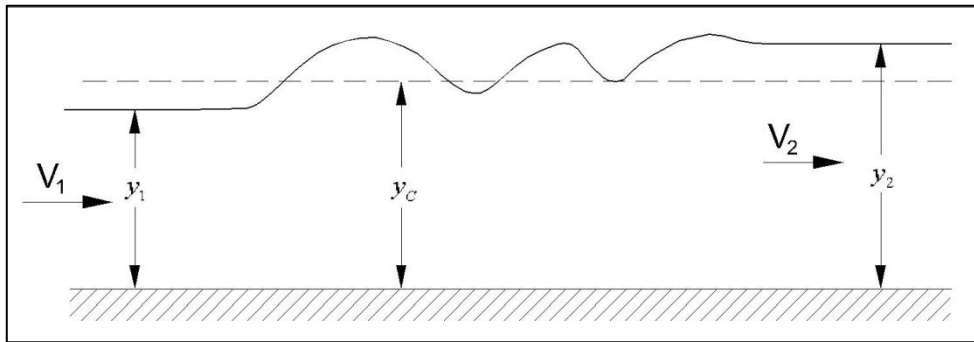


Figure 2-12: Undular Jump

Undular jumps have also been called as the pre-jump. The upper limit of incoming Froude number, F_1 is 1.7 for undular forms and this result is consistent with the kinematic value of Leliavsky (1959).

Submerged Jump;

Supposing all conditions are the same with undular jump, but the downstream level starts to rise, toe of the hydraulic jump moves gradually towards the gate, until the conditions are such as are shown in Figure 2-13. This type of jump is described, as a submerged hydraulic jump.

In literature, the flow pattern of the submerged jump is defined with not only supercritical Froude number, but also the "submergence ratio" $\sigma_r = y_r/y_2$. In which y_r represents the downstream depth actually measured, whilst y_2 is the conjugate depth required for hydraulic jump to form.

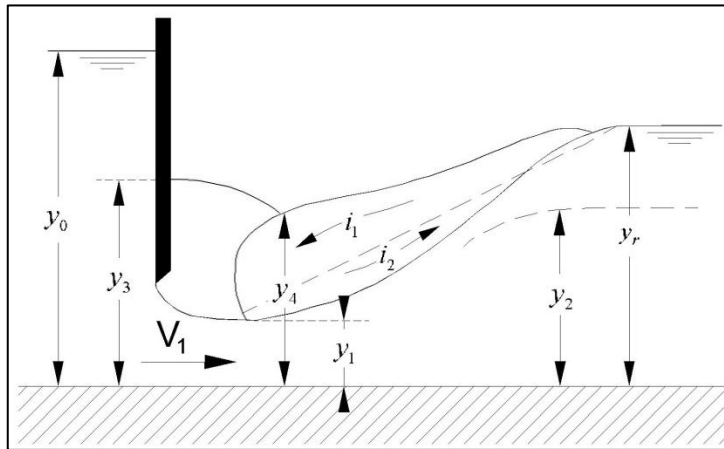


Figure 2-13: Submerged Wave

Smetana (1943) studied the flow structure and velocity distribution through submerged jumps for different incoming Froude numbers and tailwater depths. He represented the results of the study in tabular form. An example of experimental result is given in Figure 2-14.

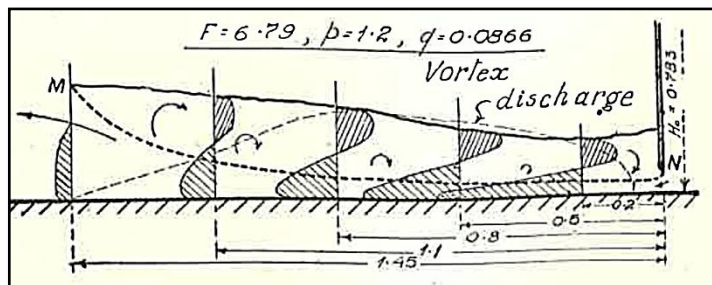


Figure 2-14: Experimental Results of Smetana (Leliavsky, 1959)

Classical Hydraulic Jumps;

The hydraulic jump in a horizontal, rectangular channel is generally referred as classical jump. The classical hydraulic jumps have distinctive characteristics depending on the incoming Froude number. The increase of F_1 causes

increases the transformation to turbulent energy as discussed in Section 2.2.6 hence the energy dissipation along hydraulic jump.

Five different types of jump had been defined for classical jumps. The basic parameter of this classification is founded on shapes of hydraulic jumps; however the borders are defined with incoming Froude number. The first category is pre-jump stage or undulating jumps, the type is already explained.

i. Weak Jump; $1.7 < F_1 \leq 2.5$:

The surface roller makes its appearance at $F_1 \approx 1.7$ and a number of small rollers are formed on the water surface, although the downstream water surface remains smooth. The energy dissipation is very small, E_1/E_2 changes from 5% at $F_1 = 1.7$ to 18% at $F_1 = 2.5$ approximately.

ii. Transition or Oscillating Jump; $2.5 < F_1 \leq 4.7$:

For these range of Froude numbers, a true hydraulic jump does not fully develop. The jet at the entrance to the jump oscillates from the bottom to the top in a random manner and these oscillations produce large surface waves in irregular period. Each irregular oscillation produces a large wave which may persist for a long distance downstream of the jump, damaging and eroding the banks. If possible this range of F_1 should be avoided at design stage. Energy dissipation is change from 18% to 45% by the increase in Froude number.

iii. Steady Jump; $4.5 < F_1 \leq 9$:

True hydraulic jump form for Froude numbers greater than 4.5. Position of steady jump is the least sensitive type to fluctuations in the tailwater elevation and forms steadily at the same location. The relative energy loss E_1/E_2 changes from 45% to 70%. This type of jump serves the best economic conditions for the design of stilling basins.

iv. Strong or Choppy Jump; $F_1 > 9$

The difference between the conjugate depths is large; the water surface profiles along jump and downstream of the jump are rough and wavy. Water rolling down the front of the jump face hits into high-velocity jet and generates additional waves at irregular intervals. Although relative energy loss is greater than 70% and up to 85%, it should be avoided because of channel bed erosion risk.

Free and Forced Jumps

The jumps have also been classified according to condition of tailwater level.

- i. Free jump:* The tailwater depth available at the end of the jump is equal to the conjugate depth y_2 .
- ii. Forced jump:* The tailwater depth available at the end of the jump is smaller than the conjugate depth y_2 . The formation of jump is aided by use of appurtenances such as chute blocks, baffle piers or high end sills.

Hydraulic Jumps on Sloping Apron;

According to geometry of apron, hydraulic jumps are also classified as A-type, B-type, C-type, or D-type as shown in Figure 2-15 (Khatsuria, 2005).

A-jump: The toe of the hydraulic jump is at the same location with the junction of a sloping channel with the horizontal floor.

B-jump: The toe of the jump is on the slope but end point of jump is on the horizontal floor.

C- jump: This type of hydraulic jump occurs in sloping channels with the toe of the jump is on the slope but end point of jump is at the intersection point.

D-jump: The entire jump is formed on the sloping portion.

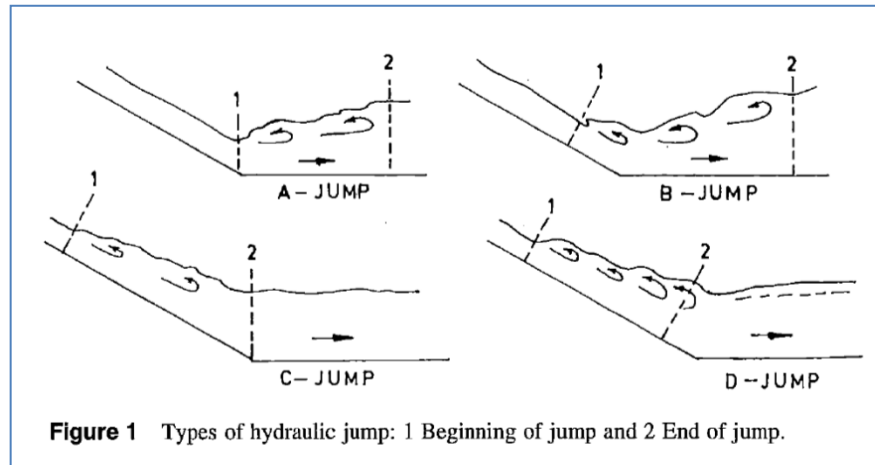


Figure 2-15: Hydraulic Jumps on Sloping Aprons (Khatsuria, 2005)

2.3 Jump on Rough Beds

Turbulent flow over a rough surface is an important problem and it has been subject of diverse fields. The flow over a surface with transverse, rectangular roughness elements often used as a simple model to study roughness effects on friction factor, heat transfer, and hydraulic jump.

Using roughness elements at the bottom of the flow causes increase in resistance to the flow hence accelerate the upstream flow development and increase in amount of kinetic energy, converted into the turbulent energy. In this manner, usage of roughened beds at stilling basins where hydraulic jumps formed increases amount of dissipated energy along jump.

In smooth horizontal channels, transformation to turbulent energy occurs only along roller and somehow downstream of the roller. Position of the jump along channels depends on H3 profile of supercritical flow and H2 profile of the subcritical flow. Any change in tailwater depth changes the position of the jump significantly because the depth of supercritical flow changes gradually along channel as in H3 profile and the change in position of the jump much more higher than the change in required supercritical flow depth. On the other

hand, if roughened beds are used along channels, resistance of flow greater than smooth surfaces, so changes in depth along H3 profile is more rapid when compared with smooth surfaces. Hence position of the jump on rough beds is less sensitive to change in tailwater depths than jump on smooth surfaces.

Ead and Rajaratnam (2002) and Ayanlar (2004) examined the reduction of tailwater depth due to corrugated beds experimentally. Reduction of tailwater depth found about 25% by Ead and Rajaratnam (2002) and found about 20% by Ayanlar(2004). It is an important point that efficiency of corrugated beds are higher than USBR stilling basins Type II and Type III (Peterka, 1958) when reduction of tailwater depths are compared. Furthermore it was observed that the length of jump on corrugated beds is approximately one half of those of the classical jumps.

Early experimental works have shown that the pitch ratio z/w is an important parameter for flows on roughened beds where w is the distance between two roughness elements and z is the height of roughness element as shown in

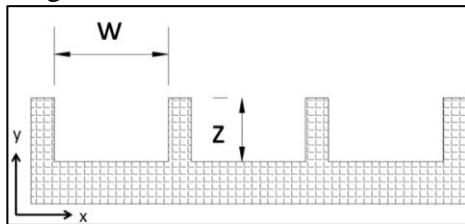


Figure 2-16 (Tani, 1987). If the ratio, w/z , smaller than 4, this type of roughness is called as d-type roughness (Cui et al., 2003). For d-type roughness, roughness elements so closely spaced that, crests of the ribs do not penetrate into flow hence effect of roughness elements on friction and eddy formation is negligible. A vortex fills the cavity between the two ribs and effects of a pitch on bulk flow look like effect of a cavity on bulk flow for this range of pitch ratio or this type of roughness.

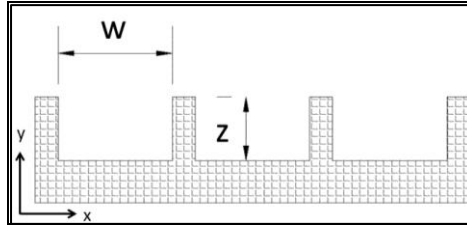


Figure 2-16: Geometrical Properties in the Study of Tani (1987)

If pitch ratio is equal to 4, it is known as intermediate roughness, the length of vortex formed in the cavity is equal to length of the gap between roughness elements, this vortex prevents the outer flow from attaching to the channel bed and streamlines above the pitch nearly parallel except near the roughness element (Cui et al., 2003).

If the pitch ratio is greater than 4, it is called as k-type roughness, vortex formed in the cavity is smaller than pitch, and hence outer flow attaches to the channel bed. Roughness elements penetrate into flow and friction factor depends on the size of roughness elements. Flow structure in the gaps for these three type of pitch ratios are shown in Figure 2-17.

Formed vortexes for k-type and intermediate type roughness increase turbulent intensities in the plane of crests of roughness elements, hence also increase Reynolds shear stresses.

Furthermore pressure drag on the roughness elements is much higher than friction drag of smooth channel and increases resistance to the flow. Cui et al. (2003) indicated that for k-type roughness resistance to the flow is 6 times higher than resistance of smooth channel, whereas for intermediate type roughness this ratio is about 4.6.

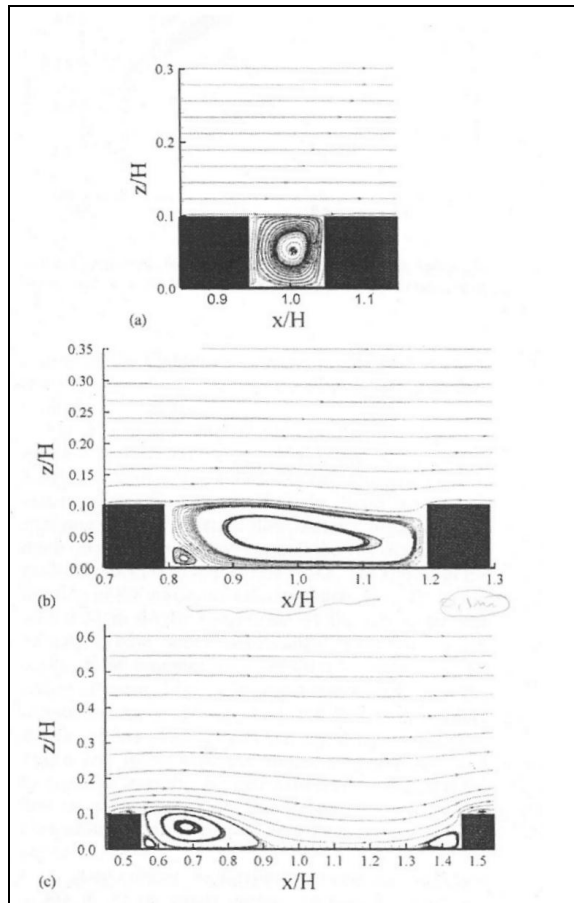


Figure 2-17: Mean streamlines for (a) d-type roughness, (b) intermediate roughness, and (c) k-type roughness (Cui et al., 2003)

2.3.1 Literature Review

According to Izadjoo and Bejestan (2007) and Nikmehr and Tabebordbar (2010), Rajaratnam (1968) was the first scientist who systematically studied the hydraulic jumps over rough beds. He analyzed the effects of bed roughness on length and sequent depth ratio with incoming Froude numbers ranging between 3 and 10 in his experiments. His results indicated that the sequent depth ratio was dependent on both the incoming Froude number and the roughness height; and also, the length of jump formed on a roughened bed was approximately half of that on smooth bed. Rajaratnam(1968) stated that the

length of the roller, L_r , decreases significantly on rough bed when compared that on smooth bed.

Perry and Joubert (1969) who studied the turbulent boundary layer over a wall roughened by transverse ribs, proposed dividing the roughness into two types; k-type and d-type, where,

- in k-type roughness, roughness function is determined by the height of the roughness, z , and,
- in d-type roughness, height of roughness element is not important and main parameters for the roughness function are, δ , the boundary layer thickness, δ_1 , pipe diameter or channel height, d_h .

Leuthesusser and Schiller (1975) experimented the development of supercritical channel flow in a horizontal and roughened rectangular open channel flume with varying bed roughness to observe the characteristics of mean turbulent motion upon the incoming jet. The selected roughness patterns through their study were spherical and strip roughness. They found that the existence of a development of supercritical flow upon rough bed is faster than smooth bed, hence requires less length in comparison to smooth bed.

Hydraulic jump characteristics on artificially roughened beds in a horizontal rectangular flume were also investigated by Hughes and Flack (1984) who utilized parallel square bars bonded to plexiglass base and closely packed gravel particles to simulate the roughness elements. They concluded their experimental results as the tailwater depth reduction and jump length are functions of both the initial Froude number and the degree of roughness.

Hager and Bremen (1989) investigated the effect of wall friction on the sequent depth ratio both theoretically and experimentally. They found a slight difference between the Belanger equation results and experimental results for the sequent depth ratio. They observed that this difference became more

significant when the incoming flow depth was small. They concluded that a deviation up to 5% would be logical; however, viscosity effects must be taken into account for deviations greater than 5%.

Mohamed Ali (1991) conducted a series of experiments with cubic roughness elements and studied the effect of roughness on hydraulic jump length to determine the optimum length of jump considering hydraulics and economy. He applied statistical methods to generate practical equations and proposed that the most efficient length of roughness is $L/z = 28$, where, L is the length of roughness, and, z is the height of roughness elements,

Hager (1995) stated that hydraulic jumps in non-rectangular channels are much less stable than the jump in the rectangular channel, and from the technical point of view cannot be used without appurtenances like baffle blocks, sills, etc.

Rajaratnam (1995) stated that an increase in the roughness of the bed can reduce the tailwater depth. For a given classical jump, if roughness height, k_s is of about $0.5 y_1$, the required tailwater depth is about 80% of required subcritical depth.

Ead et al. (2000) investigated the velocity field in turbulent open channel flow in circular corrugated culverts. Their results indicated that the corrugations increased Reynolds shear stress and caused intense mixing along the plane of the crests. They added that the velocity near the boundary was significantly smaller than average velocity of the flow.

Ead and Rajaratnam (2002) further investigated the corrugation effects on hydraulic jump length L_J , tailwater depth y_2 , integrated bed shear stress $F\tau$, and dimensionless depth deficit parameter D in rectangular channels. With Froude numbers from 4 to 10 and three relative roughness t/y_1 values at 0.50, 0.43, 0.25 (where t is the amplitude of the corrugations), they studied the effect of

corrugations; and stated that the tailwater depth required to form a jump on corrugated beds is notably smaller, the length of jump on corrugations is about half and integrated bed shear stress is about ten times when compared to jumps on smooth beds. They also concluded that the corrugations acted like cavities and the t/y_1 values have no effect on sequent depth ratio y_2/y_1 .

Cui et al. (2003) utilized ribs as roughness elements and studied the turbulent flow over rough surfaces for various pitch ratios. They analyzed the turbulence structure, interaction between the roughness layer and outer flow, flow in the roughness layer and the roughness function associated with the time and space averaged velocity profile. Their conclusions were such that:

- for d-type roughness; $w/z < 4$, streamlines beyond the rib height and cavity are nearly parallel,
- for intermediate roughness, $w/z = 4$, streamlines above the cavity are nearly parallel except near the rib
- for k-type roughness; $w/z > 4$, flow separates at points between two roughness elements (Figure 2-17).

Çelik et al. (2003) compared the effect of prismatic roughness elements on hydraulic jump properties in smooth and rough channels. They concluded that the length and the sequent depth of a hydraulic jump are smaller in a rough channel.

Tokyay (2005) introduced aluminum sheets with different wavelengths and variable incoming Froude numbers (F_1 ; where $4 \leq F_1 \leq 12$) to investigate the effect of corrugated beds on hydraulic jump properties. It was found that corrugations reduce the required tailwater depth for given upstream conditions, y_1 and F_1 , when compared to the results of hydraulic jumps on smooth bed. It was reported that an sequent depth reduction factor, D , 0.2 was observed in experiments and the decrease in the length of the hydraulic jump was in average about 35%. It was also stated that as the Froude number increases, G

(the gain in energy loss for the jumps on corrugated beds) decreases and tends to stabilize at a constant value of 7% when the Froude number is greater than 8. These results confirm the findings of Ead and Rajaratnam (2002).

Evcimen (2005) investigated the hydraulic jump properties by increasing the bed roughness in rectangular channels, where he placed rectangular prismatic strips parallel to the channel bed to investigate the effects of roughness. The different roughness heights, spacing and incoming Froude numbers on hydraulic jump formation were investigated. With increased bed roughness, the average tailwater depth was about 80% of that on free jump on smooth surface and the decrease in the length of hydraulic jump was about 40%. It was also stated that the average energy loss in hydraulic jumps on rough beds was 5~10% larger than that for free jumps on smooth beds.

Şimşek (2006) investigated the effect of non protruding strip and staggered-roughness arrangements on hydraulic jump characteristics. Through his experimental study, different length and pitch ratios were used. He concluded that the non-protruding roughness elements increases the energy dissipation by 3 to 7% and the tailwater depths are smaller by 7 to 15% when compared with jumps formed on smooth beds.

Carollo et al. (2007) investigated the effect of an artificially roughened bed, made up of closely packed crushed gravel particles cemented to the bottom, on hydraulic jump properties. They showed that the boundary roughness reduced the sequent depth ratio and offer a new form of Belanger equation (Eq.(2.23)).

$$\frac{y_2}{y_1} = \frac{1}{2} \left(-1 + \sqrt{1 + 8(1 - \phi)F_1^2} \right) \quad (2.23)$$

where, ϕ is coefficient to satisfy equation in rough beds and given as;

$$\varphi = \frac{2}{\pi} \arctan \left(0.8 \left(\frac{k_s}{y_1} \right)^{0.75} \right) \quad (2.24)$$

where, k_s is roughness height.

Ead and Elsebaie (2007) continued experiments with different shapes of corrugated beds, i.e. sinusoidal, triangular and trapezoidal corrugations with the same amplitude and wavelength. He investigated their effects on hydraulic jump characteristics and indicated that for all shapes of corrugated beds, the tailwater depth required to form a jump was appreciably smaller than that for the corresponding jumps on smooth beds, and the length of the jump on the different corrugated beds was less than half of that on smooth beds. He also stated that the integrated bed shear stress on the corrugated beds was more than 15 times that on smooth beds.

Izadjoo and Bejestan (2007) investigated the effect of trapezoidal shape corrugations experimentally on flow characteristics of hydraulic jump. They stated that when compared with classical jump on smooth bed; the conjugate depth is reduced 20%, length of the jump is reduced by 50%, the amount of bed shear stress is increased 10 times and it is a function of a Froude number. They also stated that the length of the jump roller depend on corrugate spacing rather than to their height.

Khatsuria (2009) concluded that due to reproducing most of roughness elements is impractical in nature, very little development towards the practical implementation of rough beds. It was stated that construction of corrugations, i.e. sinusoidal, trapezoidal or triangles are difficult and maintaining is hard during operation phase . It was claimed that the practical ways of construction would be casting small size cubes or blocks with the base concrete of the panel and, casting large rectangular strips spaced at close interval.

Salehian et al. (2011) investigated the effect of natural bed roughness with two different size crushed sedimentation materials on hydraulic jump characteristics. They showed that two different rough beds reduce relative sequent depth 13.5% and 19.5%; roller length of 11.1% and 21.4%; jump length 31.5% and 39.8%, respectively.

Ezizah et al. (2012) investigated the effect of U-shape roughness elements on hydraulic jump flow characteristics for Froude number range 3 to 11 experimentally. U-shaped roughness elements were installed channel bed such that the upper side of U towards to upstream. It was reported that when the U-shape and other roughened shapes compared, the best performance was achieved when using the U-shape roughness. According to their findings, sequent depth ratio, y_2/y_1 and L_j/y_1 decreases with the increasing intensity of roughness, I . For the roughness intensity of $I = 12.5\%$, reaching a minimum value and then start increasing for larger values of I for all incoming Froude number values, F_1 . It was found that the relative sequent depth decreases 14-20% and the relative jump length decreases by 28-47%.

CHAPTER 3

HYDRAULIC JUMP IN TRAPEZOIDAL CHANNELS

Hydraulic jumps in trapezoidal basins may be beneficial for the further reduction of tailwater depth, necessary length of the protected zone and construction costs when compared to the rectangular basins in some cases. The benefits can be listed as:

- i. The whole excavated volume can be used as the trapezoidal basin; no need for an additional working space as in construction of rectangular basins.
- ii. The transitions between the channel base and side walls do not enhance bending moments, decrease reinforcement cost significantly.
- iii. External formwork, support system, and a crane is not required
- iv. Backfilling and compaction works are minor, can be neglected.

However, the disadvantages of the trapezoidal basins over the rectangular basins are:

- i. The lack of practical experience with prototype trapezoidal stilling basins at present. Detailed experimental observations for basins of arbitrary geometry do not exist either. Only the application in large scale is Mongla dam, in Pakistan.

- ii. Along the stilling basin, significant surface currents exist especially, near the side walls downstream of the trapezoidal basin.
- iii. For trapezoidal channels, the length of a hydraulic jump is longer than jumps, formed on rectangular ones.
- iv. The required trapezoidal stilling basin volume is bigger than the volume of a rectangular basin.

3.1 Dimensional Analysis

A hydraulic jump in a rough trapezoidal channel bed is defined by the variables shown in (Figure 3-1) for a two dimensional flow case.

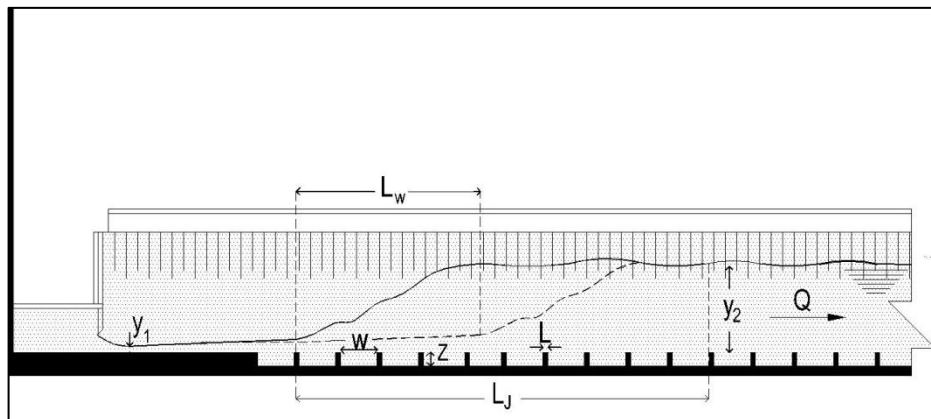


Figure 3-1: Hydraulic Jump in Trapezoidal Channel

- where, y_1 = the incoming flow depth [m]
 y_2 = the tailwater depth [m]
 b = the width of channel at the bed [m]
 L_j = the length of the jump [m]
 L_w = the length of wing oscillations [m]
 x_1 = the point where the jump starts, measured from inlet [m]
 z = the height of the roughness element [m]

- L = the length of roughness element [m]
 w = the distance between two roughness element [m]
 Q = the discharge [m]
 m = the cotangent of side slope angle
 I = the uniform intensity of roughness, The areal ratio of roughness elements and channel bed at plan view
 g = the acceleration of gravity [m/s^2]
 ρ = the mass density of water [kg/m^3]
 μ = the dynamic viscosity of water [kg/ms]

The tailwater depth y_2 , length of jump L_j and length of wing oscillations L_w , are affected by the following parameters;

$$y_2 = f_1 (y_1, b, Q, z, L, w, m, I, g, \rho, \mu) \quad (3.1)$$

$$L_j = f_2 (y_1, b, Q, z, L, w, m, I, g, \rho, \mu) \quad (3.2)$$

$$L_w = f_3 (y_1, b, Q, z, L, w, m, I, g, \rho, \mu) \quad (3.3)$$

If the parameters (y_1, Q, ρ) are chosen as repeating variables, the following dimensionless parameters are obtained:

$$\frac{y_2}{y_1} = f_4 \left(\frac{Q^2}{g y_1^5}, \frac{L}{y_1}, \frac{z}{y_1}, \frac{w}{y_1}, \frac{b}{y_1}, \frac{\mu y_1}{Q \rho}, I, m \right) \quad (3.4)$$

$$\frac{L_j}{y_1} = f_5 \left(\frac{Q^2}{g y_1^5}, \frac{L}{y_1}, \frac{z}{y_1}, \frac{w}{y_1}, \frac{b}{y_1}, \frac{\mu y_1}{Q \rho}, I, m \right) \quad (3.5)$$

$$\frac{L_w}{y_1} = f_6 \left(\frac{Q^2}{g y_1^5}, \frac{L}{y_1}, \frac{z}{y_1}, \frac{w}{y_1}, \frac{b}{y_1}, \frac{\mu y_1}{Q \rho}, I, m \right) \quad (3.6)$$

The term $Q^2/(g y_1^5)$ is called the square of the Froude number, and proportional to the square of the ratio of the inertial forces over the weight of water.

Viscous forces are not significant with respect to the gravitational force, so a form of the Reynolds number $\mu y_1/(Q \rho)$ can be neglected. The first term is equal to the incoming Froude number, hence Equation 3.4 is changed to;

$$\frac{y_2}{y_1} = f_7 \left(F_1, \frac{b}{m y_1}, I, \frac{w}{z}, \frac{w}{L} \right) \quad (3.7)$$

and w/L and I represent the same physical parameter, thus equation may be rewritten as,

$$\frac{y_2}{y_1} = f_8 \left(F_1, k, I, \frac{w}{z} \right) \quad (3.8)$$

Similarly Eq. 3.5 and Eq. 3.6 can be written as:

$$\frac{L_j}{y_1} = f_9 \left(F_1, k, I, \frac{w}{z} \right) \quad (3.9)$$

$$\frac{L_w}{y_1} = f_{10} \left(F_1, k, I, \frac{w}{z} \right) \quad (3.10)$$

Term, $k = b/m y_1$ is called as shape factor for trapezoidal channels. It has been used in analysis by many authors and it was first time analytically represented by Silvester (1964). The Term, I was called as roughness intensity and w/z is called as pitch ratio by Cui et al. (2003).

3.2 Literature Review

The physical characteristics of the hydraulic jump in trapezoidal channels have been conducted by many researchers. Although the investigation of the effect of systematically applied prismatic roughness element on hydraulic jump in

trapezoidal channel is still empty, hydraulic jump characteristics such as flow structure, sequent depth ratio, length of hydraulic jump, energy dissipation characteristic, and velocity profile inside hydraulic jump have been studied.

3.2.1 Flow Structure

Posey and Hsing (1938), reported by Wanoschek and Hager (1988), investigated hydraulic jump on trapezoidal channels. They stated that the flow features were quite different from jumps in rectangular channels. In contradiction to classical hydraulic jump, trapezoidal jumps are not straight; hence they are called as oblique jump. The result of obliquity is the energy of the high velocity stream that is concentrated over the band of water of upstream width and hence, the triangular side areas at the downstream end permit a certain degree of recirculation.

Posey and Hsing (1938) reported by Silvester (1964) stated that these recirculation produces greater energy dissipation. Recirculation reaches upstream and this assists in producing a triangular leading edge to the jump and called as "wings."

Ohtsu (1976) made a classification of hydraulic jumps in trapezoidal channels; His classification criteria based on the symmetry and steadiness of main current, and one type of jump was attributed to every domain of m and F_1 (in total 4 types).

- i. The forward flow does not deflect to the side, and the jump is symmetric with respect to the central plane of channels.
- ii. Though the size of surface eddy on one side is a little different from the one on the other side, the jump is almost symmetric.
- iii. The size of surface eddies on the side wall changes unsteadily, and the flow often reverses itself from side to side.

iv. The forward flow deflects, and the jump is unsymmetrical.

Ali and Ridgway (1977) investigated hydraulic jump properties in both trapezoidal and triangular channels. They defined jumps in sloping side walls as oblique jump. While the effects of friction and of velocity distribution were taken into account, extensive measurements of water profiles and pressure distributions were conducted. It was stated that, although the form of the hydraulic jump in a rectangular channel is defined by the incoming Froude number, the sectional geometry of a trapezoidal channel is also affected the form of jump.

Ali and Ridgway (1977) claimed that oblique jump was observed for all ranges of incoming Froude numbers and it was always veer to the same side except at Froude numbers close to the unity where the wings became symmetrical about the center line. It was also stated that the tendency for the jump to swing to one side might be due to asymmetry of the channel at entrance section, might have been too small to be noticeable in the velocity distributions (Figure 3-2). Where, F_u , is the modified upstream Froude number, equal to $F_1 \left(\frac{k+2}{k+1} \right)$, defined by Ali and Ridgway (1997).

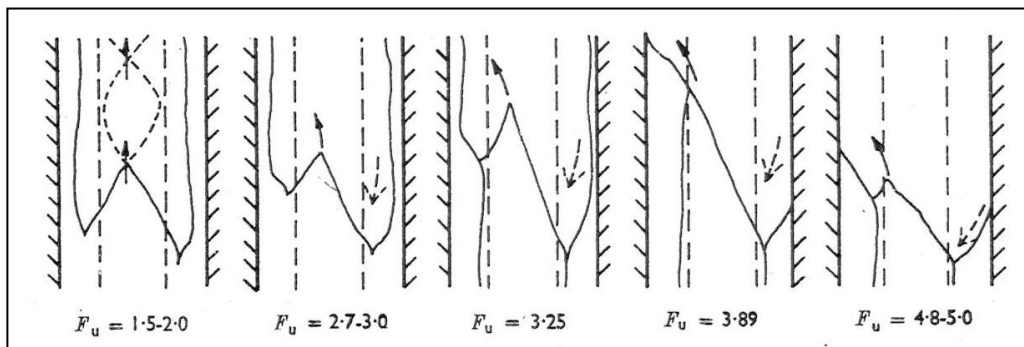


Figure 3-2: Variation of Wave Front with Froude Number for Trapezoidal Channel (Ali and Ridgway, 1977)

Sharp (1977) criticised the findings of Ali and Ridgway (1977) on oblique jumps. He pointed out that oblique jump was not observed at values of F_1 less than 4 and became apparent at Froude numbers above about 4. Furthermore, at Froude numbers greater than about 9, the oblique jump always formed and nondependent from channel geometry. The other comment was, oblique jump did not always slew to the same side and it was easy to change the direction of jump by inserting, and then withdrawing an obstacle to the flow.

Ali and Ridgway (1977) implemented a 0.3 m long sluice gate to the trapezoidal experimental model after the discussion of Sharp (1977). This modification overcame the tendency for the hydraulic jump to swing to one side of the channel.

Sharp (1977) stated that at high Froude numbers (i.e. $F_1 > 9$) the roller height was always greater than that of the subcritical sequent depth. He concluded that this roller and reversed flow can cause problems in trapezoidal stilling basins. In order to eliminate these unwanted phenomena baffle blocks, guide walls, lateral contraction and a vertical downwards step in the bed added in physical model and only a vertical downwards step in the bed stabilized the jump to a remarkable extent.

USBR (1987) stated that the triangular areas along the sides of the trapezoidal basin do not oppose the incoming high velocity jet, hence jump tend to form obliquely at the central part of the channel. At the sides there is reverse flow and this phenomenon tends to interrupt the jump formation. The hydraulic jump in a trapezoidal basin is much less complete and less stable than it is in the rectangular basin and severe scouring can occur beyond the triangular stilling basin.

Wanoschek and Hager (1988) investigated the internal flow features of hydraulic jumps in trapezoidal channels, the sequent depths, the spatial extension of the bottom roller, and the length characteristics. They stated that

no surface roller exist, jump shifts spontaneously from the left to the right side at irregular time intervals and the toe of the jump oscillates ± 0.2 m about its average longitudinal position. They also stated that for higher incoming Froude numbers, jumps were more symmetrical and the spontaneous shifting of the main current (zone 2 at Figure 3-3) was more frequent. If incoming Froude number is low, the time interval for the spontaneous shifting of the main current increases.

Wanoschek and Hager (1988) concluded that the presence of a bottom roller through a jump in a trapezoidal channel makes flow phenomena significantly differ from the classical hydraulic jump. Based on 3-D observations, they divided flow into 7 parts and these parts of the hydraulic jump are given in Figure 3-3.

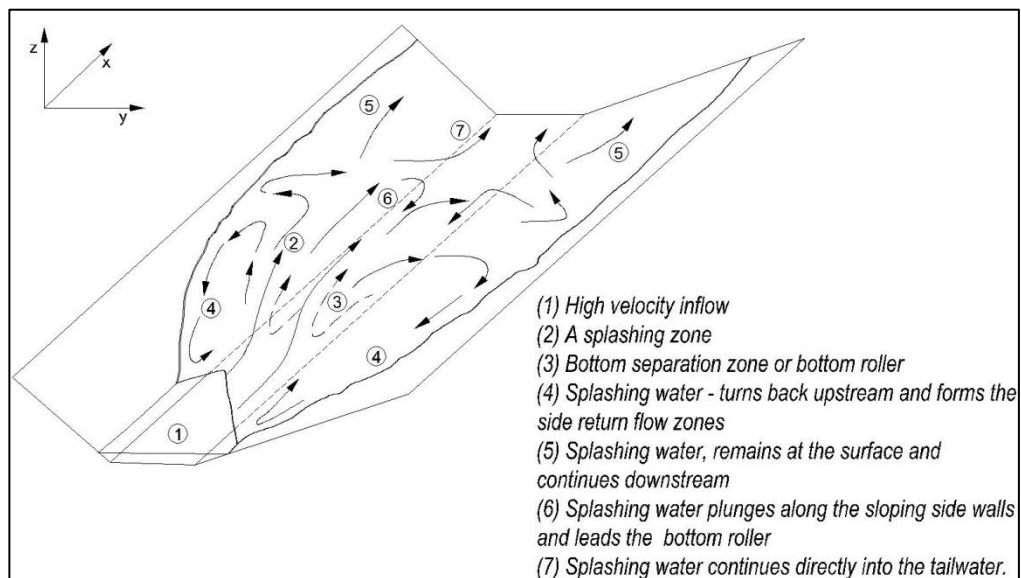


Figure 3-3: Parts of the Flow for Hydraulic Jump in Trapezoidal Channel

(Reproduced from Wanoschek and Hager, 1989)

Wanoschek and Hager (1989) expressed that the presence of the bottom roller entails several differences to the classical hydraulic jumps based on detailed 3D observations for an inflow Froude number $F_1 = 4.94$. These differences are,

- i. The velocity along the bottom are significantly reduces,
- ii. The main stream is lifted to the surfaces and diverges to both channel sides,
- iii. The maximum velocities occur along the side walls near the free surface.

3.2.2 Sequent Depths

Posey and Hsing (1938) in Wanoschek and Hager (1988) indicated that the observed sequent depth ratios with the prediction based on the conventional momentum approaches compared well.

Sandover and Holmes (1962) conducted experiments in trapezoidal channels with side slopes of 30° , 45° and 60° . They had difficulties while correlating their data with the sequent depths predicted by the momentum approach and they could not establish the length characteristics. The poor experimental facilities and/or low inflow Froude number F_1 , maybe the cause of those deficiencies, in which the maximum F_1 was 4.

Silvester (1964) compared the theoretical results with data obtained in rectangular, triangular, parabolic, circular, and trapezoidal channels. Exact solutions were provided for the conjugate depths and energy loss. French (1987) concluded that the curves plotted in Figure 3-4 provide an adequate method for estimating the value of y_2/y_1 for a given value of F_1 . Where, D is the diameter of the circular conduit.

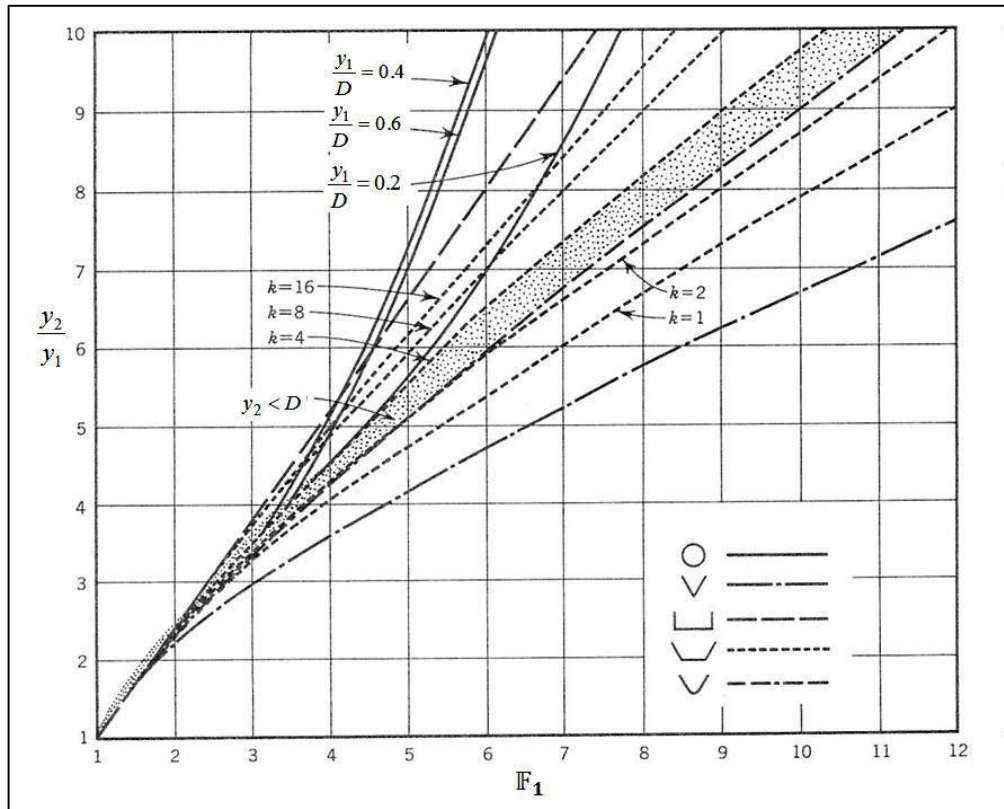


Figure 3-4: Analytical Curves for Sequent Depths (Silvester, 1964)

Mohed and Sharp(1971) conducted experiments in a 5 m long trapezoidal channel with a base width of 0.20 m and side slopes of $m = 0.925$. Inflowing depths ranged between $6.4 \text{ mm} < y_1 < 33 \text{ mm}$, where the corresponding Froude numbers were $3.67 < F_1 < 11.35$. They presented a design chart for the sequent depth ratio.

Mohed and Sharp (1971) compared the graphical representation of theoretical curves with conducted experiments (Figure 3-5). The individual points were also represented on the graphical solution. It was stated that, although graphical solution estimates higher depths than experimental values, design chart can be used for design purposes, due to it estimates safe maximum conjugate depth ratio approximately.

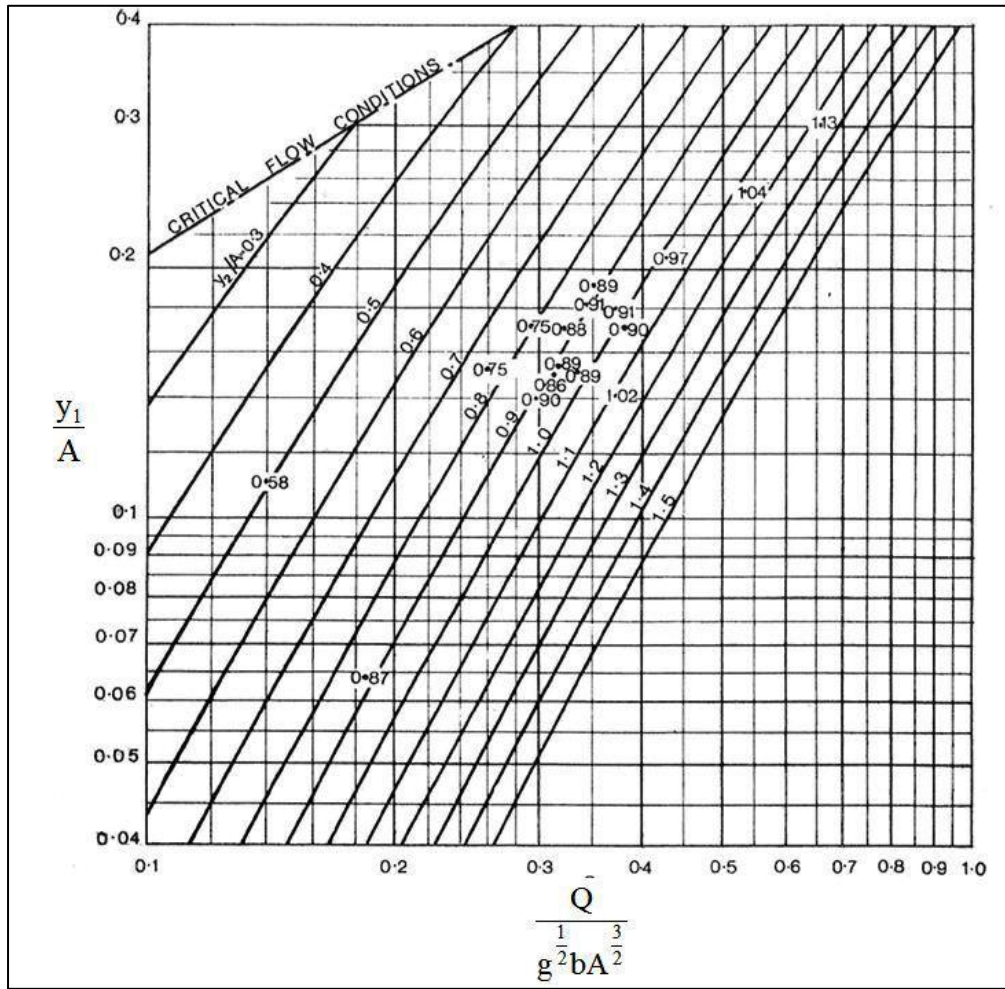


Figure 3-5: Design Chart for Upstream and Downstream Depth (Mohed and Sharp, 1971)

Ali and Ridgway (1977) defined a Froude number for supercritical flow in a trapezoidal channel and presented a general design chart (Figure 3-6) for the solution of the hydraulic jump assuming momentum correction factors equal to unity, $\beta_1 = \beta_2 = 1$, and boundary friction force is equal to zero. Froude number for supercritical flow was defined as,

$$F_U = F_1 \sqrt{\frac{k+2}{k+1}} \quad (3.11)$$

where k = Shape factor; b/my_1

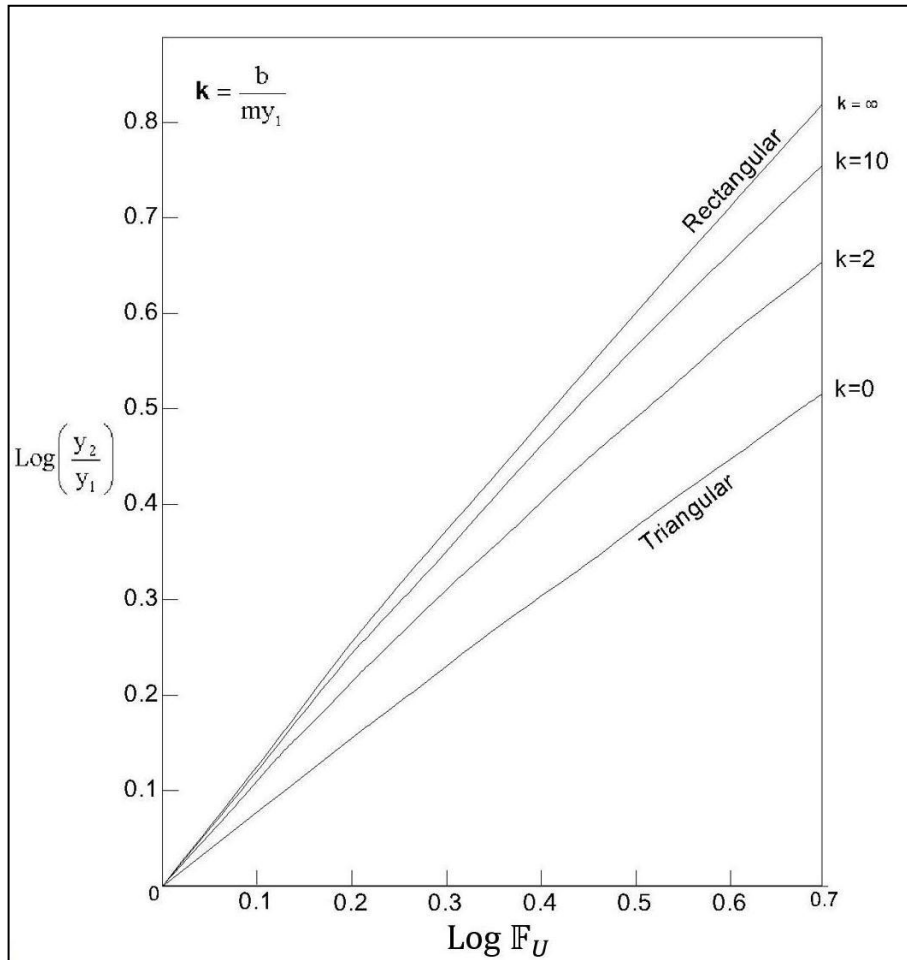


Figure 3-6: Theoretical Chart for the Hydraulic Jump in Trapezoidal Channels
(Reproduced From Ali and Ridgway, 1977)

Wanoschek & Hager (1989) stated that, the ratio of sequent flow depths may be computed by the conventional momentum approach as a function of F_1 for trapezoidal channels as in Eq. 3.12.

$$F_1^2 \left[1 - \frac{1+M}{Y(1+MY)} \right] = \frac{1+M}{Y(1+MY)^2} \left[Y^2 \left(1 + \frac{2MY}{3} \right) - \left(1 + \frac{2M}{3} \right) \right] \quad (3.12)$$

where Y = Sequent depth ratio, y_2/y_1
 M = $1/k = my_1/b$ (k = shape factor)

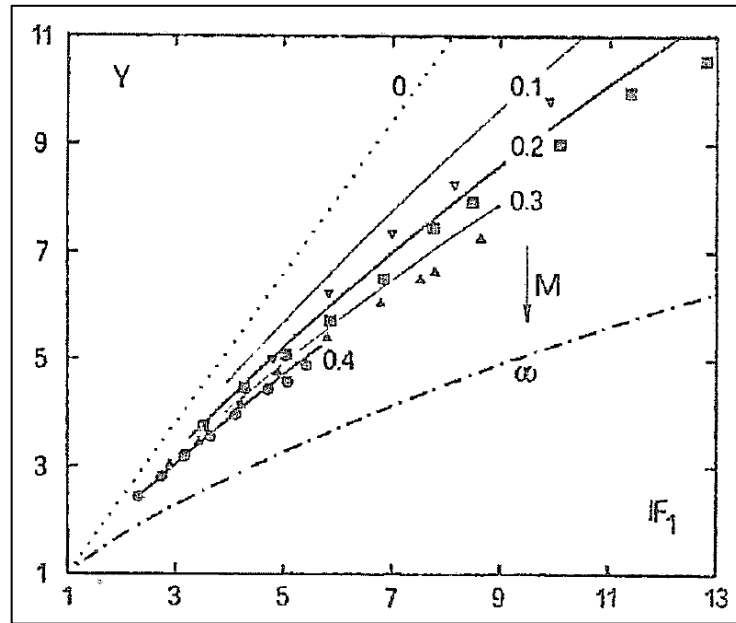


Figure 3-7: Sequent Depth Ratio for Various M. (Wanoschek and Hager, 1989)

The values of $M=0$ and $M=\infty$ correspond to the rectangular and triangular channels, respectively. Therefore, the value of M is $0 < M < \infty$ for trapezoidal channels.

3.2.3 Jump Length

An important characteristic of the jump in trapezoidal channels is the formation of wings at the side of the jump. These result from differentials in the water surface level across the jump. The reverse flow causes a build up at the sides whereas the centreline area is depressed throughout the length of the jump.

Afzal and Bushra (2002) and Wanoschek and Hager (1988) stated that Posey and Hsing (1938) expressed the average length of hydraulic jump as,

$$\frac{L_J}{y_2} = 5 \left[1 + 4 \left(\frac{T_2 - T_1}{T_1} \right)^{\frac{1}{2}} \right] \quad (3.13)$$

where, $T=b+2my$ is the surface width of flow, b is the bottom width, m is the side wall slopes of and y is the depth of flow. The scatter of data was given as $\pm 5\%$.

Sandover and Holmes (1962) stated that the length characteristics of hydraulic jumps on trapezoidal sections were impossible to establish.

Silvester (1964) conducted experiments, the sides of the channel were made of perspex, and the jump was in each case photographed with the aid of a high speed flash. Jump length was measured by projecting the image on a screen. Mean lines were drawn through undulating surfaces.

Silvester (1964) has hypothesized that a functional relationship exists between the ratio L_J / y_1 for prismatic channels of any shape

$$\frac{L_J}{y_1} = \sigma(F_1 - 1)^\Gamma \quad (3.14)$$

where σ = The shape factor, obtained experimentally, presented by Silvester (1964)
 Γ = The shape factor, obtained graphically, presented by Silvester (1964)

The length of the jump for the various shapes of channel is obtained in terms of the upstream depth and Froude number in study of Silvester (1964). It was stated that the constants in Eq. 3.15 should be determined experimentally because it is dependent on the general dimensions and proportions of any given channel shapes.

$$\frac{L_J}{y_2 - y_1} = 7.1[1 + 10M] \quad (3.15)$$

where, $M=my_1/b$.

It was stated that, Eq.3.15, fairly well expressed with the experimental results of Figure 3-8.

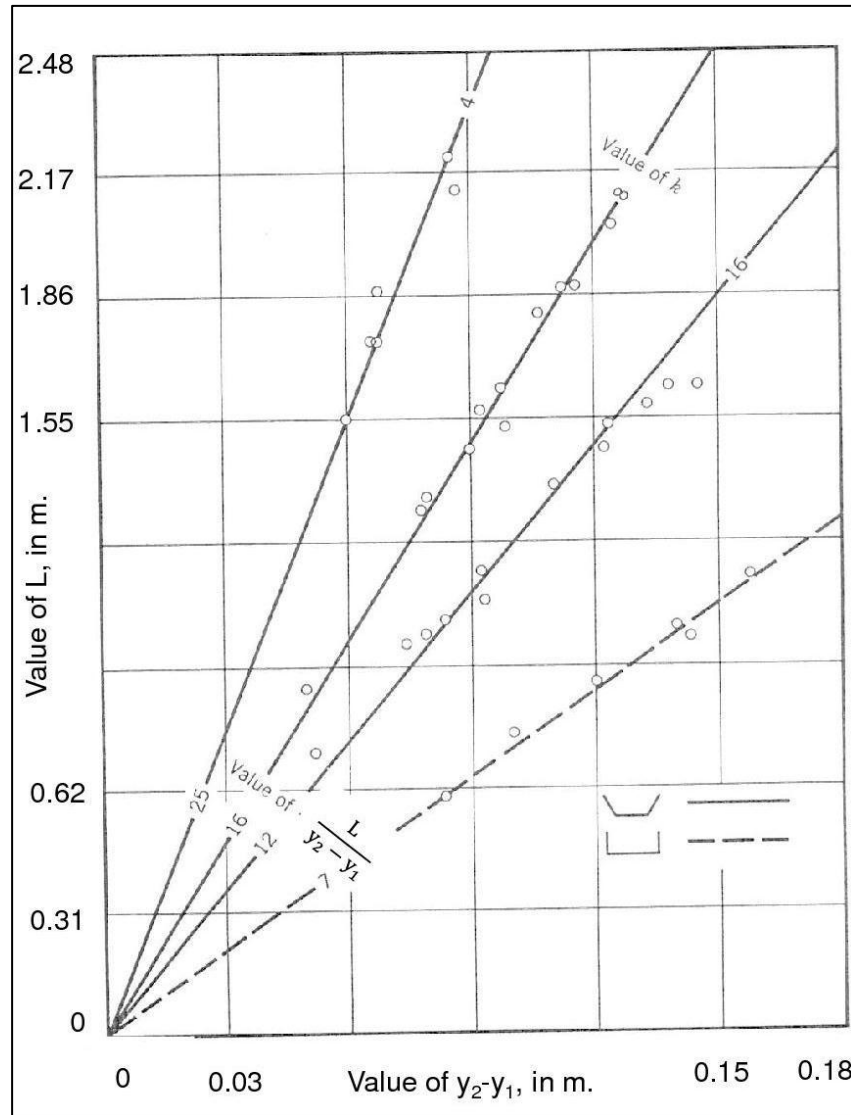


Figure 3-8: Results of Tests on Rectangular and Trapezoidal Channels (Silvester, 1964)

Figure 3-8 shows experimental results of Silvester (1964) on hydraulic jump length for different section factor, k . Silvester (1964) stated that for the jump length measurements, centreline distance is greater than the length recorded on the walls of the channel. Also the extra turbulence along the centerline,

especially at the downstream end, can make the identification of this end of the jump more difficult than if it were made near the side walls. He was stated that a consistent relationship for jump length should be obtained, which can then be used with some safety factor in design.

Mohed (1970) performed experiments in a wooden trapezoidal channels side slope of 1.0 vertical to 0.93 horizontal. A design chart was prepared for conjugate depths and compared with the results obtained from the experimental measurements.

Mohed and Sharp (1971) described the phenomenon as being unstable and noted that it was possible to direct the jump to either channel side by inserting and then withdrawing an obstacle. They have taken the end of the jump to be the cross-section where eddies disappeared and the transverse surface profile became nearly horizontal. They did not present any results regarding the length characteristics.

Ohtsu (1976) defined jump length such a way that, jump begins at the upstream end of the side wings and ends at the point where surface boil vanishes. In the light of this definition, the experimental data was able to correlated as

$$\log_{10} \left(\frac{L_o}{\Delta H} \right) = -1.71\psi + 0.315m + 1.58 \quad (3.16)$$

where, L_o is Ohtsu's jump length, $\psi = \Delta H / H_1$, ΔH is the energy loss in the jump, H_1 is total upstream head, m is the slope of side walls

Ali and Ridgway (1977) used several different methods to define the length of the jump and lengths of the jump were plotted non dimensionally as in (Figure 3-9).

- Direct observation of the water surface: the point, water surface rises suddenly accepted as starting point of the jump and the point, where the water surface became horizontal again accepted as jump end.
- Measuring water surface profile through the centre line of the jump.
- Measuring static pressure distribution: the point, the pressure first began to rise sharply accepted as starting point of the jump and the point, where the static pressure and water surface profile coincided accepted as jump end.

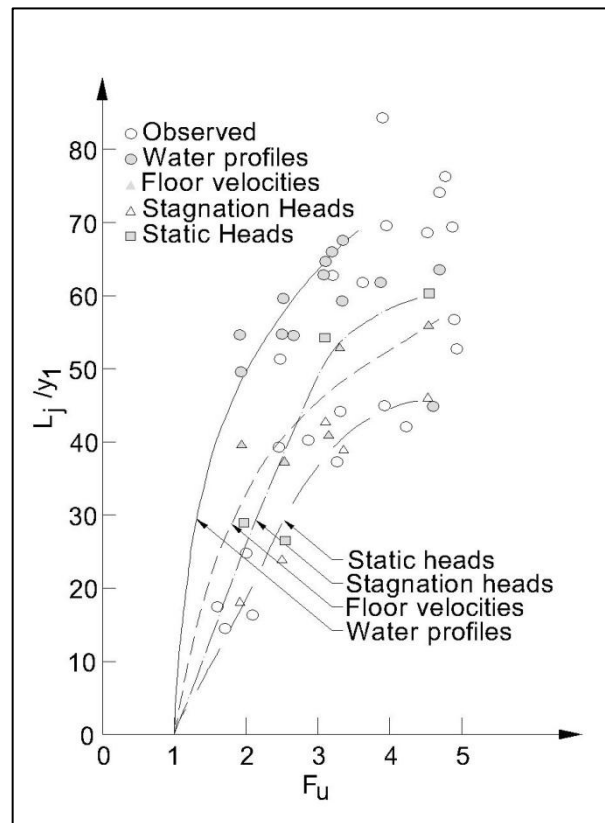


Figure 3-9: Variation of L_j/y_1 in Trapezoidal Channels
(Reproduced From Ali and Ridgway, 1977)

- Stagnation head method: the total pressure head close to the floor of the channel was measured along the centre line of the jump. The point,

where the total head began to drop steeply accepted as starting point of the jump and the point, where the variation in total head with distance became very small accepted as jump end.

- Floor velocity method: the floor velocities through the centre line of the jump were measured. The beginning and end of the jump were determined via the stagnation head method.

Wanoschek and Hager (1988) defined the end of the jump temporally averaged position where the surface boil vanishes. The end of the jump visualized both by eye and by photographs. According to their study, the beginning of the jump was taken as the average locations of both wings.

Afzal & Bushra (2002) stated that the surface profile is very flat towards the end of the jump, large personal errors are introduced in the determination of jump length L_j . They also stated that the beginning of the hydraulic jump is not precisely defined.

3.2.4 Energy Dissipation

Silvester (1964) presented a theoretical curve for energy loss in various shapes of channel. It is seen (Figure 3-10) that all shapes of channels give a greater percentage energy loss than the rectangular channel for any given Froude number. Where, D is the diameter of circular conduit.

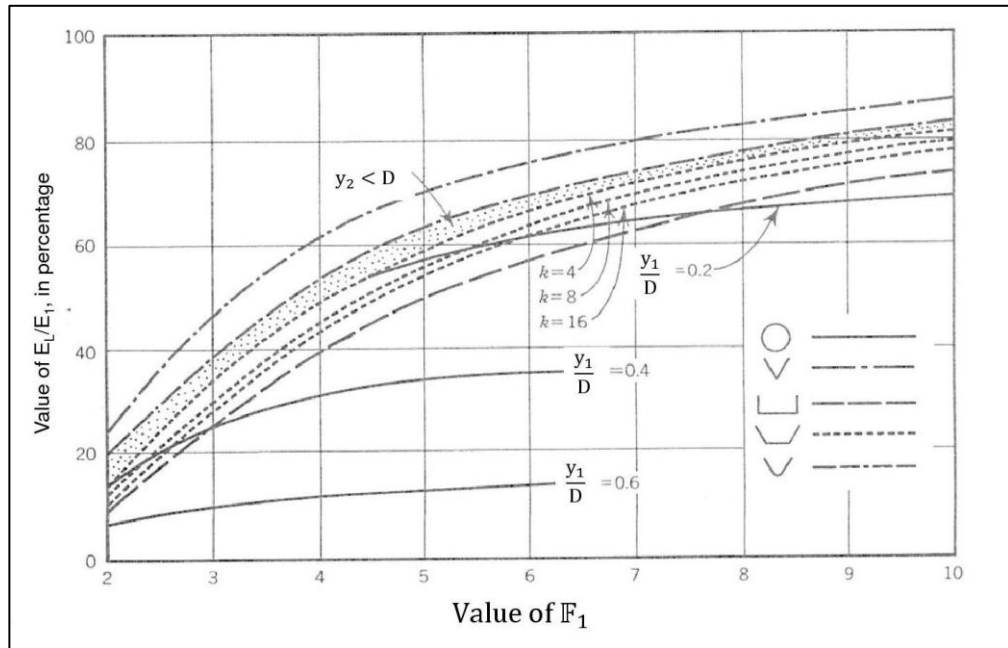


Figure 3-10: Theoretical Curves for Energy Loss (Silvester, 1964)

Ohtsu (1976) conducted experiments on several different trapezoidal hydraulic jump flumes and presented the following equation for the relative energy loss. It was also concluded that the cross sectional form of trapezoidal channels has only a little effect on the relative energy loss in a free hydraulic jump.

$$\frac{E_L}{E_1} = \frac{2(1 - Y) + \frac{(1 + \frac{1}{k})}{(1 + 2\frac{1}{k})} \left[1 - \frac{(1 + \frac{1}{k})^2}{(1 + \frac{1}{k} Y)^2 Y^2} \right] F_1^2}{2 + \frac{(1 + \frac{1}{k})}{(1 + 2\frac{1}{k})} F_1^2} \quad (3.17)$$

where $Y = y_2/y_1$, Sequent depth ratio.
 $k =$ Shape factor, b/my_1

Rajaratnam (1995) affirmed for jumps in prismatic and non-rectangular channels, the supercritical Froude number should be expressed in terms of the hydraulic depth, $D_H = A/T$. Where A is the cross-sectional area and $T = b + 2my$

is the surface width of flow. He concluded that the relative energy loss is highest for triangular section, than for circular sections and the lowest for the rectangular section. Depending on channel geometry, expressions for the relative energy loss E_L/E_1 in terms of incoming Froude number was given (Figure 3-11).

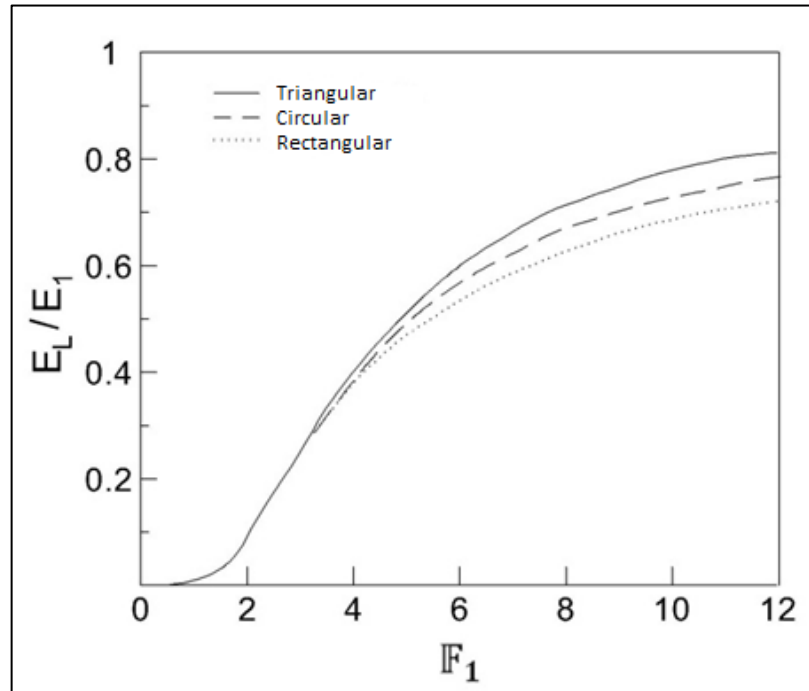


Figure 3-11: Energy Loss of Hydraulic Jump in Different Channels
(Reproduced From Rajaratnam, 1995)

CHAPTER 4

EXPERIMENTAL SETUP

Experimental setup was constructed in Hydromechanics Laboratory, METU. A similar subject, The Effect of Roughness on Hydraulic Jump Characteristics was studied by Ayanlar (2004) and Evcimen (2005). In the light of these studies, the experimental setup was designed, constructed and tested.

4.1 Dimensioning of Physical Model

There are several factors, which affect the selection of the dimensions of an experimental model. These factors can be summarised as follows;

- i. Past studies in the same or close fields
- ii. Physical conditions of laboratory
- iii. Available measurement equipment
- iv. Economical sources
- v. Amount of skilled labour

The studies, conducted in the past are given in Table 5-1. The average dimensions of past studies respect to width, length and depth are 38 cm, 800 cm and 50 cm. For the experimental setup, dimensions were selected as width of channel bed was 32 cm and side angles were 60° with vertical. The reason of the selection of side angles 60° was due to its optimum hydraulic

performance from discharge capacity point of view throughout trapezoidal channels. Experimental model of the present study is presented in Figure 4-1.

Table 4-1: Experimental Model Dimensions of Previous Studies

Reference	Area of interest	Dimensions			
		Width (m)	Length (m)	Depth (m)	Side Slope (h/v)
Silvester, 1964	Jump Characteristics (T)	0.21	-	-	-
Rajaratnam, 1965	Pressure field, velocity field, boundary shear stress (R)	0.31	4.88	0.90	-
Leutheusser et al, 1972	Air Entrainment (R)	0.39	15.25	-	-
Mohed, 1970	Jump Characteristics (T)	0.21	5.00	-	1.08
Ali & Ridgway, 1977	Jump Characteristics (T+R)	0.15	6.10	-	1
Wanoschek & Hager (1989)	Jump Characteristics (T)	0.20	8.00	0.70	1
Küçükali and Çokgör (2006)	Air Entrainment (R)	0.50	5.80	0.45	-
Carollo et al.(2007)	Jump Characteristics (R)	0.60	14.40	0.60	-
Küçükali and Chanson (2008)	Air Entrainment (R)	0.50	3.20	0.45	-
Salehian et al. (2011)	Jump Characteristics (R)	0.30	7.50	0.40	-
Present Study	Jump Characteristics (T)	0.32	6.00	0.30	0.537

R: Rectangular in cross section

T: Trapezoidal in cross section



Figure 4-1: Experimental Model of the Present Study

4.2 Experimental Equipment

The discharge was supplied by a constant head tank, a pressure conduit of diameter 0.15 m and a regulating valve. The transition from the pressure conduit to the channel was accomplished by a pressure tank (Figure 4-2). The discharge capacity of the tank is 50 l/s.

The following requirements dominated the design of the experimental model.

- i. Present study is mainly concentrated on measurement and observation of hydraulic jump characteristics as discussed in Section 2.2. In order to observe such characteristics i.e. length of the jump, flow structure, aeration, the flume should be transparent.
- ii. Trapezoidal channel should have a trapezoidal gate to satisfy regular inlet conditions and delete any transition before hydraulic jump in open channel flow. The designed inlet conditions can be practically implemented in nature. Past studies i.e. Rajaratnam (1965, 2002) solved the measurement difficulty by designing an inlet. An inlet section was designed by considering these requirements.

- iii. It was known that, it is hard to measure incoming supercritical flow depth just before hydraulic jump because of unstable feature of hydraulic jump in trapezoidal channels and water surface oscillations. Validity of measurements is the most important point of experimental setup design. If any dimension, which was claimed to be measured and was not able to be measured, this means waste of time and money. A reliable inlet design was required to overcome this problem.
- iv. Different roughness patterns should be practically applied both on bed and side walls of the trapezoidal channel. In order to avoid cavitation, roughness elements should be installed to the channel bed with such an arrangement that the crest of roughness elements will be at the same level of upstream bed.
- v. In order to measure discharge, a measurement device and structure was required. It was decided that a discharge measurement flume should be constructed.
- vi. A downstream gate was required to regulate the location of hydraulic jump in upper flume.

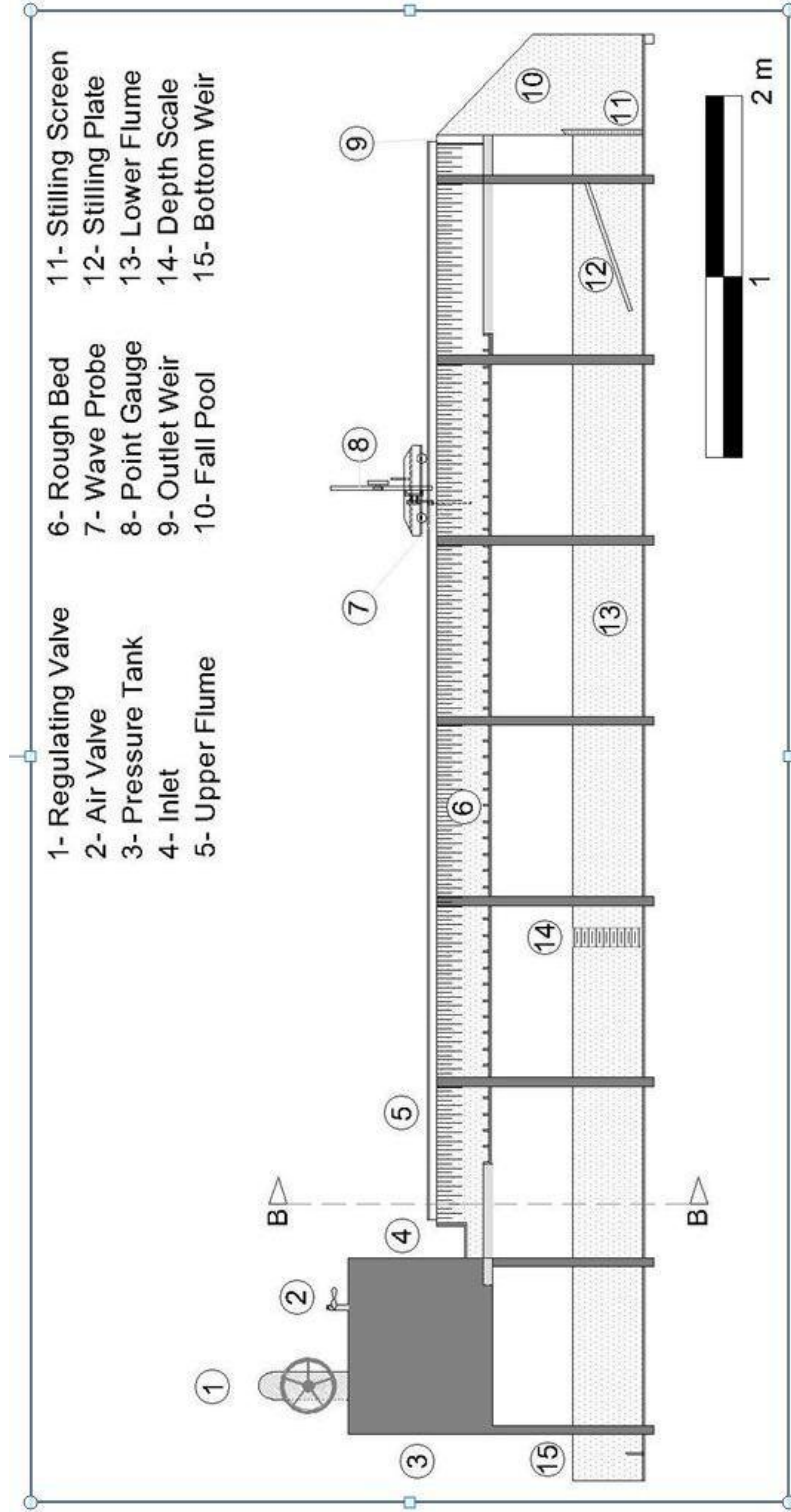


Figure 4-2: Experimental Model and its Parts

4.2.1 Hydraulic Jump Flume

The present tests were conducted in a prismatic, symmetrical trapezoidal channel of 0.324 m base width and side slope of 60° ($m = 0.577$). The depth of the channel amounted to 0.26 m, such that a top width of 0.60 m resulted. The length of the horizontal channel was 6 m (Figure 4-3). Hydraulic jump flume has a horizontal bed hence the effect of weight on flow direction was eliminated.

Both bed and sidewalls were made up five layers of plexiglass sheets and steel sections were used for the construction of pressure tank and framework of the flume. Roughness patterns can be installed on the bed and the side walls of the flume in such a way that the upmost three layers of fiberglass sheets can be detached one by one and, roughness elements can be installed on remaining plexiglass sheet. Such a design was done to provide such condition that, the crests of prismatic roughness elements are at the same level as the upstream bed.

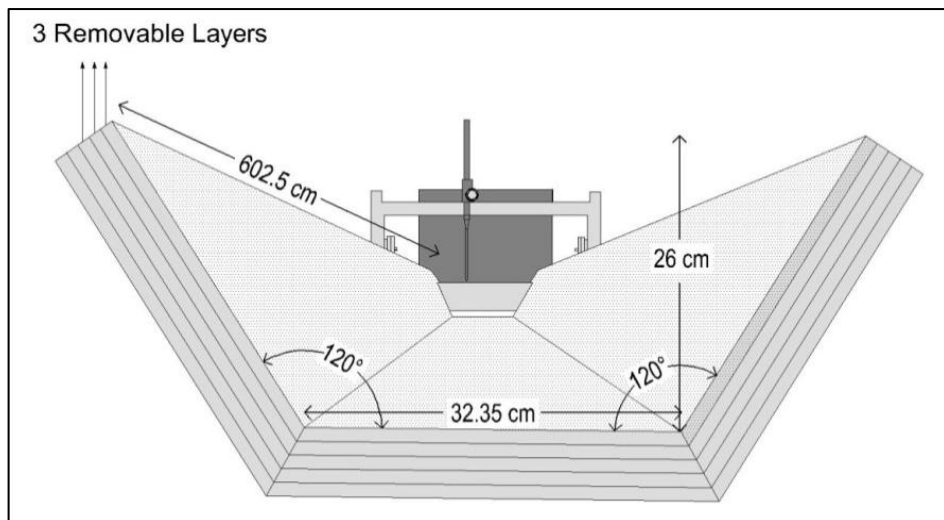


Figure 4-3: Physical Dimensions of Experimental Model

The reasons of selection the dimensions of experimental model can be summarized as;

- i. The dimensions should be similar with past studies,
- ii. The selected cross section of trapezoidal channel should be optimum from the discharge point of view; hence the discharge measurement interval would be extensive.
- iii. The minimum amount of plexiglass sheets should be consumed to produce channel sections and roughness elements.

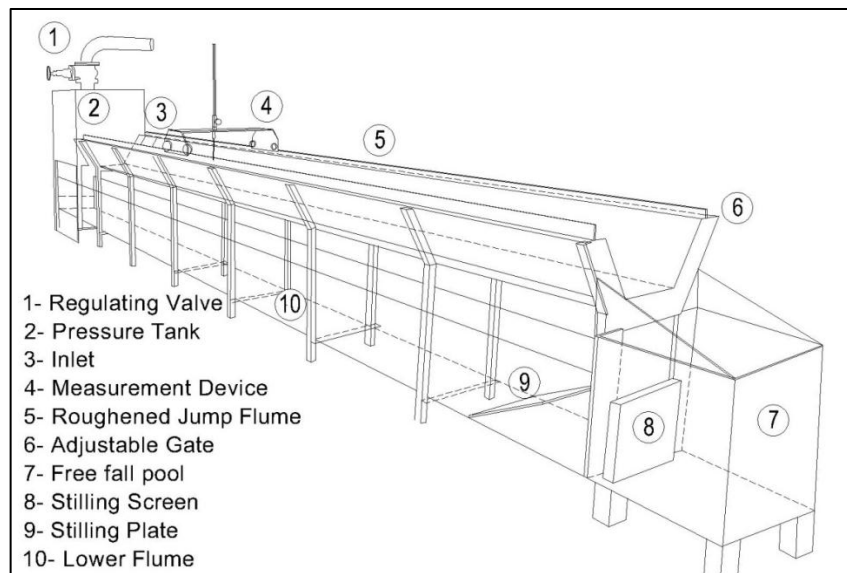


Figure 4-4: Experimental Model – Isometric View

The jump location was controlled by an upstream regulating valve and by a downstream overshoot gate (Figure 4-4).

4.2.2 Inlet Gate Design

As mentioned in Section 2.2.2, it is hard to measure incoming supercritical flow depth just before hydraulic jump with high accuracy. This problem was solved with designing a special inlet section by Rajaratnam (1965) by a nozzle (Figure 4-5-a).and, Rajaratnam and Subramanya (2002) by a curved lip (Figure

4-5-b) and Figure 4-5-c) shows the inlet sections at present study. The both studies of Rajaratnam investigated hydraulic jump characteristics in rectangular channels and, the location of the jump, was just downstream of inlet, controlled by a sliding gate which was installed at the end of the experimental flume. Gate opening accepted as the supercritical incoming flow depth.

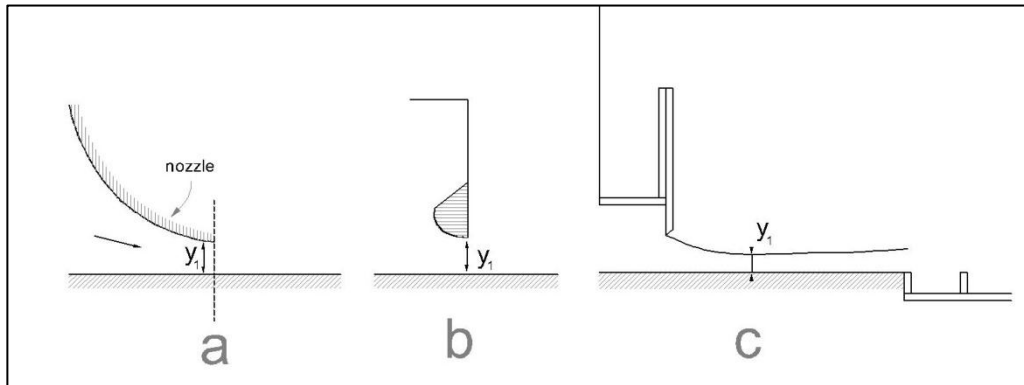


Figure 4-5: Three Different Inlet Types for Experimental Studies

Ali and Ridgway (1977), stated that hydraulic jumps swing to one side of the channel. In the discussion, Sharp (1977) criticised Ali and Ridgway findings and commented that oblique jump did not always slew to the same side. Ali and Ridgway (1977), stated that overcome the tendency for the hydraulic jump to swing to one side of the channel could be solved when a 0.3 m long sluice gate was used in the trapezoidal channel.

Wanoschek and Hager (1989) used a damping pointer gauge through their experimental study to eliminate the effects of violent splashing and eruptions in the jump region. They stated that due to the longitudinal oscillations of the entire hydraulic jump, the actual uncertainties of the measured water depths were ± 5 mm.

Hager and Bremen (1989) indicated that, for flows in which the incoming flow depth y_1 is small, there exists a significant scale effect on sequent depth ratio.

In the light of such information, it was decided that a transition section should be constructed between the just downstream of the pressure tank.

There were two geometric alternatives for the construction of inlet gate; rectangular or trapezoidal gates in shape. Rectangular gate would require a transition from rectangular to trapezoidal section in channel, on the other hand the trapezoidal gate require a transition from the pressure tank to the gate. In order to eliminate problems due to scale effect on open channel flow, the transition from the pressure conduit to the channel was accomplished by a pressure tank, the transition section and a trapezoidal gate (Figure 4-5-c), (Figure 4-6). A smooth transition section was also added between the trapezoidal gate and rough channel to investigate the outlet conditions of inlet gate.

Design of an experimental model should not incorporate any questions pertaining to applications on the nature. The flow velocity is high especially at just downstream of sluice gates or spillways, prismatic roughness elements can be subjected to cavitation and abrasion. This situation causes damages and maintenance costs at operating stilling basins and millions of dollars are spend each year.

To avoid cavitation, roughness elements should be installed to the stream bed with such an arrangement that the crest of roughness elements will be at the same level of upstream bed. Hence, the roughness elements would not be protruding into the flow and subjected lower intensity of cavitation when compared with protruding roughness. Experimental setup constructed according to this approach and the crest of roughness elements will be at the same level of upstream bed; the bed of tank outlet is 3 cm higher than channel bed.

Four trapezoidal gates, G1, G2, G3, and G4 were produced from plexiglass for gate openings, 1 cm, 2cm, 3 cm and 4 cm, respectively. These gates were

screwed onto the end of transition region to ensure the gate opening and, clamped onto end of transition region to provide self-sealing (Figure 4-6). On the other hand, this design does not allow attaching any streamlined part behind the gate to satisfy the condition, gate opening is equal to incoming flow depth. Upstream side of the gate is also pressurized; hence a vena contracta would form.

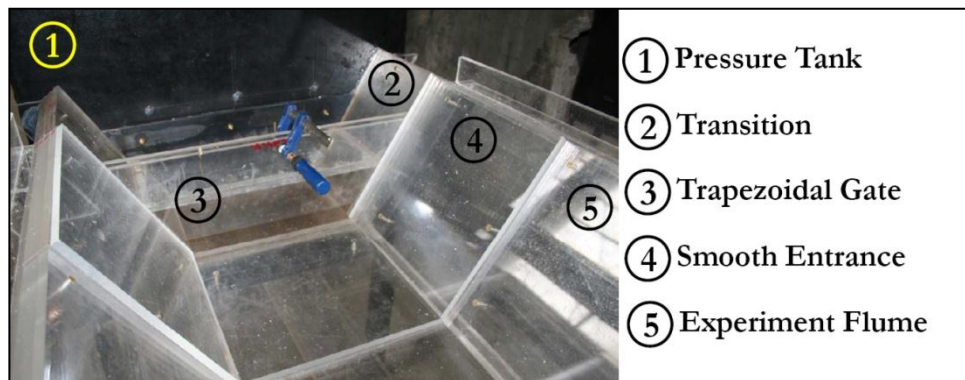


Figure 4-6: Inlet section

4.2.2.1 Calibration of Inlet Section

After experimental setup was constructed, preliminary experiments was performed to determine the flow conditions on smooth entrance section (Figure 4-6-4).

There was some leakage problems at the inlet section, It was solved by using some plexiglass (Figure 4-7) pieces. The leakage was able to be stopped by the help of dough or rag in permanent way (Figure 4-8).



Figure 4-7: Plexiglas Pieces to Improve Inlet Conditions



Figure 4-8: Dough at Sides to Improve Inlet Conditions

The flow conditions were investigated along inlet after improvements was completed to see if any further improvement is necessary and to understand if any flow properties which might be helpful during experimental studies.

It was observed that depth of incoming water decreases up to vena contracta, and then increases. Flow conditions were smooth enough to measure flow depth with a point gauge. Calibration study was done up to 28.5 cm downstream of the inlet. Figure 4-9 shows a picture for the inlet section. The investigation of inlet conditions of experimental model showed that, the flow surface profiles are similar for four gates. It was observed that when the gate opening increases, vena contracta moves further downstream.



Figure 4-9: Calibration Study at Inlet Section

Study was conducted with 3 cm measurement intervals for G1, G2 and G4 (Table 4-2) and, measurement intervals of 1.5 cm just for gate G3 (Table 4-4). The normalized flow depths, obtained by dividing flow depth with related gate opening, are also presented in Table 4-3 and Table 4-5. The calibration showed that, vena contracta forms at downstream of inlet gate and its contraction coefficient is 0.673 for the vena contracta.

$$C_c = 0,673$$

(4.1)

Table 4-2: Measured Flow Depths along Inlet Section for G1, G2 and G4

X (cm)	Measured Flow Depths, cm									
	Sets with G1			Sets with G2				Sets with G4		
	1	2	3	1	2	3	4	1	2	3
0	1	1	1	2	2	2	2	4	4	4
1.95	0.69	0.69	0.69	1.42	1.4	1.38	1.37	3.25	3.15	3.09
4.95	0.76	0.72	0.72	1.39	1.37	1.34	1.34	2.72	2.69	2.78
7.95	0.87	0.81	0.78	1.52	1.45	1.42	1.37	2.74	2.76	2.85
10.95	0.95	0.85	0.78	1.57	1.49	1.46	1.4	2.76	2.97	3.01
13.95	1	0.88	0.8	1.62	1.57	1.55	1.43	2.84	3.2	3.1
16.95	1.16	0.94	0.82	1.69	1.65	1.59	1.46	3.06	3.36	3.23
19.95	1.05	0.96	0.81	1.75	1.7	1.66	1.5	3.1	3.32	3.09
22.95	1.1	0.96	0.83	1.77	1.73	1.66	1.5	3.25	3.38	3.12
25.95	1.07	0.95	0.83	1.8	1.77	1.66	1.53	3.4	3.45	3.07
28.95	1.15	0.99	0.85	1.87	1.8	1.8	1.56	3.47	3.51	3.11

Table 4-3: Normalized Flow Depths along Inlet Section for G1, G2 and G4

X (cm)	Sets with G1			Sets with G2				Sets with G4		
	1	2	3	1	2	3	4	1	2	3
0	1	1	1	1	1	1	1	1	1	1
1.95	0.69	0.69	0.69	0.71	0.70	0.69	0.69	0.81	0.79	0.77
4.95	0.76	0.72	0.72	0.70	0.69	0.67	0.67	0.68	0.67	0.69
7.95	0.87	0.81	0.78	0.76	0.73	0.71	0.69	0.69	0.69	0.71
10.95	0.95	0.85	0.78	0.79	0.75	0.73	0.70	0.69	0.74	0.75
13.95	1.00	0.88	0.80	0.81	0.79	0.78	0.72	0.71	0.80	0.78
16.95	1.16	0.94	0.82	0.85	0.82	0.80	0.73	0.77	0.84	0.81
19.95	1.05	0.96	0.81	0.88	0.85	0.83	0.75	0.78	0.83	0.77
22.95	1.10	0.96	0.83	0.89	0.87	0.83	0.75	0.81	0.85	0.78
25.95	1.07	0.95	0.83	0.90	0.89	0.83	0.76	0.85	0.86	0.77
28.95	1.15	0.99	0.85	0.93	0.90	0.90	0.78	0.87	0.88	0.78

Table 4-4: Measured Flow Depths along Inlet Section For G3

X (cm)	Measured Flow Depths, cm					
	Sets with G3					
	1	2	3	4	5	6
0	23.29	23.29	23.29	23.29	23.29	23.29
1.95	22.54	22.53	22.53	22.52	22.51	22.51
3.45	22.33	22.31	22.32	22.31	22.3	22.29
4.95	22.36	22.37	22.35	22.37	22.36	22.37
6.45	22.42	22.44	22.41	22.41	22.41	22.42
7.95	22.53	22.5	22.5	22.51	22.49	22.49
9.45	22.63	22.61	22.61	22.59	22.59	22.58
10.95	22.73	22.7	22.67	22.66	22.65	22.64
12.45	22.77	22.74	22.72	22.71	22.7	22.68

Table 4-5: Normalized Flow Depths along Inlet Section for G3

X (cm)	Sets with G3					
	1	2	3	4	5	6
0	1.00	1.00	1.00	1.00	1.00	1.00
1.95	0.75	0.75	0.75	0.74	0.74	0.74
3.45	0.68	0.67	0.68	0.67	0.67	0.67
4.95	0.69	0.69	0.68	0.69	0.69	0.69
6.45	0.71	0.71	0.70	0.70	0.70	0.71
7.95	0.75	0.74	0.74	0.74	0.73	0.73
9.45	0.78	0.77	0.77	0.76	0.76	0.76
10.95	0.81	0.80	0.79	0.78	0.78	0.78
12.45	0.82	0.81	0.80	0.80	0.80	0.79

Figure 4-10 represents the normalized flow surface profiles at inlet section. Where, F_e represents the Froude number at the gate opening. Flow depths were normalized with dividing measured water surface profiles by gate opening.

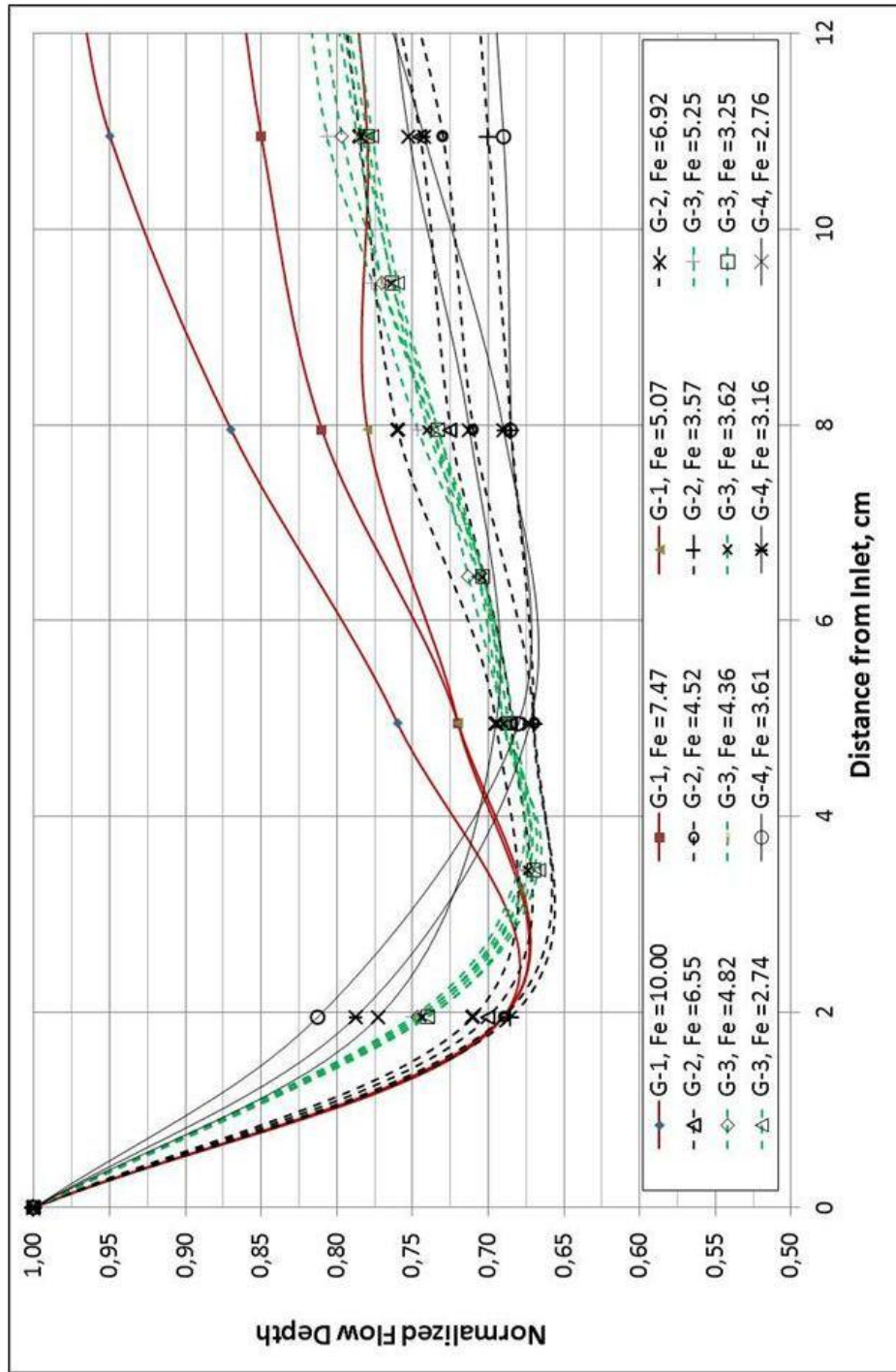


Figure 4-10: Normalized Flow Surface Profiles at Inlet

4.2.3 Overshoot Gate and Free Fall

For the experimental model, implementing a sliding gate at the end of the flume and positioning jump precisely just using this gate is an expensive and not practical solution due to operational difficulties, some extra equipment should be added to overcome water tightness problem. An overshoot gate was more practical and economical. However the ability of regulating the location of a hydraulic jump is limited depending thickness of the overshoot bars. A total of six bars were produced to regulate the downstream conditions of jumps to overcome the limited ability of overshoot gate, the location of jumps was adjusted via the regulating valve and overshoot gate.

An overshoot gate was implemented (Figure 4-11) at the end of upper flume with several plexiglass parts. The discharge on upper flume overtops the gate and falls on the stilling pool.

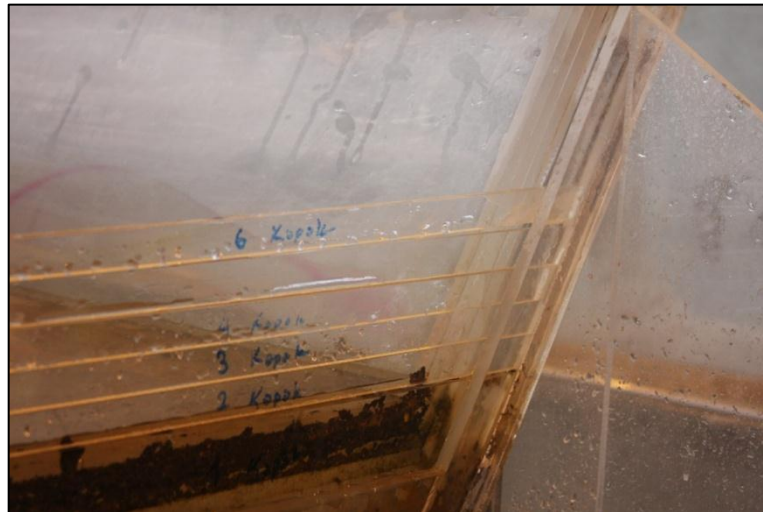


Figure 4-11: Overshoot gate at the end of upper flume

4.2.4 Downstream Basin

The main function of the downstream basin is to collect water from trapezoidal channel and divert it to measuring flume without any significant wave action.

The downstream basin composed of three parts, a stilling pool (Figure 4-12 - a), a stilling screen (Figure 4-12 - b), and a stilling plate (Figure 4-12 - c).

- a. Pool is made of plexiglass. Its height, width and length are 85 cm, 65 cm and 70 cm, respectively.
- b. The frame of stilling screen is made of plexiglass and screen is made of plastic mesh. Plastic mesh smoothened out the conditions of flow.
- c. The stilling plate is made of wood, it was attached the upper flume from its upstream side by two wires. Its width is slightly shorter than the lower flume width; hence its downstream part can be float in the lower flume. Its oblique position helps to damped out the wave action in a short distance.

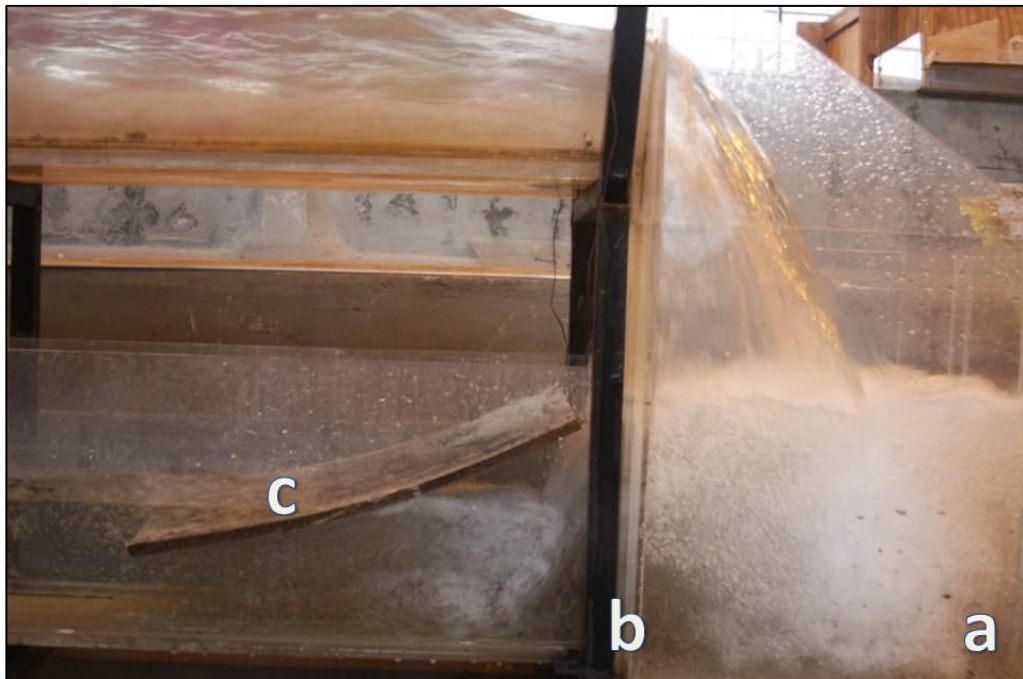


Figure 4-12: Downstream Basin

4.2.5 Roughness Setup

Khatsuria (2009) stated that the practical ways of construction would be casting small size cubes or blocks with the base concrete of the panel and, casting large rectangular strips spaced at close interval.

The roughness elements and arrangements were selected in that way, the application in nature should be practical. Casting small size cubes or blocks in stilling basins requires great amount of detailed labour and, formwork. On the other hand, casting rectangular strips is much more practical; right after casting of apron bed, green cut methodology can be applied and rectangular strips can be casted on dowel bars (Figure 4-13).

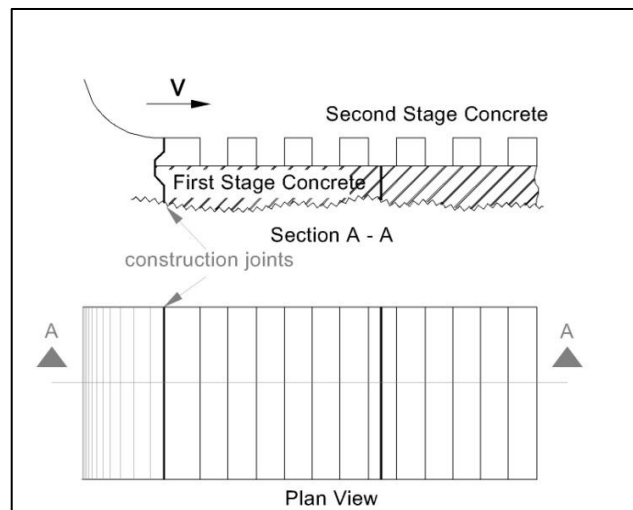


Figure 4-13: Application Detail of Strip Roughness at Aprons
(Reproduced from Khatsuria (2009))

The selected roughness pattern should be easily applied nature in a practical way. Rectangular in cross section strips obey the definition of Khatsuria (2009). The cross section and plan view

Figure 4-13) of Khatsuria is the best representation of the roughness pattern of present study.

4.2.5.1 Adjustable rough bed and walls

The adjustable rough channel designed in a way that different roughness patterns could be practically applied both on bed and side walls of the trapezoidal channel. As mentioned in Section 4.2.1, bed and side walls of upper flume composed of five layers of plexiglass sheets. The outer layers of channel bed and walls were directly connected to steel frame. Its function is to providing tightness and horizontality and, bearing the weight of other plexiglass layers and water.

The second plexiglass layer from outside was fixed to the outer layer by screws. Its surface level is three cm below than inlet surface at bed and side walls. Due to three cm elevation difference between its surface and inlet section bed surface, when roughness elements having three cm height attached on it, their upper surface have the same level with surface of inlet section. Each roughness element was attached to smooth surface of the layer by two screws. The distance between two successive screw taps was three cm in flow direction. A total of 124 roughness element can be installed on three surfaces of hydraulic jump flume.

The upper three plexiglass layer can be detached one by one and, roughness elements can be mounted on plexiglass sheets as in Figure 4-14.

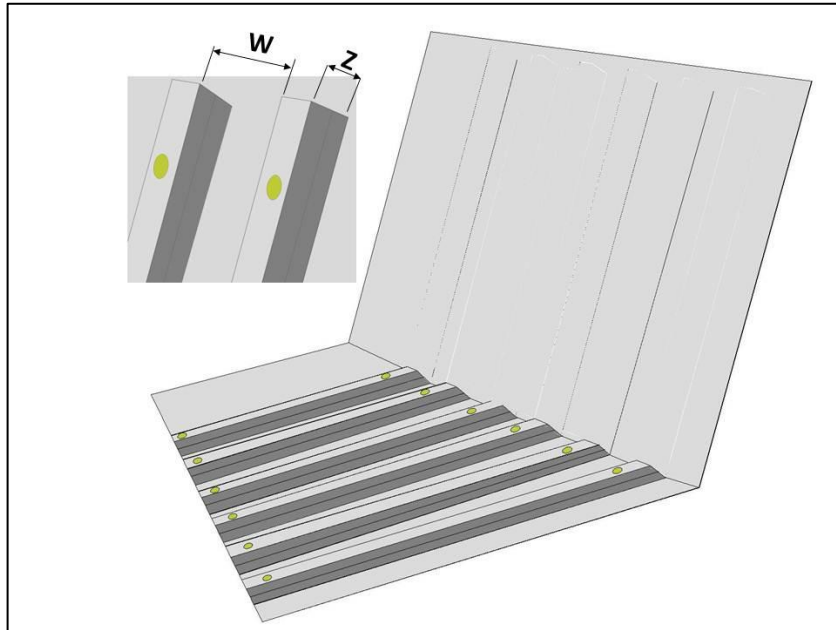


Figure 4-14: Installation of Roughness Elements on Channel Bed

Towards from outside to inside third and fourth layers could be installed on previous layers by screws. Due to elevation difference between their smooth surfaces of sheets and smooth surface of inlet section bed, roughness elements having appropriate height attached on them. Upper surfaces of roughness elements should have the same level with surface of inlet section bed.

The inner layer was connected the layer below by screws and it was installed only during when smooth surface was required either at side walls or at channel bed.

4.2.5.2 Roughness Elements

Three different sizes of fiberglass roughness elements were used in the experiments. Because of the geometry of the trapezoidal channel, roughness elements were trapezoidal in cross section. To obtain different roughness height strip roughness elements are produced such that three different roughness elements in length could be stowed to each other and create a roughness pattern with three cm in height (Figure 4-15).

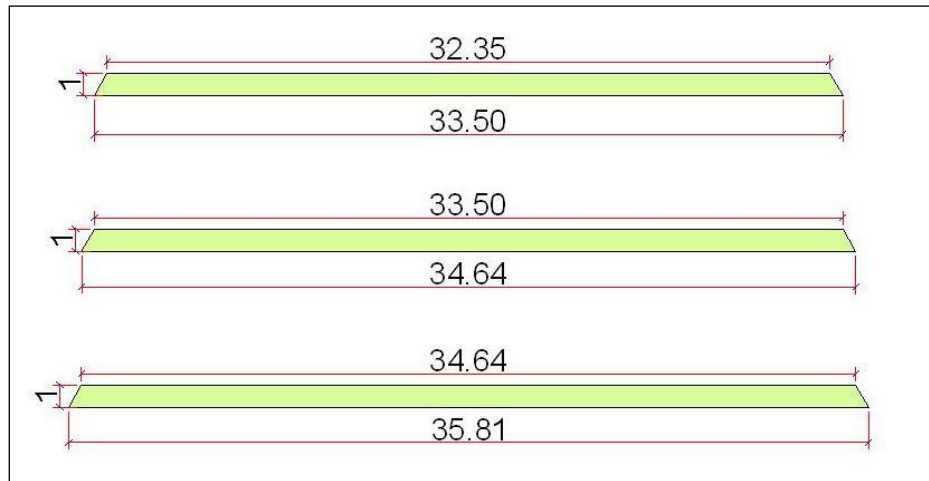


Figure 4-15: Widths of strip roughness elements (in cm)

Roughness elements could be screwed into fiberglass sheets in such a way that the wavelength, distance between the crests of two successive roughness elements, of roughened beds would be 3 cm, 6 cm and 9 cm.

4.2.5.3 Roughness Arrangements

Nine different roughness arrangements were investigated through experimental study both for channel bed and side walls. Geometrical properties of roughness setup are represented in Table 4-6.

The related parameters in table-3 illustrated with roughness patterns investigated through experiments. The roughness patterns having the same roughness height was named with the same letter in Figure 4- 16.

Table 4-6: Geometrical Properties of Roughness Setup

Roughness Pattern	Height z (cm)	Wavelength (cm)	Pitch w(cm)	Length L (cm)	Pitch Ratio (w/z)	% Intensity (I)
A1	1	3	2	1	2	33.33
A2	1	6	5	1	5	16.66
A3	1	9	8	1	8	11.11
B1	2	3	2	1	1	33.33
B2	2	6	5	1	2.5	16.66
B3	2	9	8	1	4	11.11
C1	3	3	2	1	0.66	33.33
C2	3	6	5	1	1.66	16.66
C3	3	9	8	1	2.66	11.11

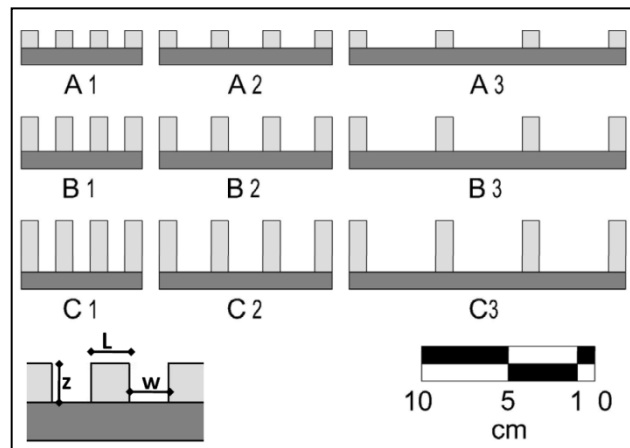


Figure 4-16: Bed Roughness Patterns in the Study

4.2.6 Portable Ultrasonic Flowmeter

Initial calibration of lower discharge measurement flume was conducted by the help of Tokimec UFP-10 portable ultrasonic flowmeter. The UFP-10 flowmeter can measure discharge by fixing the transducer outside the pipe Figure 4-17-a). The ultrasonic pulses created, and the propagation velocity is measured by the transducer. The propagation velocity of ultrasonic pulses in a liquid varies according to flow velocity. UFP-10 includes an onboard microprocessor with functions i.e. velocity measurement and flow calculation Figure 4-17-b). The device is applicable for pipe diameters from 13~5000 mm.

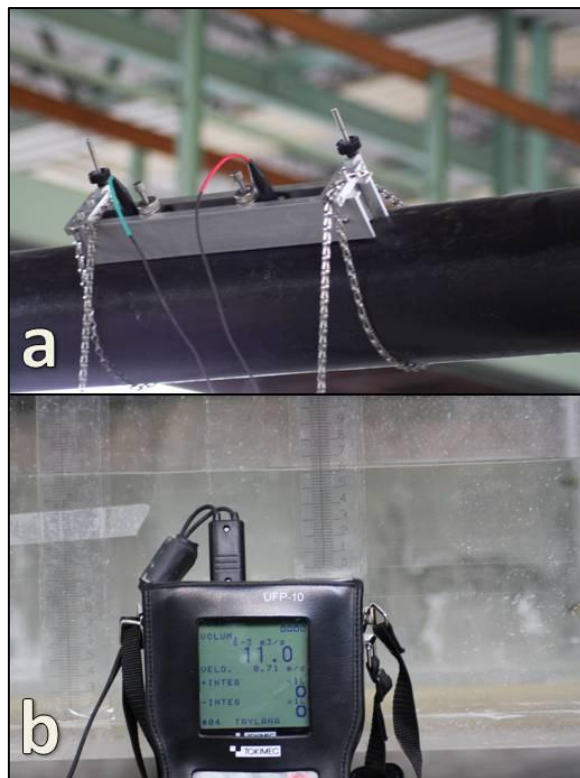


Figure 4-17: Portable Ultrasonic Flowmeter

4.2.7 Discharge Measurement Flume

To measure the discharge, a rectangular lower flume was designed with transparent side walls under the trapezoidal channel as shown in Figure 4-2.

Depth measurements were done by a transparent scale, which was stucked on outer side of the walls.

4.2.7.1 Calibration of Discharge Measurement Flume

The calibration of the lower flume has been conducted before starting hydraulic jump experiments. UFP-10 portable ultrasonic flow meter (Figure 4-17) was fixed on main pipeline and water level measurements have conducted on lower flume. A total of 157 measurements were conducted for 40 different discharge values.

For each discharge value, measurements done with reading scale attached on the side wall of flume. The accuracy of the readings was checked by analyzing high resolution photographs, taken during each measurement set. The average depth, H, for each discharge value was determined and a depth-discharge curve was obtained (Figure 4-18).The relation (Eq. (4.2)) was obtained for lower flume and discharge was calculated with this relation through all experimental runs.

$$Q = 0.807 H^{1.448} \tag{4.2}$$

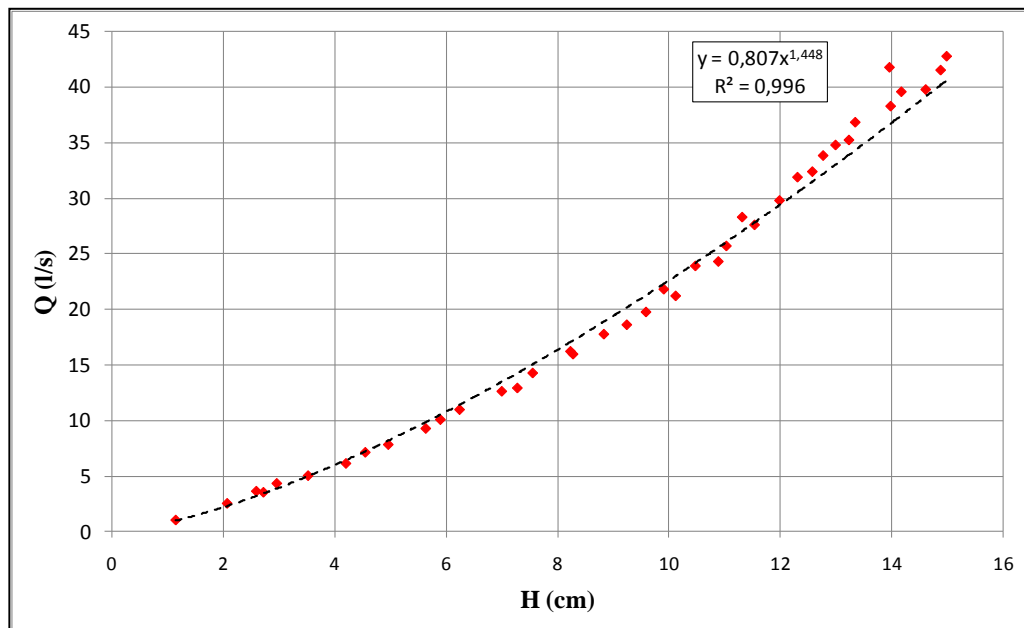


Figure 4-18: Discharge Calibration Curve

4.2.8 Wave Monitor

Subcritical flow depth was measured by the help of H.R. Wallingford Wave Probe Monitor (Item Code CLE3 C30) (Figure 4-19-b). Wave Probe, (Figure 4-19-a), was fixed to the measurement car, which can move along the channel.

The flow depth was measured along the channel axis. Hereby, the tailwater depth was defined as the asymptotic water depth and measured 0.5 m upstream of the point, where roughness pattern ends.

By the help of a Ms-Dos program, called as 470, voltage signals were converted to numerical values and a note pad file and graphical demonstration of these numerical values were prepared by computer. The Ms-Dos program, 470, has a parameter (Figure 4-20) and an output screen (Figure 4-20-b, c).

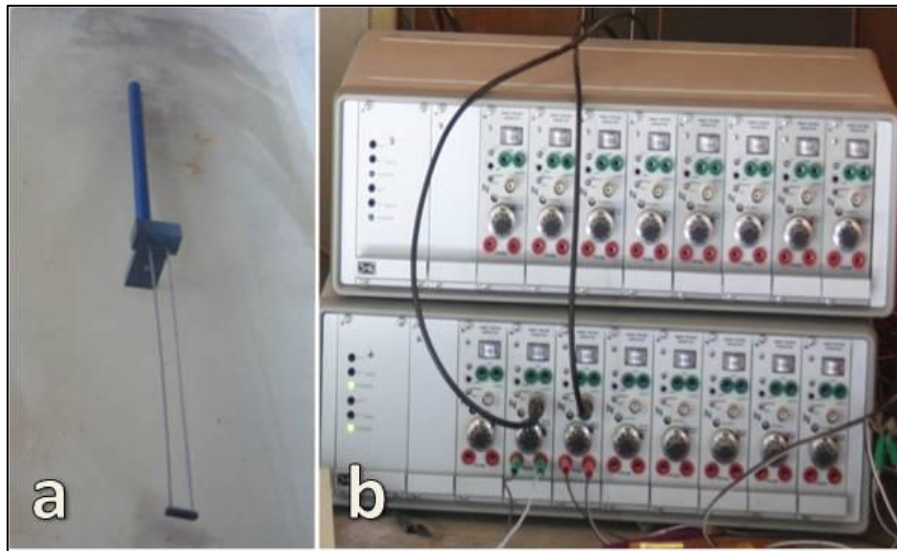


Figure 4-19: (a) Wave Probe (b) Wave Probe Monitor

The result on output screen after a hydraulic jump measurement (Figure 4-20-b) and after a calibration (Figure 4-20-c) is illustrated.

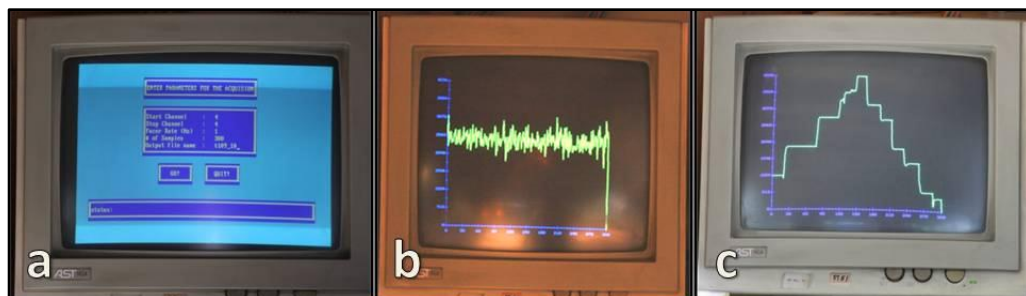


Figure 4-20: The Parameter Screen of Ms-Dos Program, 470

4.3 Experimental procedure

To determine the hydraulic jump characteristics, sequent depth ratio, length, energy dissipation, and wing oscillations, the discharge, Q , the water depth of incoming flow just before jump, y_1 , the subcritical tailwater depth, y_2 , the upmost point of wing oscillations, X_1 , the farthest point of wing oscillations, X_2 , length of jump L_j , were measured in every set of experiments.

4.3.1 Calibration of Tailwater Measurement System

In order to use the wave probe, the probe monitor and the pointer, the calibration of the system was conducted before each experiment set. The calibration of the probe was made by sinking the wave probe into calm water with known depths.

4.3.2 Hydraulic Jump Formation

The locations of hydraulic jump were arranged in such a way that the upmost points of wings were as close as possible to vena contracta. The starting points of hydraulic jump were arranged with overshooting gate and regulating valve. The upmost points of hydraulic jump were arranged such that, they were at the first 30-100 cm of 600 cm long trapezoidal channel. The average distance from trapezoidal gate was 40 cm.

4.3.3 Measurement of Incoming Water Depth

Hydraulic jumps have been investigated in terms of the upstream Froude number since the study by Bakhmeteff and Matzke in 1936. Such an approach provides extrapolation of model test result confidently to any installation.

In preliminary experiments, it was observed that at high Froude numbers, smooth surface conditions rapidly changed and due to aeration of the water surface became irregular on rough bed. Measuring depth with point gauge may cause substantial errors. It was decided that supercritical flow depth at vena contracta can be used as incoming water depth, y_1 .

4.3.4 Tailwater measurement

When calibration procedure for wave probe was carried out (Sec. (4.3.1)) according to procedure (Sec. (4.2.8)), tailwater measurement system was ready for the experimental runs.

4.3.5 Length measurements

The length of the hydraulic jump has not yielded to an analytical solution. Empirical relationships have, therefore, been derived for certain shapes by model tests. These tests have necessarily been over a range of Froude numbers and difficulty has been experienced in defining the downstream end of the jump in trapezoidal channels. This inconsistency is valid for even for the rectangular section.

From the practical point of view, the jump length is may be the most important variable to define the downstream limit beyond which no bed protection is necessary.

The time averaged surface profiles could be obtained with the help of wave probe and measurement car. On the other hand, the axis of a hydraulic jump and axis of flume does not intersect in trapezoidal channels. Measurements should also be conducted on triangular side walls of the flume. Experimenting with this method also requires long time intervals because of the wavy action of oblique jump.

Although many photographs were taken during experiments, exact way to state precisely the length of hydraulic jump could not be determined. Initially it was assumed that the length for extinguishing the surface turbulence was suitable solution, but this approach could not be used. It seems that it is hard to determine exact length of the jump with observations during experiments or analyzing high resolution photographs (Figure 4-21).

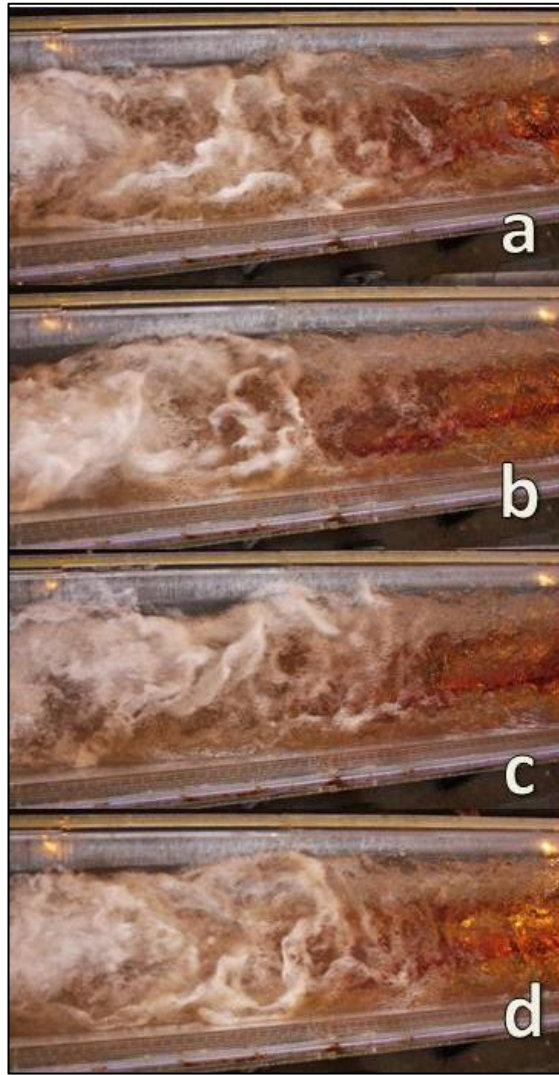


Figure 4-21: Indefinite End of Hydraulic Jump ($F_1 = 6.87$)

Aeration length, L_a , is another common method and many studies are still ongoing as discussed in Section 2.2.5. The last point, where air bubbles touch the bed of the channel was observable due to plexiglass walls (Figure 4-22).

This definition, the point where air bubbles touch the bed of the channel, explains a physical phenomenon; the aeration length in channel bed or the distance where intensity of aeration bubbles in flow field is zero.

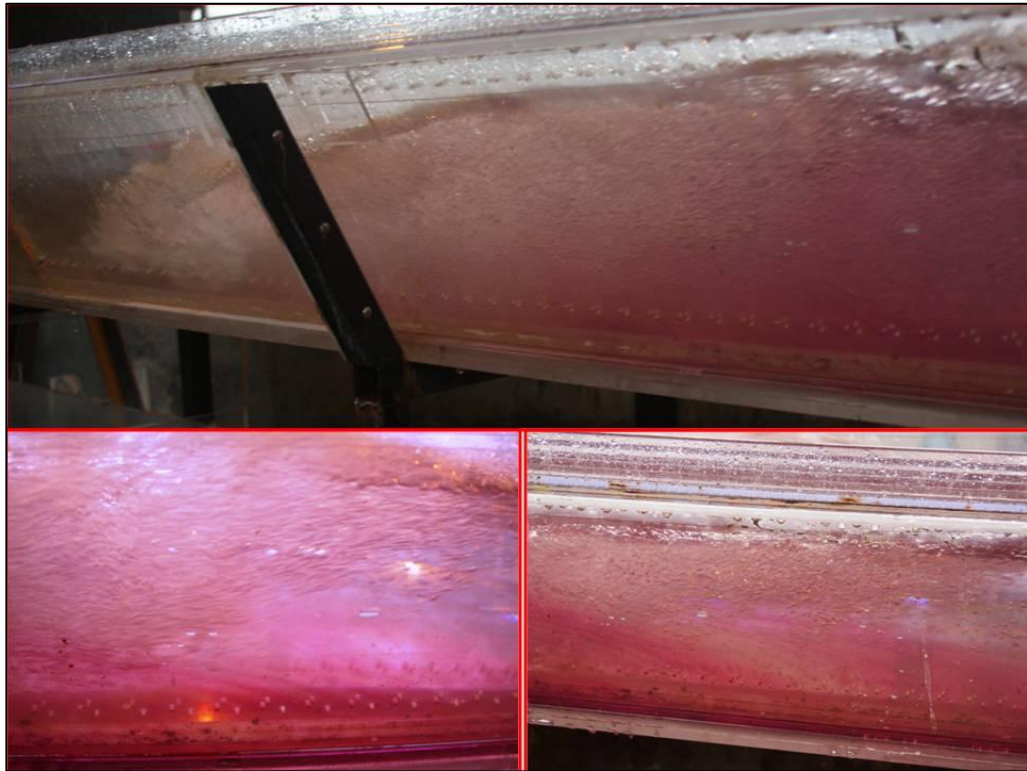


Figure 4-22: Air pockets at Downstream Flow ($F_1 = 6.87$)

The aeration length of hydraulic jump, L_a , was measured according to following definition; “The distance between upmost point of wings and the last point, where visible air bubbles touch channel bed or penetrates into two successive roughness elements in flow direction is aeration length of a hydraulic jump.

4.3.6 Wing Oscillations

As mentioned by Bakhmateff, (1932) the characteristics of the hydraulic jump are to be considered permanent only in the sense of presenting a stable average over a certain period of time. However for trapezoidal channels, due to instant eruptions and splashing, the extension of fluctuations at toe of a hydraulic jump is wider than rectangular channel. This is why side wings should be accepted as part of the hydraulic jump.

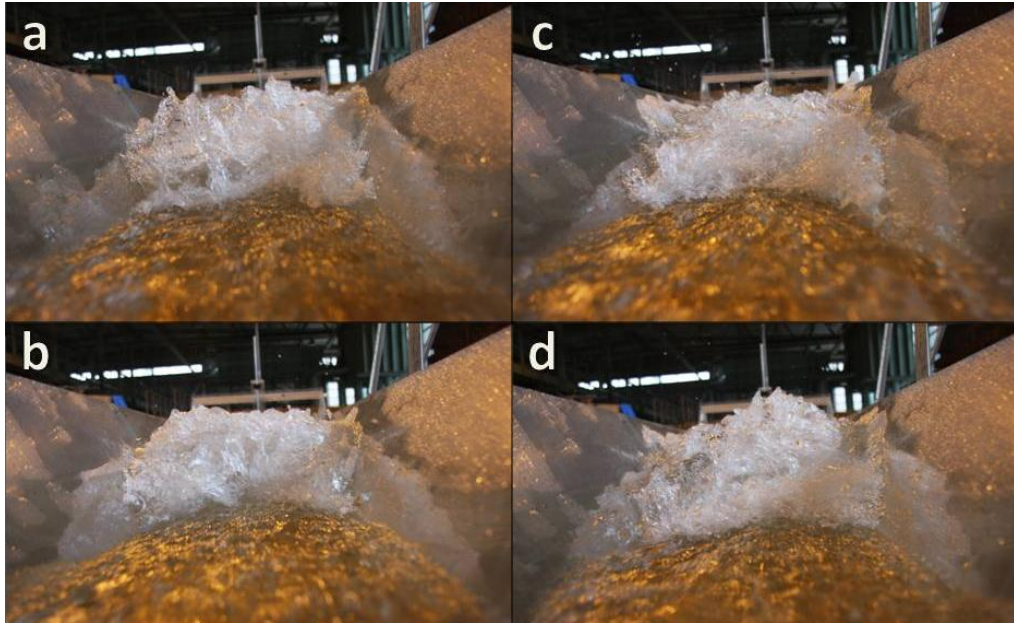


Figure 4-23: Wing Oscillations ($F_1 = 5.34$)

Although the wing oscillations of a hydraulic jump is a physical parameter and has been observed many times by several authors, the range of wing oscillations has not studied yet. It was easily understood that (Figure 4-23) hydraulic jump toe is not constant in trapezoidal jumps, dominant side wing switches its side and range of wing fluctuations are different (Figure 4-24).

The starting point of a hydraulic jump in a trapezoidal channel was assumed to be the upmost point of the wings. As aforementioned the wings of a hydraulic jump is not stable, hence for each set up, the oscillation of a wings was observed for a period of time. The closest point and the most farthest point of the wings to the inlet were recorded.

A selected example of an unstable front face of a hydraulic jump is shown in (Figure 4-23) and in (Figure 4-24). The arrangement of hydraulic jump location was done by the overflow weir and the regulating valve. The upmost points of hydraulic jump were forced such that, average starting point of hydraulic jumps is around 0.4 m downstream from inlet and 0.1 m into the rough bed.

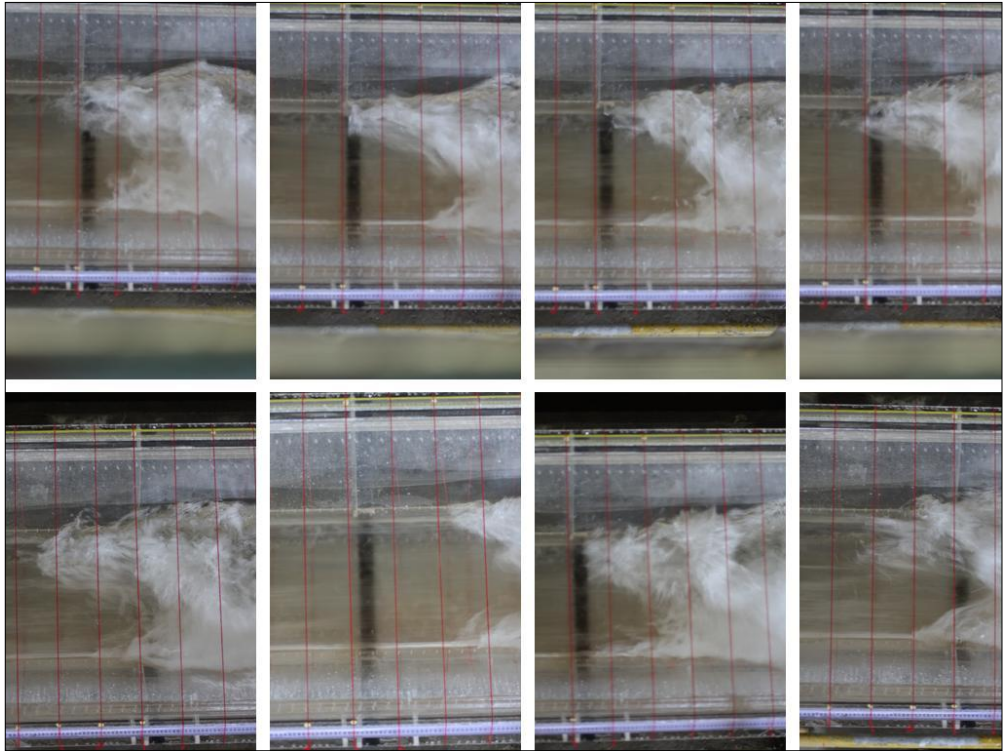


Figure 4-24: Unstable Wings for the Same Hydraulic Jump

The wing oscillations are represented with two figures. In Figure 4-23 wing oscillations are represented from the upstream side of experimental flume. For the same hydraulic jump on smooth bed eight different hydraulic jump toe location can be identified in (Figure 4-24).

The method was used to determine a wing oscillation in experimental run is;

- i. Observe wings in a period of 30 sec., determine upstream point, x_1 , and downstream point x_2 , where wing oscillates between these two points.
- ii. Observe 60 sec.; if oscillations form between these two point, x_1 and x_2 , was determined.
- iii. If the defined boundaries were exceeded by wing oscillations, wait 60sec. duration when new boundary was not exceeded.

CHAPTER 5

EXPERIMENTS, RESULTS AND DISCUSSION

The experiments were conducted in laboratory flume and hydraulic jump characteristics were analysed for three different channel beds; both bed and side walls were smooth, bed was rough only and, walls were rough only.

5.1 Experiments on Smooth Trapezoidal Channel

A total of 11 experiments were conducted on smooth trapezoidal channels. Table 5-1 represents the main parameters related with characteristics of hydraulic jump; Froude number of flow, F_1 , initial depth of jump, y_1 , the sequent depth y_2 , Froude number of supercritical flow F_2 , efficiency of energy dissipation, η , wing oscillations, L_w , and aeration length, L_a . The importance of these experiments was, results of them validate the assumptions in the study.

Measured tailwater depths and, conjugate depth of incoming flow depths, obtained according to Eq. 5.1 is compared with theory in Figure 5-1. The vertical axis represents theoretical result of specific force equation (left hand side of Eq. 5.1) and the horizontal axis represents the experimental result, produced with measured downstream depth (right hand side of Eq. 5.1). The comparison of measured tailwater depth y_2 , and calculated one by conventional momentum approach was presented in Figure 5-2.

$$\bar{y}_1 A_1 + \frac{Q^2}{gA_1} = \bar{y}_2 A_2 + \frac{Q^2}{gA_2} \quad (5.1)$$

Table 5-1: Experiments on Smooth Trapezoidal Channel

Set	F_1	y_1 (cm)	y_2 (cm)	F_2	η (%)	L_w (cm)	L_A (cm)
1	12.01	1.346	19.89	0.11	79.68	39	202
2	8.83	1.346	15.96	0.14	70.27	37	187
3	7.20	1.346	13.11	0.17	63.78	33	164
4	5.59	1.346	10.20	0.23	54.48	20	132
5	7.25	2.019	19.15	0.14	65.25	33	170
6	6.39	2.019	16.80	0.17	61.16	27	150
7	5.20	2.019	14.01	0.20	52.45	24	148
8	4.49	2.019	11.40	0.27	49.15	23	141
9	5.36	2.692	19.81	0.15	52.61	39	173
10	5.01	2.692	17.68	0.18	51.81	32	160
11	3.57	2.692	12.61	0.27	37.73	22	132

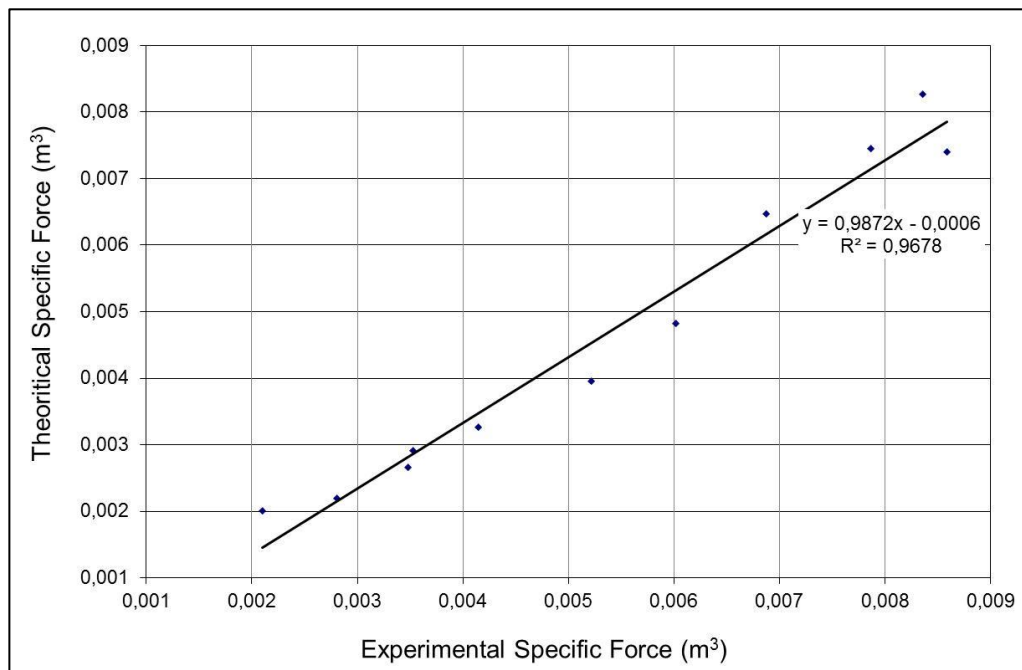


Figure 5-1: Comparison of Theoretical and Experimental Specific Force

As indicated by Hsing (1937), the observed sequent depth ratios with the prediction based on the conventional momentum approach compared well.

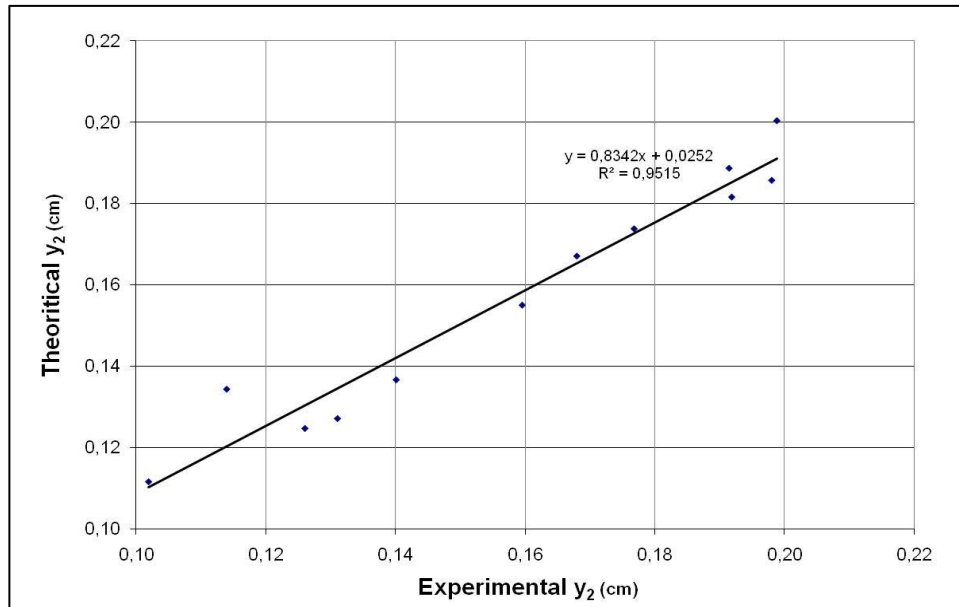


Figure 5-2: Comparison of Theoretical and Experimental Subcritical Depths

5.1.1 Flow Features

The trapezoidal jumps are not straight; hence they have been called as oblique jump. The recirculation behind jump feed up backflow and producing triangular leading wings.

Triangular areas along the sides of the trapezoidal stilling basins do not oppose the incoming high velocity jet, hence jump tend to form obliquely at the central part of the channel.

The tendency for the jump to swing to one side was not observed. According to discussion of Sharp (1977) and Ali and Ridgway (1977), the tendency for the jump to swing to one side is related with asymmetry at inlet. As a consequence, inlet design has not any asymmetry and properly works.

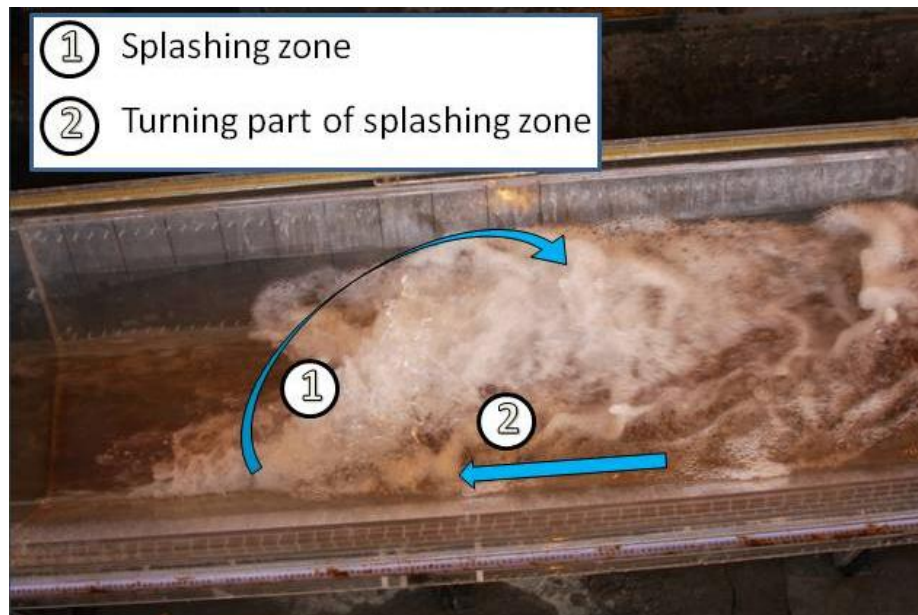


Figure 5-3: Oblique Jump and Returned Flow ($F_1 = 6.87$)

Figure 5-3 represents an ideal experimental flow. The upmost point of wings is 40 cm far from gate although difference of wings is more than 20 cm. At the sides of the jump there is reverse flow and this phenomenon tends to interrupt the jump formation. Wanoschek and Hager (1988) defined the parts of hydraulic jump (Figure 3-3) in trapezoidal channels. Figure 5-3 represents two different flow parts of Wanoschek and Hager (1988). These zones are, “the splashing zone” and “Splashing water–turns back upstream and forms the side return flow zones” with indicators 1 and 2, respectively.

It is observed from Figure 5-3 that the jump is oblique and splashes one side wall of channel. The angle of a jump in trapezoidal channel (Figure 5-4 - α) was not constant and downstream of jump was wavy and bubbly. Depending on oblique jump angle and time, bubbly regions were spreading on different parts of the surface.

Figure 5-3 and Figure 5-4 represent different backflow conditions of the same experimental set.

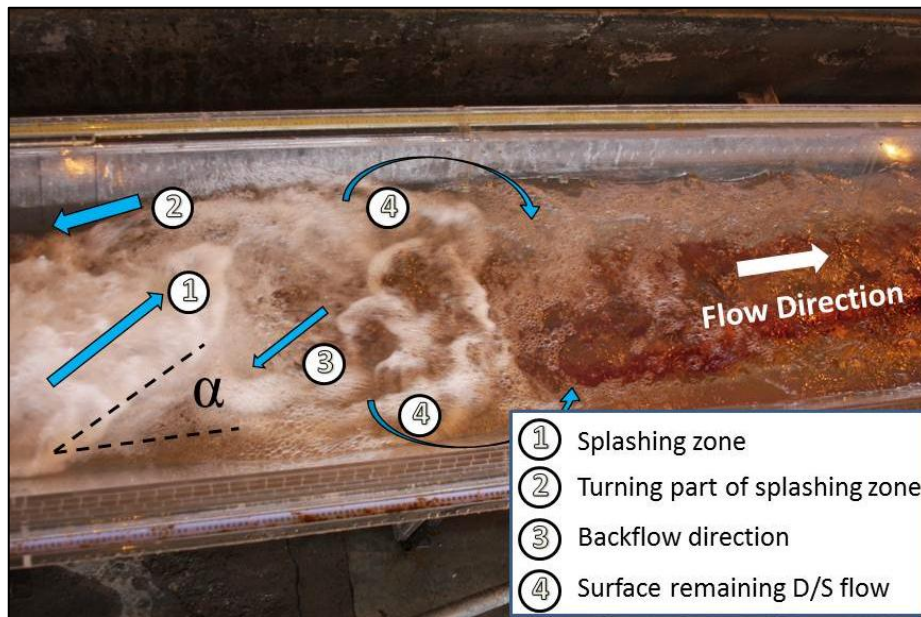


Figure 5-4: Oblique Jump, Returned Flow and Side Flows ($F_1 = 6.87$)

Hydraulic jump surface profile and the downstream flow conditions can be compared. When oblique jump splashes the wall, some part of the energy of jump transferred to flow on the splashed side, but greater amount is reflected and transfers energy and momentum other side of the channel. The transfer of energy and momentum creates a straight end line for the bubbly region in Figure 5-4.

Air entrainment was formed through all hydraulic jump, but the last entrainment point was the last bubbly regions at surface in downstream direction.

The air pockets, which entrain at the last bubbly region of the hydraulic jump rarely touch the bed of channel.

According to the definition of Wanoschek and Hager (1988), Figure 5-4 represents “the splashing zone” (Figure 5-4-1), “Splashing water – turns back

upstream and forms the side return flow zones” (Figure 5-4-2) and, “splashing water, remains at the surface and continues” (Figure 5-4-4).

However indicator 3 represents a surface wave towards upstream, which feeds upstream wings. This flow zone was not represented by Wanoschek and Hager (1988).

Figure 5-5 illustrates the flow structure at close vicinity of the channel wall, on which oblique jump ends. When the movement of a metal sheet inside the flow is investigated, the back flow is articulately displayed.



Figure 5-5: Side Flow Towards to Upstream ($F_1 = 5.34$)

Figure 5-6 illustrates the flow directions at the surface of a hydraulic jump. The added indication arrows represent the flow direction at close vicinities of arrows. Although Wanoschek and Hager (1988) defined a flow part for trapezoidal hydraulic jump “bottom separation zone or bottom roller” (Figure 3-3), this zone was not observed during experimental study. On the other hand,

arrow directions in flow field indicate there is a roller at just downstream of the oblique jump and bounded by arrows.



Figure 5-6: Flow Directions at Surface ($F_1 = 6.87$)

It is observed from Figure 5-7 that jumps in trapezoidal channel are oblique and splash one side wall of channel. The jump angle of a roller in trapezoidal channel was not constant and, downstream of jump was wavy and bubbly. Depending on oblique jump angle, bubbly regions are different. The successive photograph frames also show that the end of the hydraulic jump was not precise. When Figure 5-7-a compared with Figure 5-7-b and Figure 5-7-c, it can be deduced that determination of definite end of hydraulic jump from the surface bubbles was not possible only with observation.

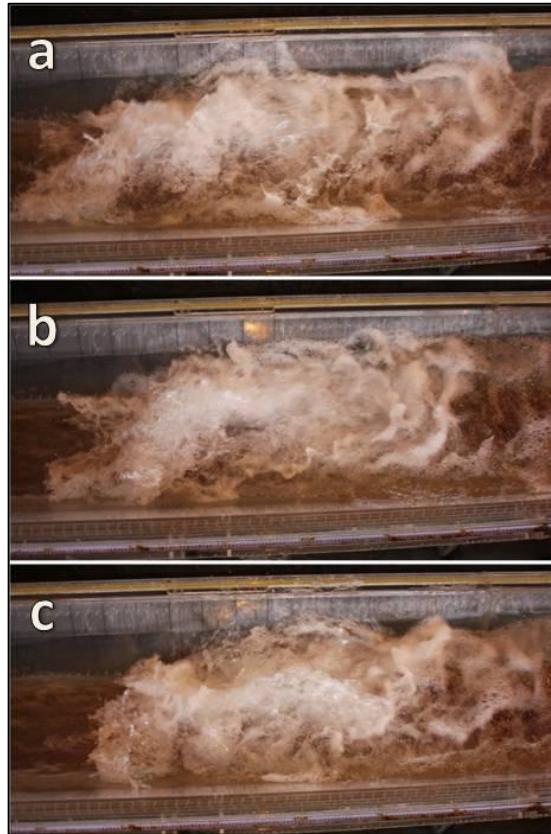


Figure 5-7: Fluctuating Toe and End of Hydraulic Jump ($F_1 = 5.34$)

The successive photograph frames (Figure 5-8) were taken from side of jump flume also shows that the end of the hydraulic jump was not precise. These pictures were taken during special light conditions, end of the jumps were illuminated to observe end of a hydraulic jump. It was observed that turbulence characteristics are similar at the end of the jump. However, without any turbulence measurement devices, the length of jump could not be determined from the surface of flow field. Selected length measurement methodology seems it is the most feasible method due to it is free from subjective errors.

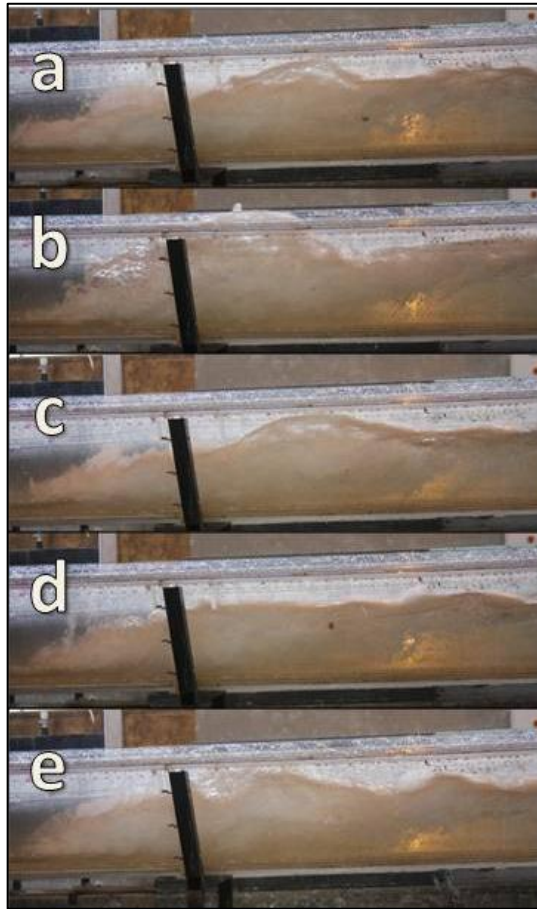


Figure 5-8: Indefinite Length of Hydraulic Jump ($F_1 = 9.81$)

5.1.2 The Sequent Depths

Figure 5-9 shows the sequent depth ratio of hydraulic jumps in smooth bed and walls. The incoming depth was accepted as the depth at vena contracta and the tailwater measurements were conducted at downstream part as mentioned in Section 4.3.4.

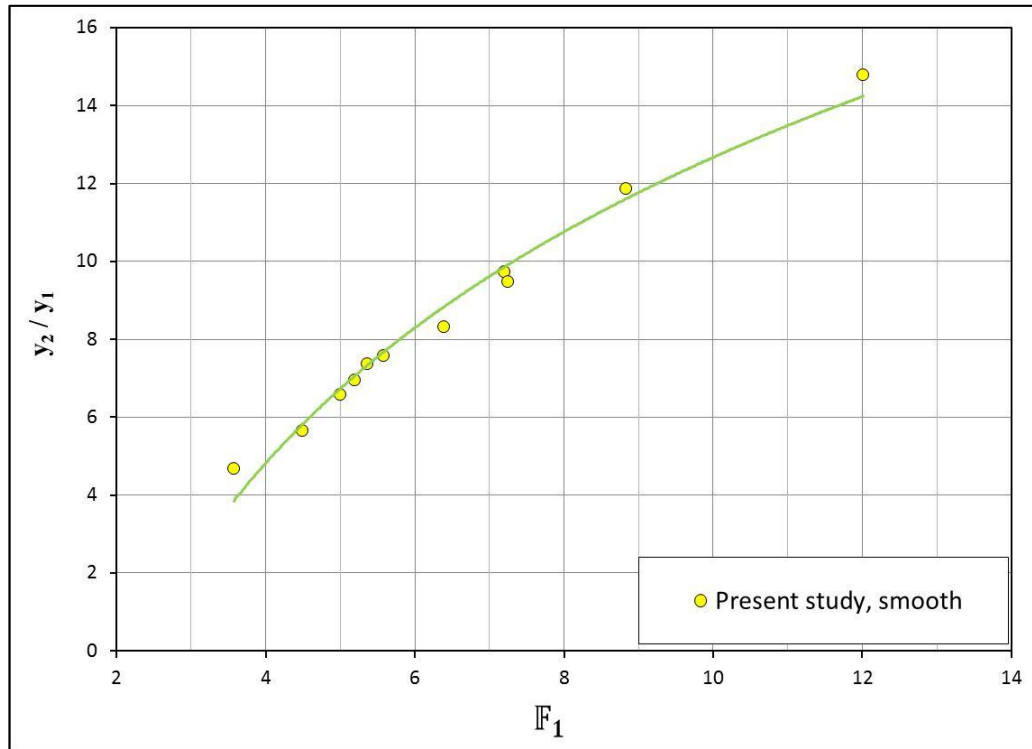


Figure 5-9: Sequent Depth Ratio on Smooth Beds

The best fit curve for the range of $3.5 < F_1 < 12$ with a correlation coefficient 0.99 is obtained as;

$$\frac{y_2^T}{y_1} = 8.5662 \ln(F_1) - 7.0537 \quad (5.2)$$

where y_2^T is the sequent depth of a hydraulic jump on a smooth bed in trapezoidal flume of present study.

Sequent depth ratios of the present study were plotted in Figure 5-10 as a function of F_1 along with the corresponding data obtained from the experiments conducted on smooth bed by Wanoschek and Hager (1988). The observed sequent depth ratios with the experimental data of other study compare well.

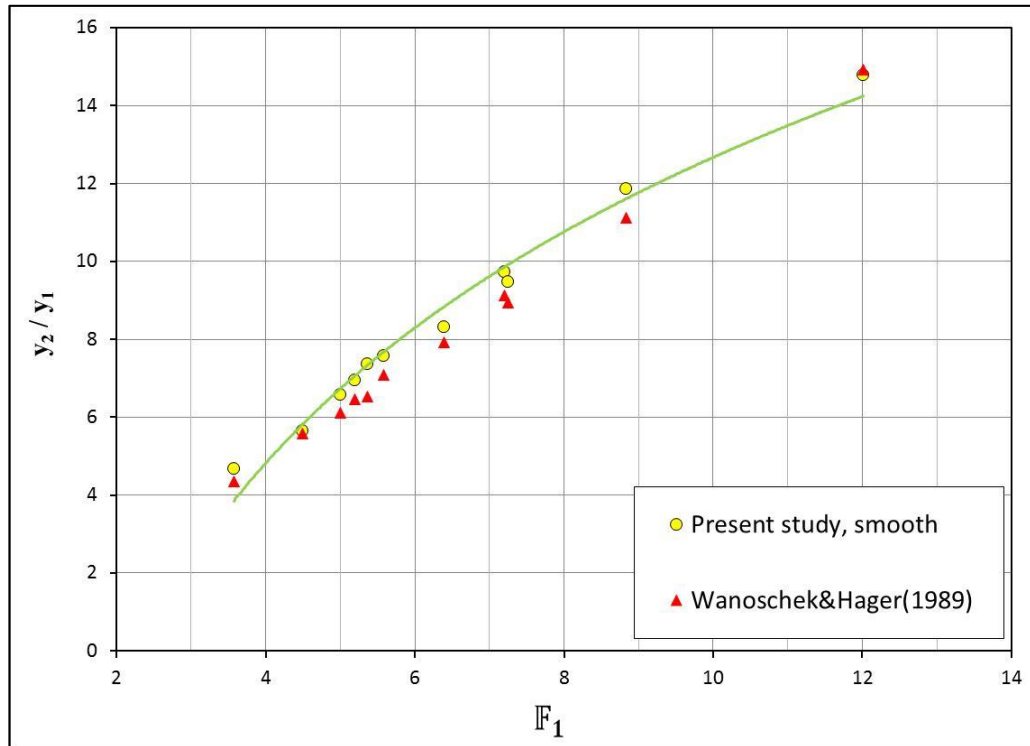


Figure 5-10: Comparison of Sequent Depth Ratio with Previous Studies

It was understood that, the efficiency of tailwater reduction was related with unstable characteristics and oblique structure of jump. The splashing direction often changed in the range of Froude numbers 4 to 9, and this action results in more energy dissipation due to secondary flows. Secondary flows can be divided into three; intersecting, downstream and upstream flows.

Ali and Ridgway (1977) investigated sequent depth ratio in rectangular, triangular and several trapezoidal channel sections. They defined a parameter $k=b/my_1$ which gives the differences between channel geometries.

The data of present study is compared with the data of Ali and Ridgway (1977) in Figure 5-11. Data obtained by digitalizing the figures of Ali and Ridgway (1977). For trapezoidal channels only the data series of Ali and Ridgway (1977), having maximum k value of 10 represented in Figure 5-11.

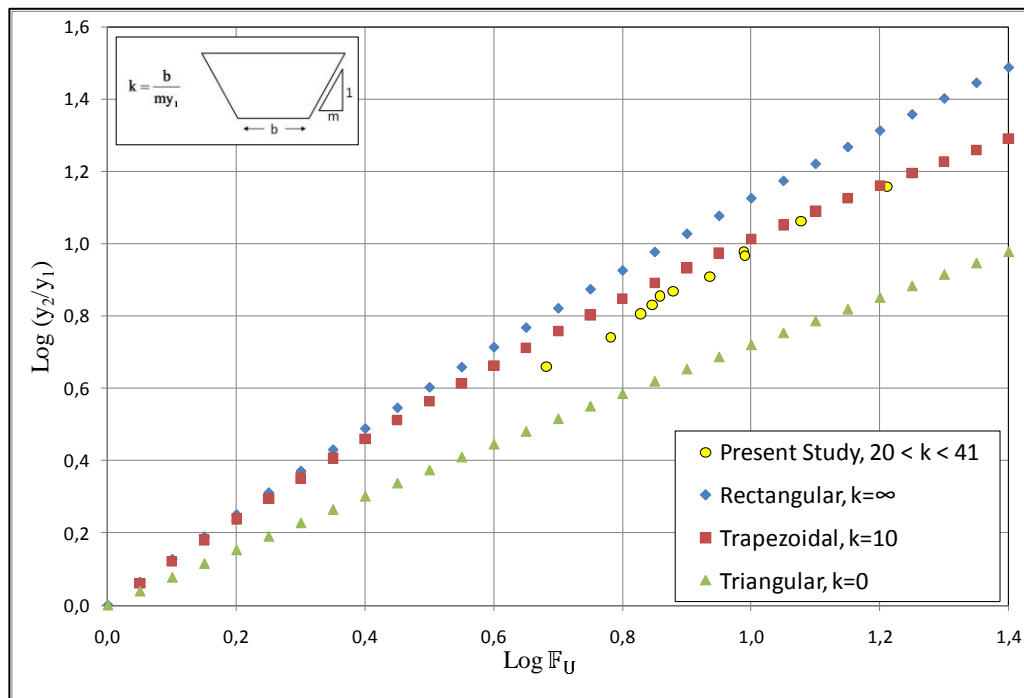


Figure 5-11: Hydraulic Jump Sequent Depths; Present study vs. Ali and Ridgway (1977)

For the smooth bed hydraulic jumps, the dimensionless channel geometry parameter, k , was from 20 to 41 in present study. The experimental results were between the boundaries drawn by Ali and Ridgway (1977) for rectangular channels and trapezoidal channels. Figure 5-11 shows that the data of present study for which the values of k is $20 < k < 41$ agrees quite well with the study of Ali and Ridgway (1977).

Ali & Ridgway (1977) analyzed hydraulic jump properties with a narrower channel (Table 4-1) and with higher incoming flow depths. The inconsistency of the present study with results of authors was probably due to scale effect. When the incoming flow depth y_1 is small, scale effect becomes significant as mentioned by Hager and Bremen (1989). The discrepancy observed between the recent and previous works might be the outcome of experimental errors, also.

5.1.3 Efficiency of Energy Dissipation

Efficiency of energy dissipation is the ratio of the dissipated energy to the specific energy of the supercritical flow in a hydraulic jump. As seen in Figure 5-12, efficiency of energy dissipation grows with increasing inflow Froude number F_1 . Similarity of the present data series with Ohtsu's (1976) proposed formula (Eq. 3.16), conducted on trapezoidal channels, and equation of Hager (1995) (Eq. 2.13) can be seen in the figure.

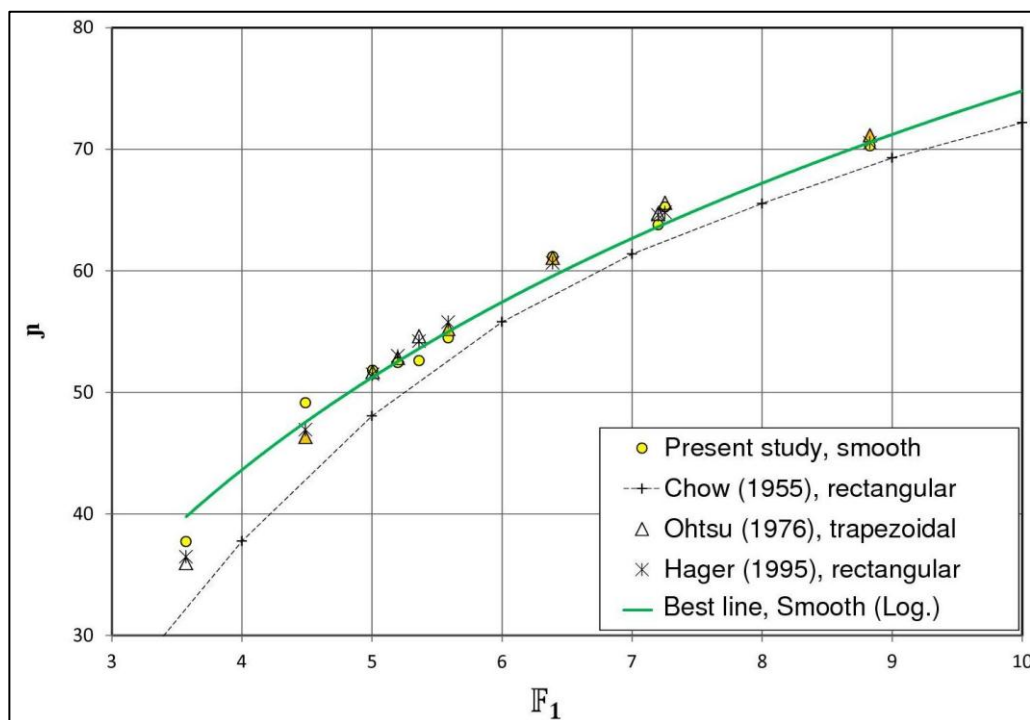


Figure 5-12: Comparison of Efficiency with the Data in the Literature

As mentioned in section 5.1.2, both cotangent of side walls, m , and channel width, b , influence the hydraulic jump characteristic. Only for experimental flume of present study, the following equation for efficiency is presented on the purpose of comparing experimental results conducted on rough bed and walls.

$$\eta = 34.11 \ln(F_1) - 3.5204 \quad (5.3)$$

Figure 5-12 indicates that there is a noticeable distinction between efficiencies of Chow (1959) (Eq. (3-12)), and Hager (1995) (Eq. (3-13)) for rectangular channels. The probable reason of such a difference is, while Chow (1959) represented the data obtained from large scale implementations, Hager represented an approximate formula for experimental data series.

In Figure 5-13, the effect of incoming Froude number on % efficiency of energy dissipation is presented with the data series of Rajaratnam (1995) for rectangular, triangular and circular cross sections. The data series of present study is between the data series of circular and rectangular channels as proposed by Rajaratnam (1995).

Figure 5-13 shows that for incoming Froude number, up to 5; all the channels having different cross sections have almost the same energy dissipation efficiency, η . After $F_1 > 5$ the effect of channel shape on η becomes more visible. Trapezoidal basins dissipates energy more efficiently than rectangular basins.

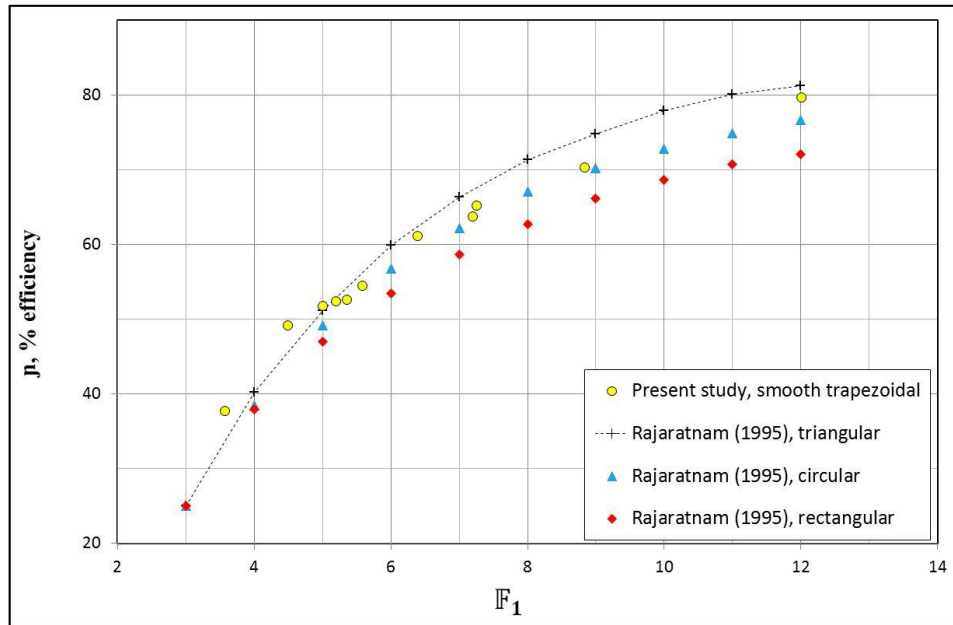


Figure 5-13: Comparison of Efficiency with Previous Studies

In a trapezoidal channel, the upstream high velocity jet enters the jump over a smaller width than the downstream water surface. The side areas, which are in triangular shape and which are not directly influenced by the jet, permit reverse flow and recirculation. Reverse flow and recirculation also occurs on the water surface of jump. These extra recirculations are probable reason of the higher energy dissipation rates in trapezoidal channels.

5.1.4 Length of Jump

The length of the hydraulic jump has not yet, yielded to an analytical solution. Empirical relationships have been derived for certain trapezoidal channels by model studies. As discussed in Section 3.2.3, difficulty has been experienced in defining the downstream end of the jump in trapezoidal channels. The side areas, which are triangular in shape and which are at upstream of jump, permit reverse flow and recirculation as mentioned in Section 5.1.1. The reverse flow is the main factor increasing jump length.

As is clear from these statements that, the width of the incoming jet affects the length of jump. Thus for trapezoidal and triangular channels, both m and b should influence the length.

In Figure 5-14, the effect of incoming Froude number on hydraulic jump length presented with the data series of Posey and Hsing (1936), Silvester (1964), Ohtsu, (1976) Hager (1995), Evcimen (2005). Although it was for rectangular channels, only Hager's (1995) Eq.(2.13) is directly comparable with present data due to it represents aeration length, L_a . Posey and Hsing (1936), Silvester (1964), Ohtsu (1976) conducted experiments on trapezoidal channels and they have measured the jump length at surface, hence they uses jump length, L_J .

There is a large degree of scatter in Posey and Hsing (1936) results for jump length. Silvester (1964) stated that the tabulated results of Posey and Hsing (1936) show a number of constant length values for different values of F_1 which must have resulted from difficulties in measuring the length accurately.

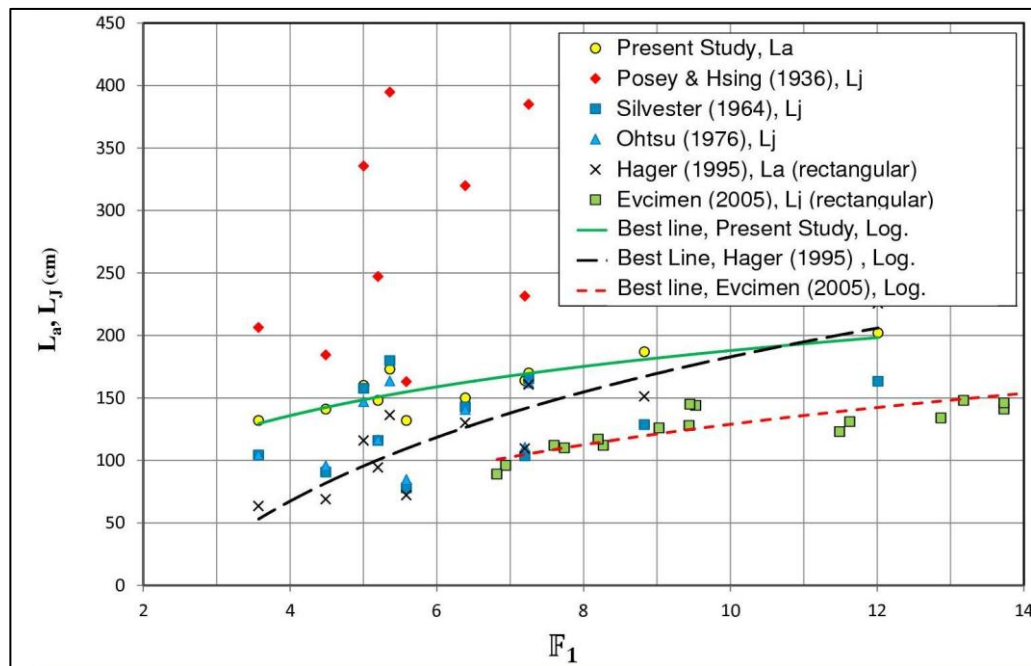


Figure 5-14: comparison of Hydraulic Jump Lengths with Previous Studies

In Figure 5-14, while the green full line represents best line of present study, black dashed line represents best line of Hager (1995) and, red line represents best of jump on rectangular channels.

When the data of Hager (1995) for aeration length L_a is compared with hydraulic jump length L_J data of Evcimen (2005) for rectangular channels, it is seen that aeration length is longer than hydraulic jump length. The difference between two lengths increases with increasing inflow Froude number F_1 .

These two comparisons validate the proposal of Hager (1995) to use L_a as a scaling parameter for hydraulic jump in trapezoidal channels. On the other hand, L_a can be used as a scaling parameter for classical hydraulic jump as in Eq. (2.13) and for hydraulic jumps in trapezoidal channels. Aeration length is longer than the length of jump.

The data of Silvester (1964) for jump length L_J shows that, when it is compared with hydraulic jump aeration length L_a data of present study, it is seen that aeration length is longer than hydraulic jump length.

5.1.5 Wing Oscillations

Figure 5-15 shows that normalized wing oscillations of hydraulic jumps in smooth trapezoidal flume. The incoming depth was accepted as the depth at vena contracta and the wing oscillations recorded by observations. The scatter of data series is small enough to compare this results with that of rough bed and side walls.

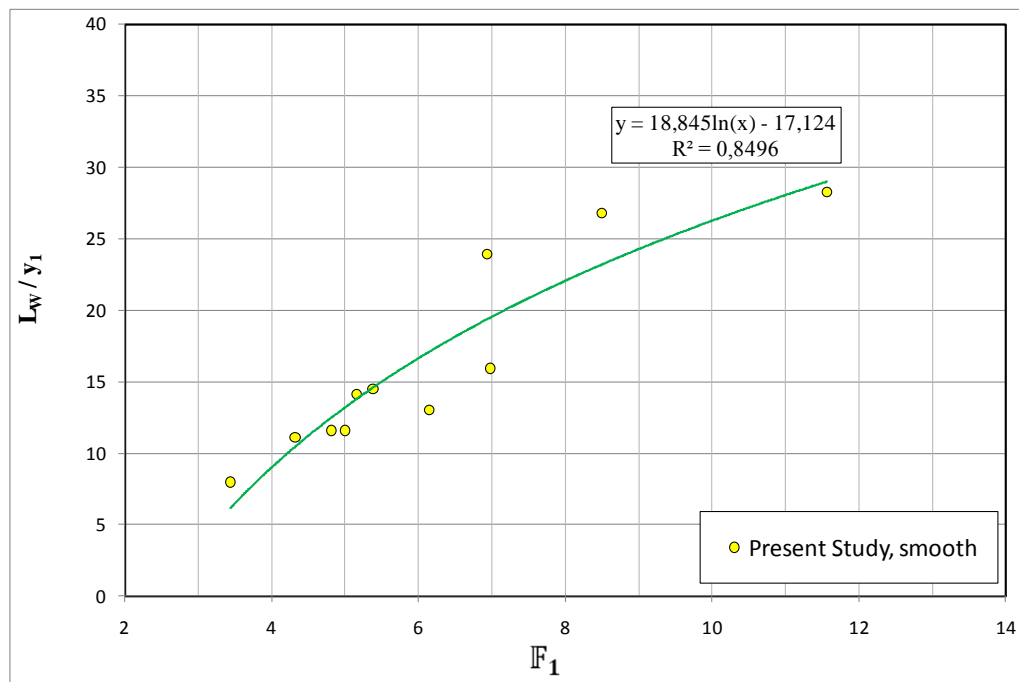


Figure 5-15: Normalized Wing Oscillations

Sharp (1977) stated that the oblique jump was not observed at small values of upstream Froude numbers, F_1 .

Oblique jump become apparent at upstream Froude numbers F_1 , above about 4 and always formed at Froude numbers in excess of 9. This might be the reason of why the data of the present study for $6 < F_1 < 9$ shows some scatter.

5.2 Experiments on Rough Beds

In this study, data of 109 sets of experiments were performed and results of these performances used to express the effect of rough beds on the hydraulic jump properties.

Along experimental studies, different roughness types, different intensities and different pitch ratios were used to investigate the effect of roughness on hydraulic jump properties. At the beginning of the study, investigation of effect of different roughness intensity and pitch ratios on flow was planned. On the

other hand for the roughness intensities 8.33% and 6.66%, the first roughness element disturbs flow significantly hence these roughness patterns were not used in the study.

5.2.1 The Sequent Depths

The sequent depth ratio y_2/y_1 versus Froude number, F_1 , is plotted in Figure 5-16 for the data obtained in the present study and data of Wanoschek and Hager (1988).

Figure 5-16 shows that the increasing bed roughness reduces the required tailwater depth for given upstream conditions, y_1 and F_1 . The line represents best fit of smooth bed results and dots represent individual experimental results.

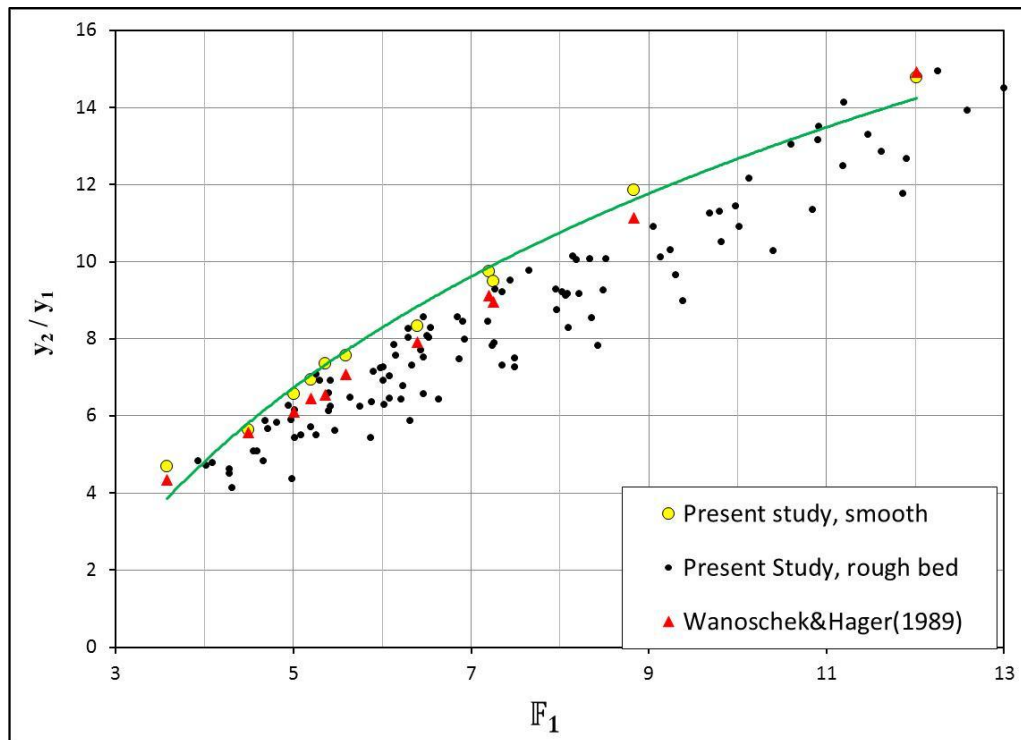


Figure 5-16: Comparison of Sequent Depth Ratio for Rough Beds

To see the effect of roughness intensity on sequent depth ratio, y_2/y_1 values versus Froude number, F_1 , are plotted for three different roughness intensities in Figure 5-17.

Figure 5-17 shows that there are noticeable differences between the sequent depth ratios of three different roughness intensities. While roughness intensity 11.11% was the most effective roughness pattern from the depth reduction point of view, roughness intensity of 33.33% was the least effective pattern.

It was observed during experimental studies that, the flow structures inside the grooves are not similar for different intensities of roughness. Cui et al. (2003) represented (Figure 2-17) the flow structures inside the grooves when they studied turbulent flow structure in a channel with rib roughness by Large-eddy simulation. They divided flow structures at grooves according to pitch ratio.

If pitch ratio is equal to 4, it was called as intermediate roughness, the length of vortex formed in the cavity is equal to length of the gap between roughness elements.

If the pitch ratio is greater than 4, it was called as k-type roughness, vortex formed in the cavity is smaller than pitch, and hence outer flow attaches to the channel bed.

If the pitch ratio is smaller than 4, roughness elements so closely spaced that, crests of the ribs do not penetrate into flow hence effect of roughness elements on friction and eddy formation is negligible.

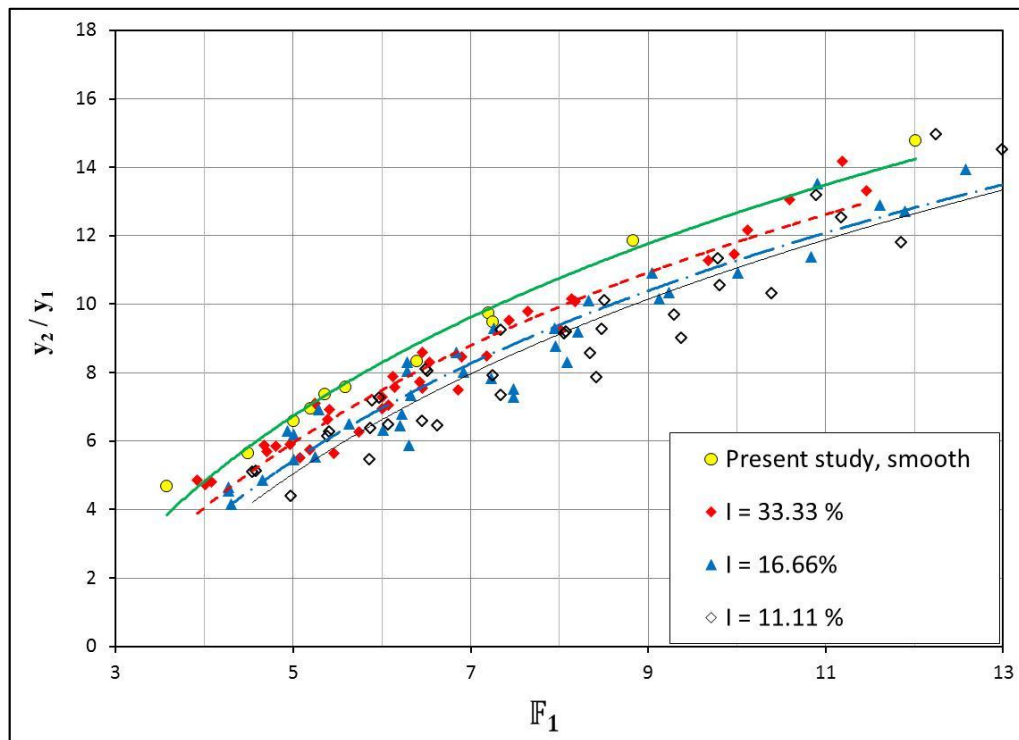


Figure 5-17: Sequent Depth Ratio for Different Roughness Intensities

When the physical characteristics of roughness patterns are examined (Table 4-6), it is observed that while the pitch ratios of 33.33% intense patterns are smaller than 2; pitch ratios of 16.66% intense patterns are 5, 2.5 and 1.66. 11.11% intense patterns had pitch ratios 8, 4 and 2.66. Therefore, the effect of 33.33% roughness intensity patterns on hydraulic jump should be similar with the effects of roughness pattern having smaller pitch ratio than 4.

Considering the obliquity of a jump in trapezoidal channel, it can be concluded that the axis of flow structure inside the grooves are not the same with channel axis through hydraulic jump. The flow structures are similar with definition of Cui et al. (2003), but the main difference is in trapezoidal channels flow structure is somehow oblique in the grooves. Because of this obliquity, the flow inside the grooves has more distance to travel, when compared with study

of Cui et al. (2003). Pitch ratio limit to define intermediate roughness should be different than 4 and somewhat smaller than 4.

This conclusion can be checked by investigating the effect of pitch ratio on hydraulic jump characteristics, i.e length and wing oscillations.

In Figure 5-18, the effect of different Pitch ratios, PR, on sequent depth ratio was investigated. For $PR > 4$, the roughness patterns was more efficient than, that for $PR < 4$ roughness patterns. The experimental series of $PR = 4$ was intermediate from the sequent depth point of view.

$PR = 4$ series approaches the $PR > 4$ at high incoming Froude numbers. The question may be answered such that while increasing Froude number, flow structure was changed inside the groove for $PR = 4$. Outer flow should be attached to the channel bed and hit the roughness element at the end of the groove. This definition was done by Cui et al. (2003), however it was for the series $PR > 4$.

This result proves the idea; pitch ratio limit for intermediate roughness should be different than 4 and somewhat smaller than 4. If intermediate roughness limit is less than 4, the effect of 11.11% intense roughness patterns on hydraulic jump characteristics should be similar with the same effect produced by $PR > 4$.

Focusing on distribution of $PR = 4$ series shows that at low Froude numbers the effect of $PR = 4$ was similar to effect of $PR < 4$ series on sequent depth ratio. Such an extraction can be done here; $PR = 4$ series shows behaviour of intermediate roughness. At low Froude numbers up to 6, have similar flow field with $PR < 4$ and, for higher Froude numbers have similar flow field with $PR > 4$.

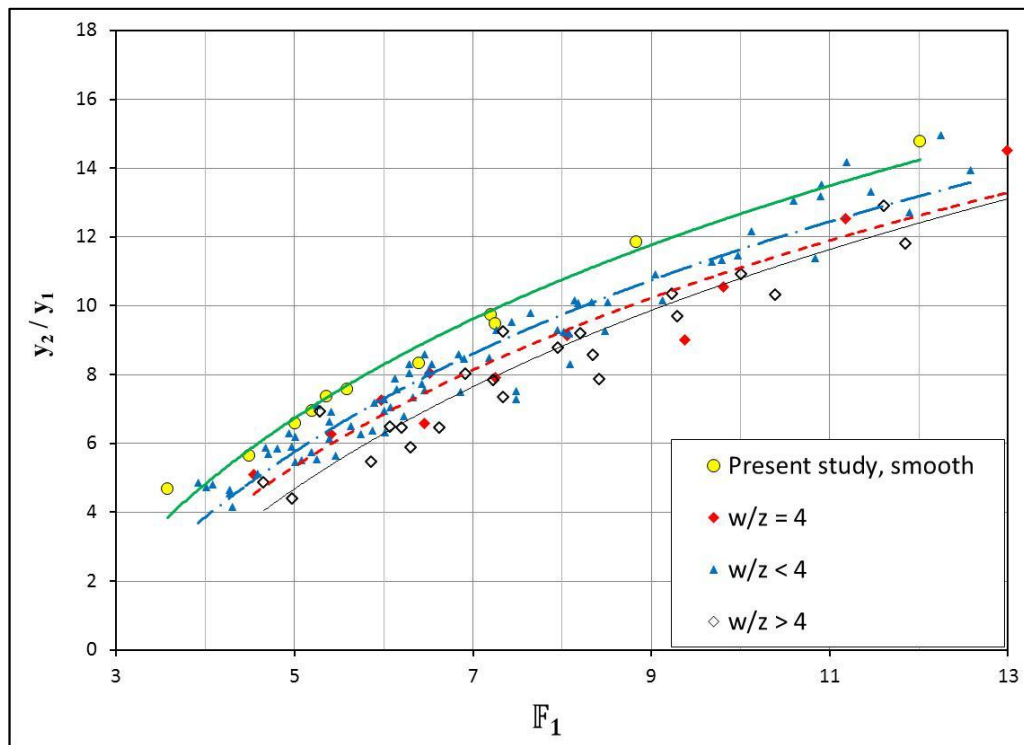


Figure 5-18: Sequent Depth Ratio for Different Pitch Ratios

Figure 5-18 also shows that, although $PR < 4$ series have smaller sequent depth ratio than on smooth channels for Froude numbers < 10 . However, when the Froude numbers were greater than 10, some experimental data have larger sequent depth ratio than that on the smooth channel. This phenomenon may be explained as follows: For $PR < 4$, the currents in the groove may remain the same as the Froude number increases and hence the influence on the flow field becomes weaker and weaker by increased Froude numbers. The normalized sequent depth ratios $(y_2 - y_1)/y_1$ values are plotted against F_1 in Figure 5-19 both for rough and smooth beds. This figure shows that rough beds reduce the sequent depth ratio considerably.

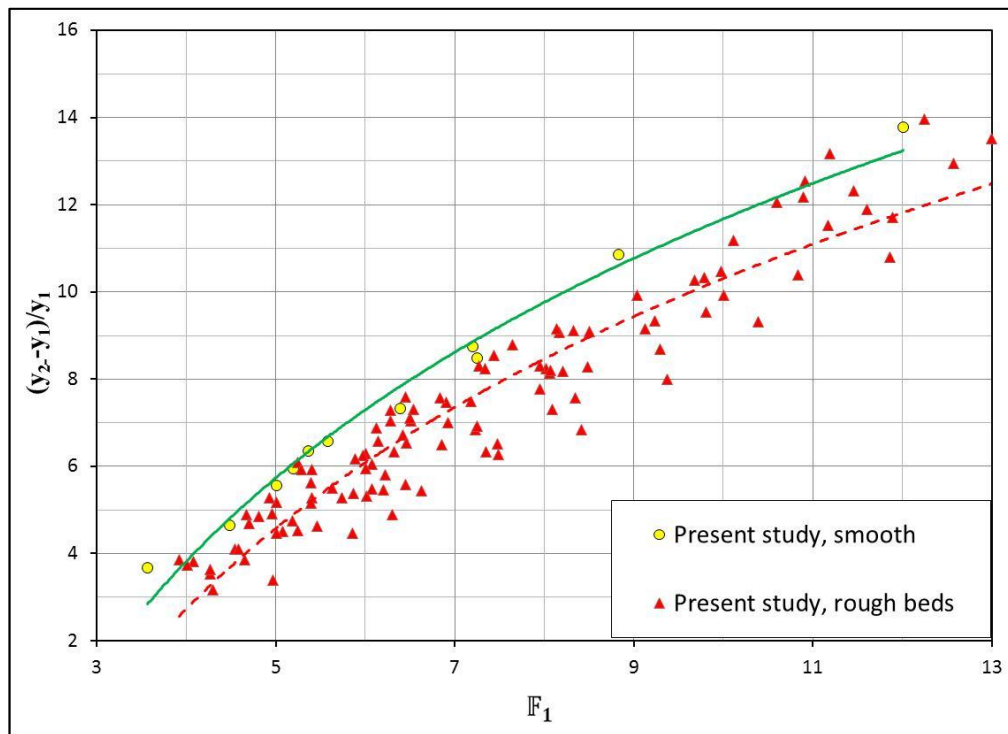


Figure 5-19: Normalized Sequent Depth Ratio on Rough Beds

Figure 5-20 represents normalized sequent depth ratio for different pitch ratios. While the most efficient series was $PR > 4$ the least effective series was $PR < 4$. The reason of such different behaviour is the same with the reason of behaviour of data series in Figure 5-18. The reason of such behaviour is directly related with the flow structure inside the grooves.

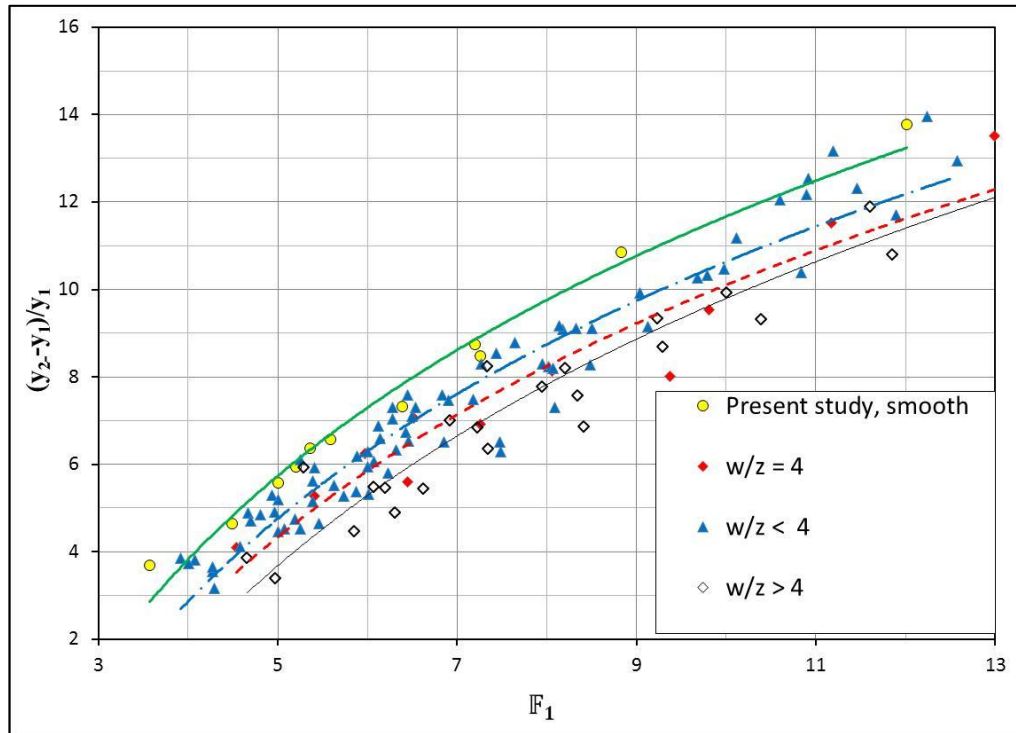


Figure 5-20: Normalized Sequent Depth Ratio for Different Pitch Ratios

5.2.2 Depth Reduction Factor

To obtain the percent reduction in sequent depth ratio, a depth-reduction factor D may be defined as Ayanlar (2004), and Ead and Rajaratnam (2002);

$$D = \frac{y_2^T - y_2}{y_2^T} \times 100 \quad (5.4)$$

Where y_2^T is the sequent depth of y_1 for corresponding oblique jump on a smooth bed. The variation of D with F_1 is shown in Figure 5-21 for different pitch ratios.

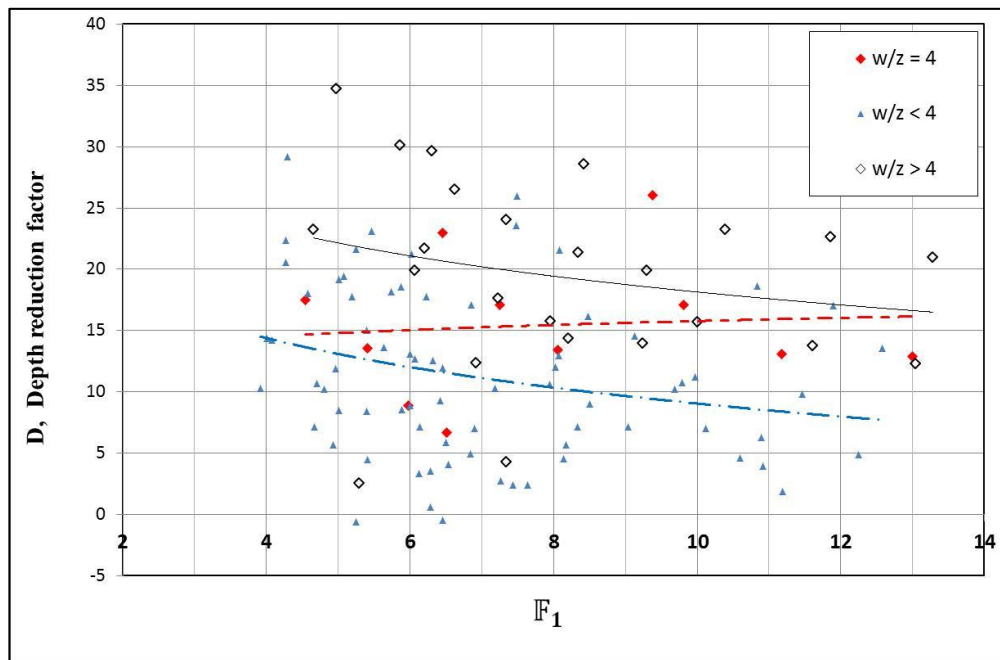


Figure 5-21: Depth Reduction Factor on Rough Beds for Different Pitch Ratios

As discussed above, focusing on distribution of PR=4 series shows that at low Froude numbers the effect of PR=4 was similar to effect of PR<4 series on sequent depth ratio. The extraction done, “PR=4 series shows behaviour of intermediate roughness” is obvious. At low Froude numbers have similar flow field with PR<4 and, at higher Froude numbers have similar flow field with PR>4.

Figure 5-22 demonstrates the distinction between sequent depth ratios of three different roughness intensities. While the most efficient roughness intensity was 11.11%, the least effective intensity was 33.33%.

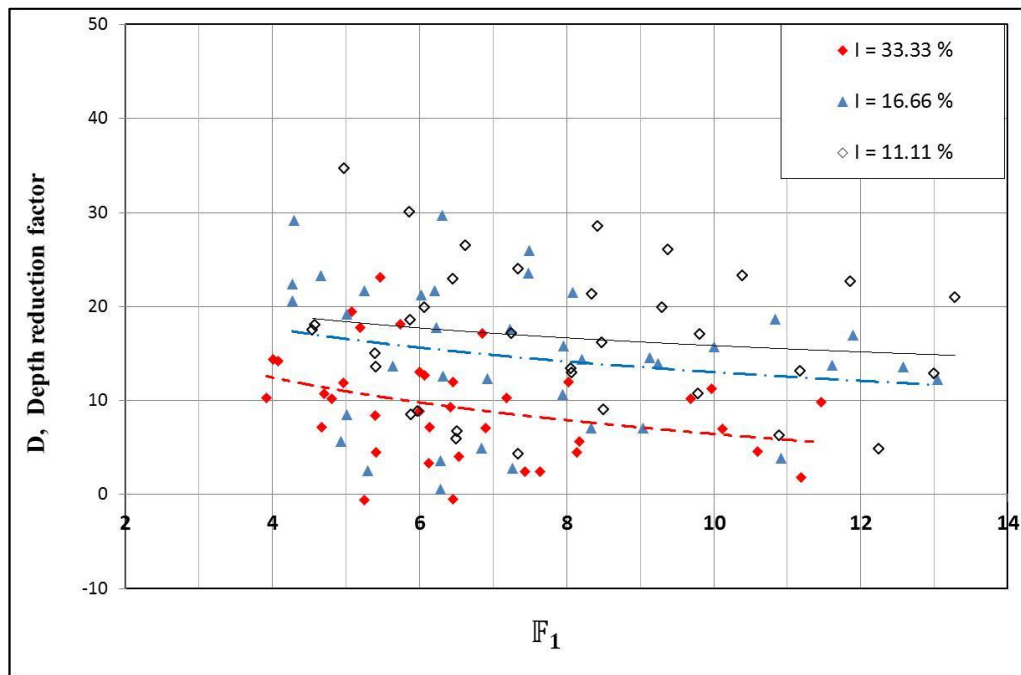


Figure 5-22: Depth Reduction Factor on Rough Beds for Different Intensities

5.2.3 Efficiency of Energy Dissipation

Figure 5-23 represents the effect of incoming Froude number on % efficiency of energy dissipation on rough beds with the data series of past studies and the results on smooth beds of present study. The dots illustrate the experimental series of rough bed combinations. Figure 5-23 shows that there is noticeable difference between efficiency of hydraulic jumps on rough and smooth beds of the present study. This distinction is also valid with proposed formula of Ohtsu (1976), Eq. 3.16, and equation of Hager (1995), Eq. 2.13.

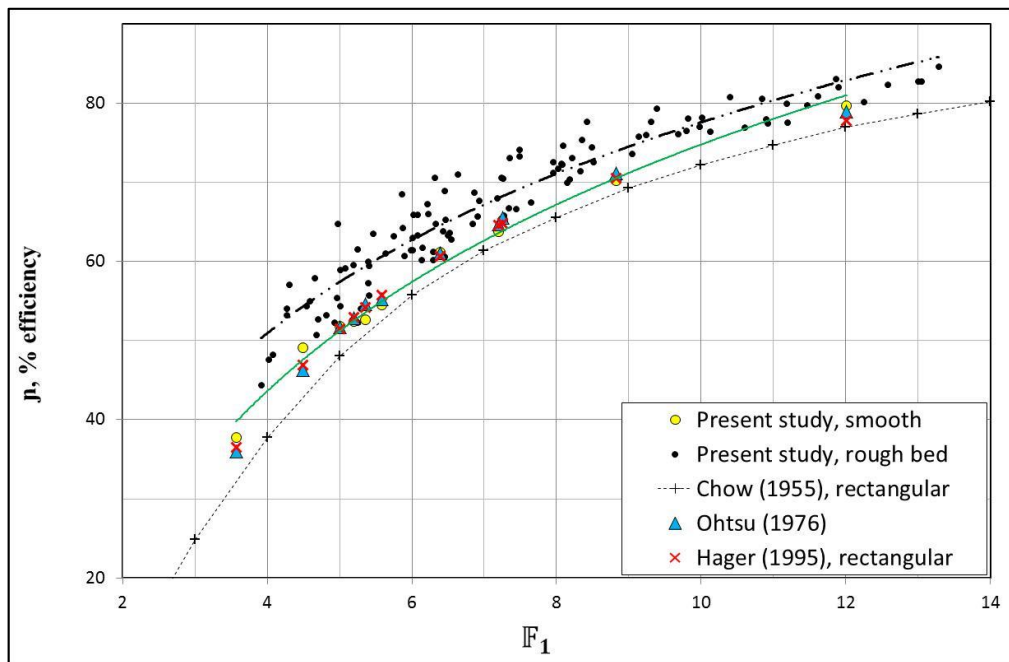


Figure 5-23: Comparison of Efficiency with Previous Studies

Figure 5-24 represents the effect of incoming Froude number on % efficiency of energy dissipation with the data series of past studies conducted on rough beds and the present study.

The dots illustrate the experimental series of rough bed combinations. Figure 5-24 shows that although data series of Ead and Rajaratnam (2002) fits the experimental results of present study, the data series of Ezizah at al. (2012) is different from all other three data series.

Experimental results on rough beds have similar efficiency figures with Ead and Rajaratnam (2002). This similarity confirms the conclusion of Ohtsu (1976): *“the cross sectional form of trapezoidal channels has only a little effect on the relative energy loss in a free hydraulic jump.”*

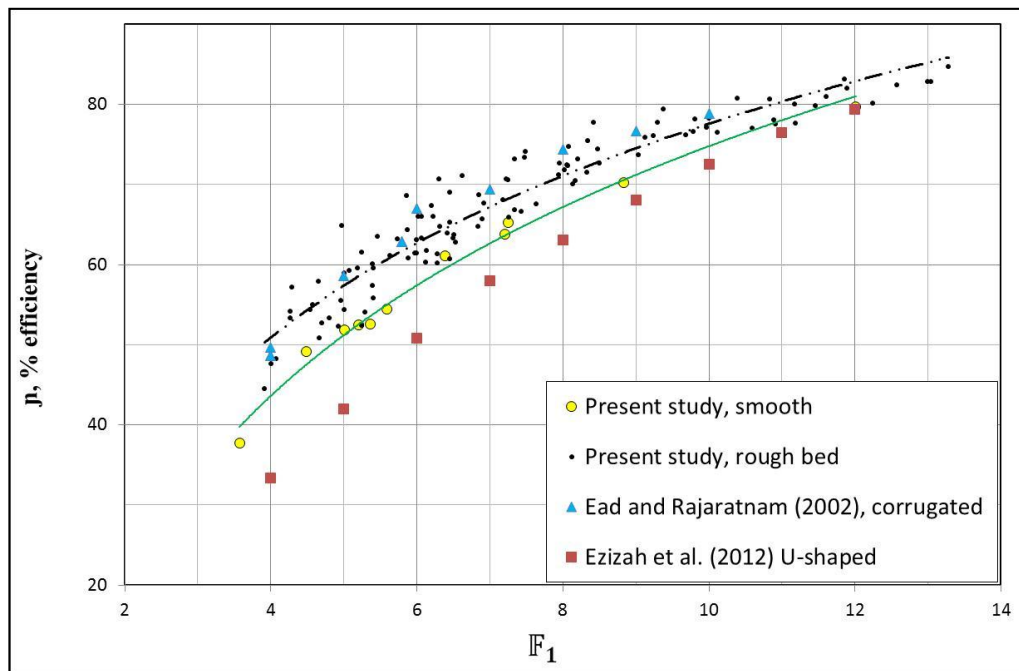


Figure 5-24: Comparison of Efficiency with Previous Studies on Rough Beds

Figure 5-25 represents the effect of different roughness intensities on energy dissipation efficiency. Figure 5-25 shows that while the least effective intensity was 33.33%, the most efficient roughness intensity was 11.11%, and the roughness intensity 16.66% is intermediate. For all rough patterns energy dissipation efficiency approaches to energy dissipation efficiency of smooth bed as Froude Number increases. This means that the effect of roughness patterns loses their effect on flow field as Froude number, F_1 , increases.

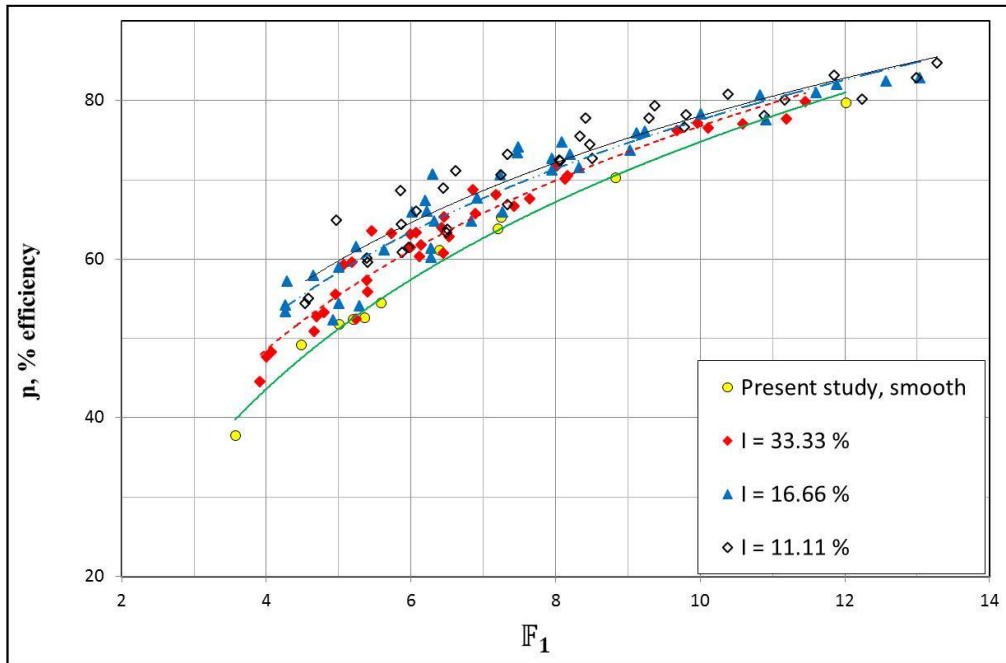


Figure 5-25: Efficiency on Rough Beds for Different Roughness Intensities

In Figure 5-26, the effect of different pitch ratios on energy dissipation efficiency was investigated. As mentioned in Sec. (5.2.1) and Sec. (5.2.2), along the different pitch ratio patterns, PR=4 series is intermediate.

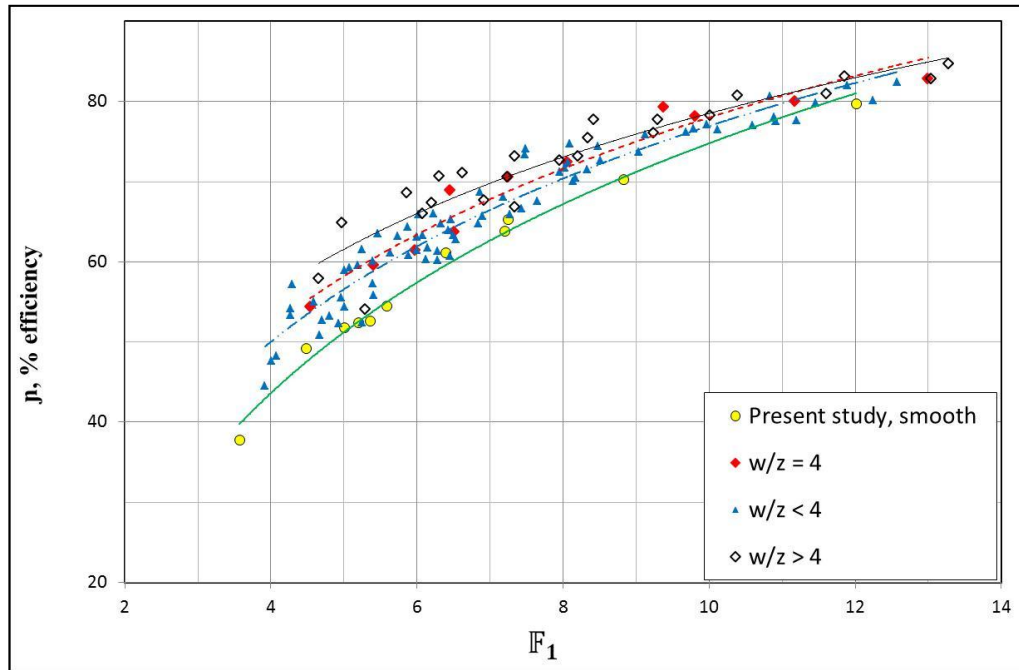


Figure 5-26: Efficiency on Rough Beds for Different Pitch Ratios

5.2.4 Gain in Energy Dissipation

“Gain in energy dissipation” parameter can be defined as the percent of the additional dissipated energy by the roughness elements with regard to the energy dissipation of a smooth jump under the same incoming Froude numbers, F_1 and flow depth, y_1 .

The parameter can be formulated as follows:

$$G = \frac{\Delta H - \Delta H^*}{\Delta H^*} \times 100 \quad (5.5)$$

where ΔH = energy loss on rough bed

ΔH^* = energy loss of hydraulic jump that would occur on smooth bed for the same incoming Froude number, F_1 , and incoming flow depth, y_1 . Obtained by means of Eq. (5.2).

The variation of the percent gain in energy dissipation G with F_1 is shown in Figure 5-27 for all experiments on rough beds.

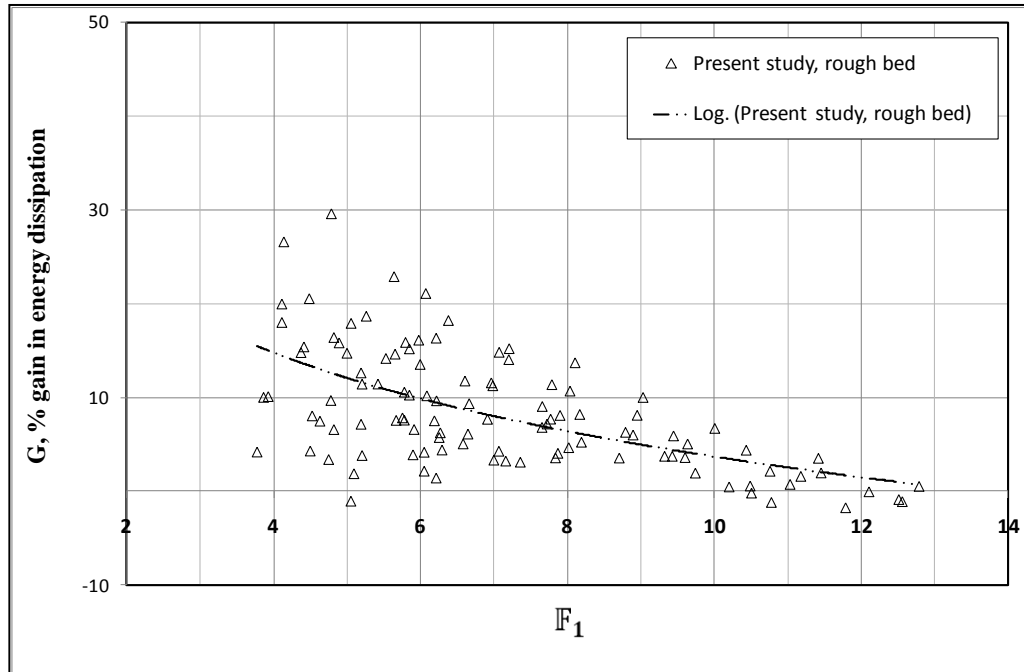


Figure 5-27: Gain in Energy Dissipation on Rough Beds

Figure 5-27 shows that the percent gain in energy loss for the jumps on rough beds decreases as incoming Froude number, F_1 , increases. The figure is the another illustration of Figure 5-23, hence it displays the same behaviour of flow field; Non-protruding roughness elements are getting less “felt” by the flow with increasing F_1 thus rough-bed characteristics converging to those of smooth bed.

The variation of percent gain in energy dissipation, G , for varying roughness intensities is presented in Figure 5-28. The gain in energy dissipation reduces with increasing non protruding roughness intensity at low and moderate Froude numbers. As mentioned before, at high Froude numbers, the effect of non-protruding roughness or flow structure inside the grooves lost their efficiency especially on energy dissipation. The reason of such a phenomenon is, while

energy dissipation is increasing by the oblique jump, the ratio of energy dissipation inside the grooves become the same or little higher.

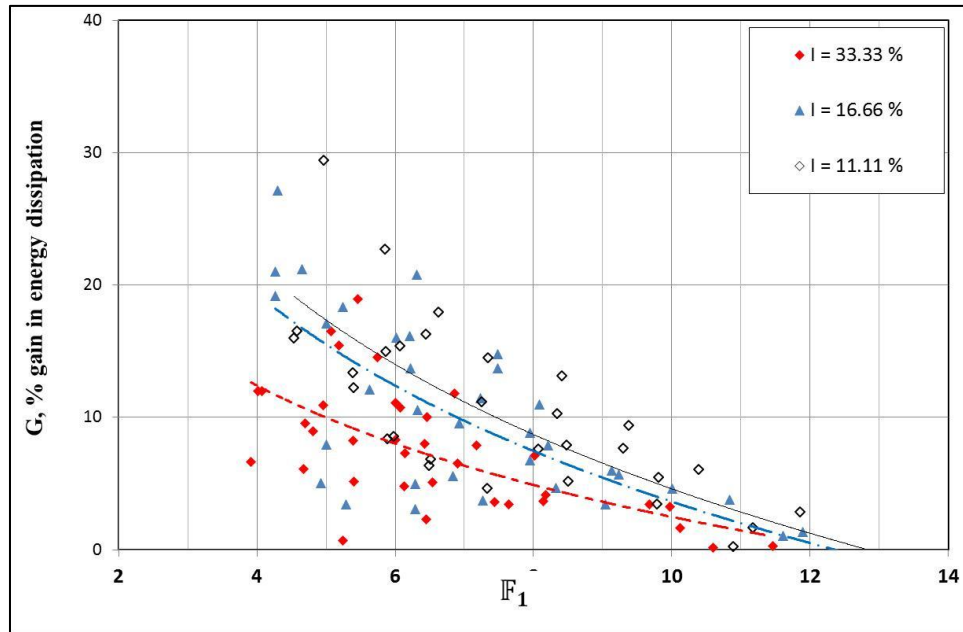


Figure 5-28: Gain in Energy Dissipation on Rough Beds for Different I Values

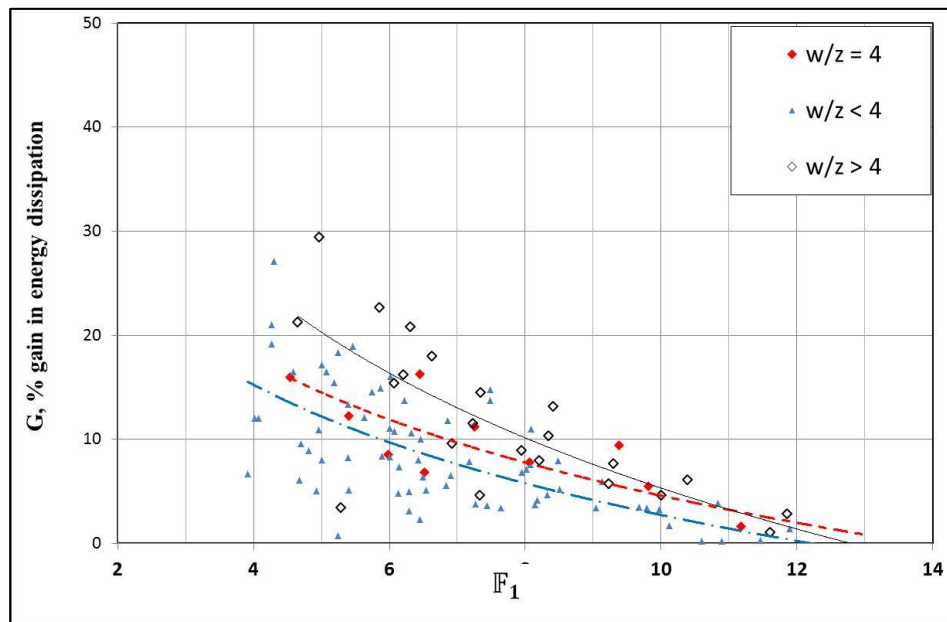


Figure 5-29: Gain in energy Dissipation on Rough Beds for Different Pitch Ratios

The variation of percent gain in energy dissipation, G , for varying pitch ratios is presented in Figure 5-29. While the pitch ratio increases, the gain in energy dissipation increases at low and moderate Froude numbers.

5.2.5 Length of Jump

Figure 5-30 shows the variation of nondimensional aeration length, L_a/y_1 with F_1 for flows over rough beds and smooth channel.

Figure 5-30 indicates that the increasing bed roughness reduces the normalized aeration length for given upstream conditions, y_1 and F_1 . While the green line represents best fit of smooth bed results, dots represents individual experiments on rough bed. Black line is the best fit of results on rough beds.

The best fit line for normalized aeration length is obtained on rough bed as;

$$\left(\frac{L_a}{y_1}\right) = 74.884 \ln(F_1) - 67.097 \quad (5.6)$$

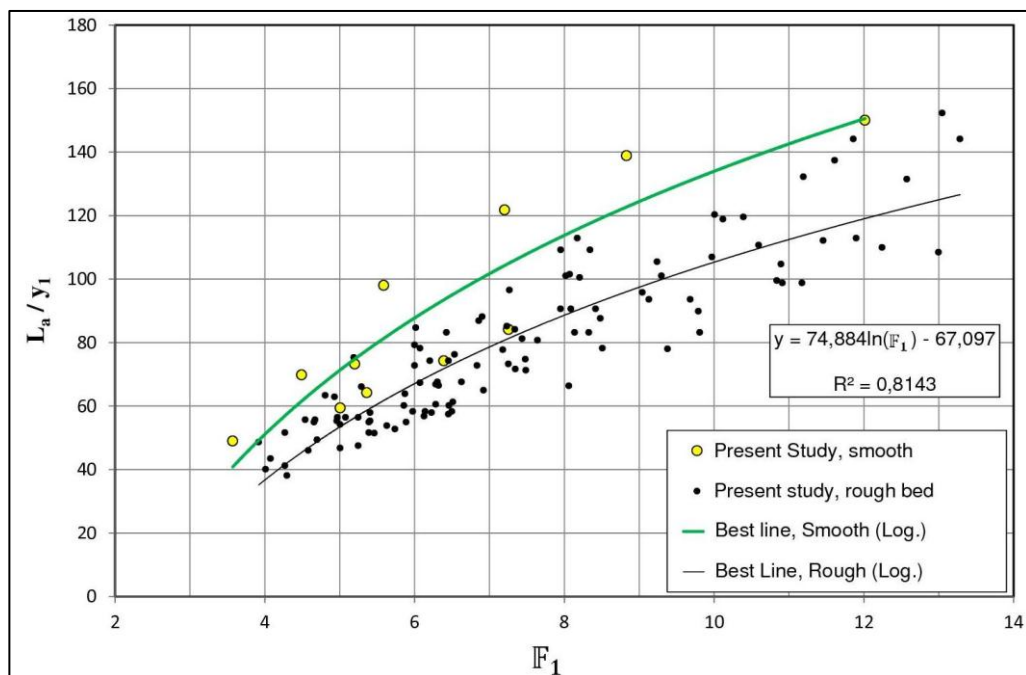


Figure 5-30: Normalized Aeration Length on Rough Beds

Figure 5-31 establishes that the effect of different roughness intensities on normalized aeration lengths. As seen from figure that, while the most efficient roughness intensity from the aeration length reduction point of view is 11.11%, the results of intensities 16.66% and 33.33% are smaller.

No significant deviance can be observed between the normalized aeration length trends of flows over roughness intensities 16.66% and 33.33%. However, it can be concluded that, while incoming Froude numbers are relatively low, the effect of intensity of 33.33% is smaller than that of intensities of 16.66%; their effects on aeration length reduction is the same at relatively high Froude numbers. Either the efficiency of 16.66% intensity loses its effect on aeration length reduction or the efficiency of 33.33% intensity increases its effect on aeration length.

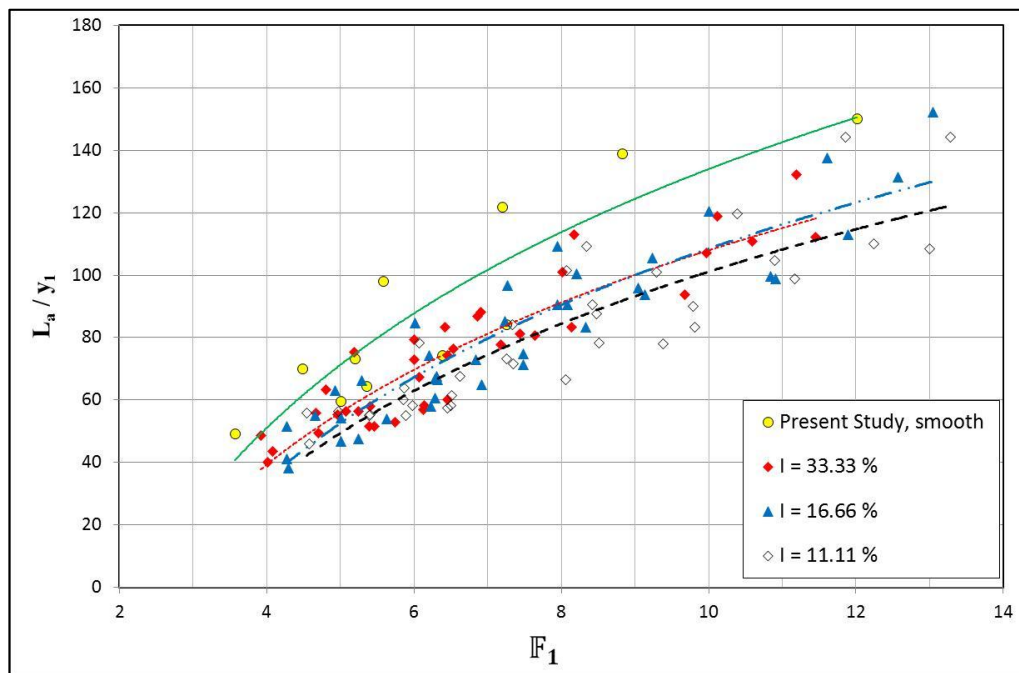


Figure 5-31: Normalized Aeration Length on Rough Beds for Different Intensities

The effect of different pitch ratios on normalized aeration length is presented in Figure 5-32. While at relatively low incoming Froude Numbers all pitch ratio patterns have similar effect on normalized aeration length, roughness patterns $PR > 4$ is less efficient than, the other roughness patterns $PR < 4$ and $PR = 4$ at high Froude numbers. In consistent to other jump characteristics, $PR = 4$ roughness pattern is more efficient than other roughness patterns with regards to normalized aeration length of a jump.

As mentioned in Section 5.1.2, the flow structure inside the grooves having different pitch ratio are different. It was also claimed that due to oblique nature of a hydraulic jump in trapezoidal channels, in contradistinction to Cui et al. (2003), the pitch ratio limit to define intermediate roughness should be different than 4 and somewhat smaller than 4.

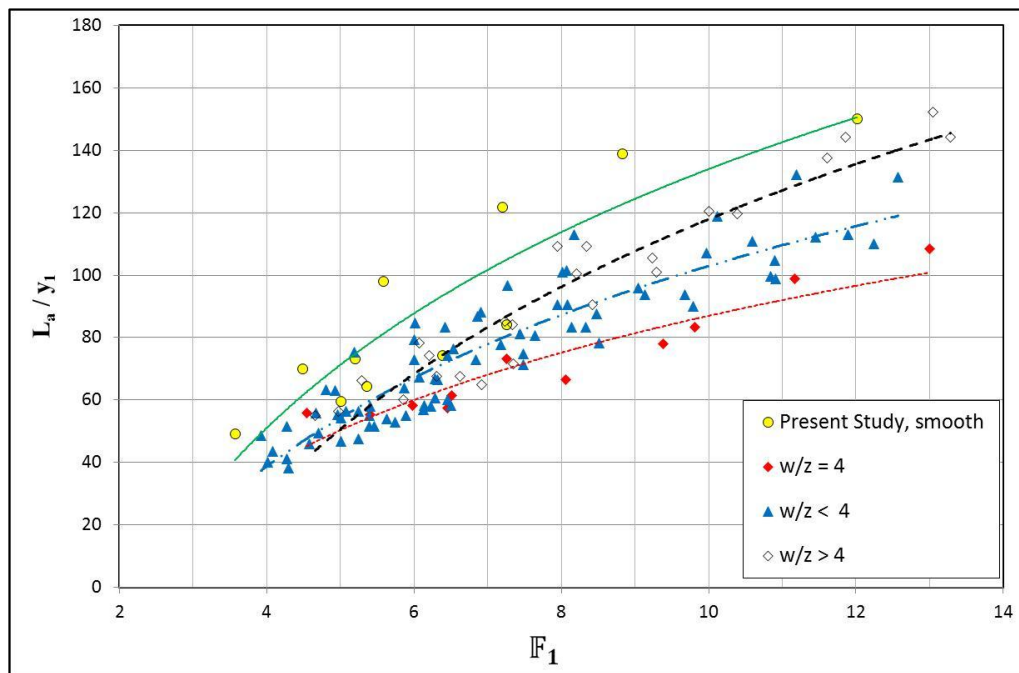


Figure 5-32: Normalized Aeration Length on Rough Beds for Different Pitch Ratios

In Figure 5-33, the percent efficiency in energy dissipation, η , is plotted against normalized aeration length. Figure 5-33 shows that PR=4 data series dissipates more energy in shorter region when compared with PR>4 and PR<4 series. In this short length of jump, due to flow coming close to the channel bed and hit the roughness element at the end of the groove and, turbulence intensity increases substantially.

For other two PR series have more streamlined flow fields inside their own grooves. Although their effect on energy dissipation was 10% different at low Froude numbers, at high Froude numbers the difference on energy dissipation distinct. Furthermore, their effect on flow field disappears at high Froude numbers.

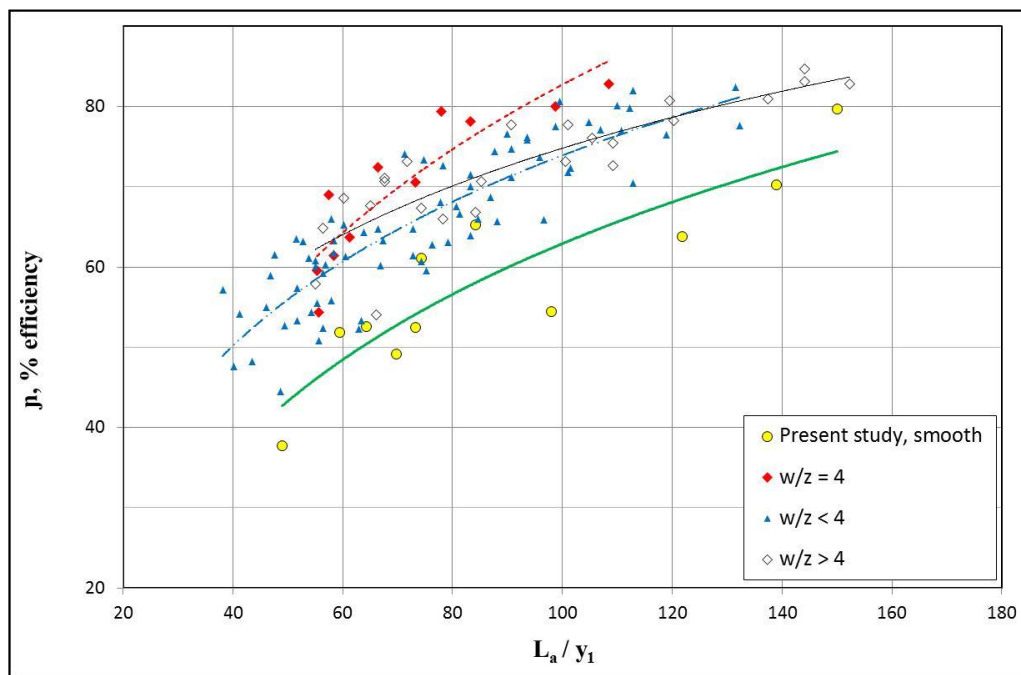


Figure 5-33: Efficiency vs. Normalized Aeration Length for Different Pitch Ratios

It was mentioned that, the loss of energy in a hydraulic jump is, in a large measure, is due to conversion of velocity head into turbulent head. Specific

energy of incoming Froude number transforms into turbulent energy first. The ratio of dissipated energy to jump length should be related with intensity of turbulence inside the flow field (Figure 5-33).

In Figure 5-33, except from relatively short jump lengths, which means low Froude numbers and flow structure inside the grooves is at pre-developing stage, PR = 4 series dissipates more energy than other series for same jump length. PR = 4 series reach the same maximum energy dissipation efficiency of series PR<4 and PR>4 at %30 shorter aeration length.

The intrusion of higher intensity level of turbulence in a short reach could be the answer of dissipating more energy in shorter length, or smaller normalized aeration lengths at same incoming Froude numbers. The rough bed pattern having PR=4 increases turbulence level immediately at the beginning of the jump and, thus the last point, where air bubbles penetrates into two successive roughness elements in flow direction is closer to hydraulic jump.

5.2.6 Wing Oscillations

Nondimensional wing oscillation L_w/y_1 values are plotted against Froude Number F_1 on Figure 5-34. Figure 5-34 shows wide spread of data. Therefore to demonstrate the effect of different roughness intensities on normalized wing oscillations Figure 5-35 is plotted. As seen from figure that, increasing bed roughness reduces the normalized wing oscillations for given upstream conditions, y_1 and F_1 . While the most efficient roughness intensity was 33.33%, the least effective intensity was 11.11%.

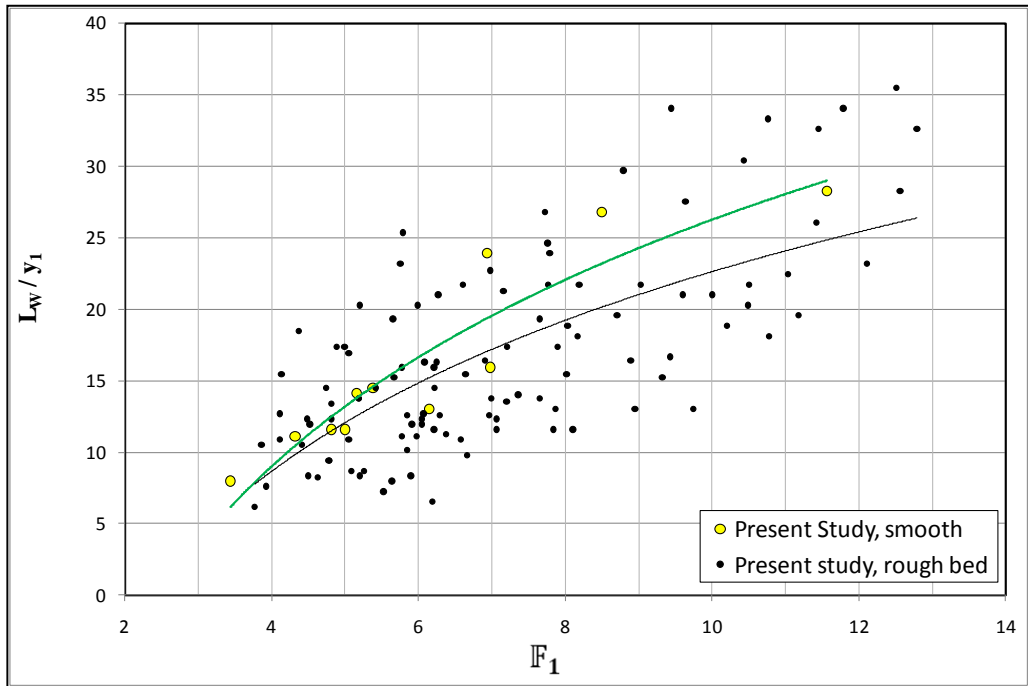


Figure 5-34: Normalized Wing Oscillations on Rough Beds

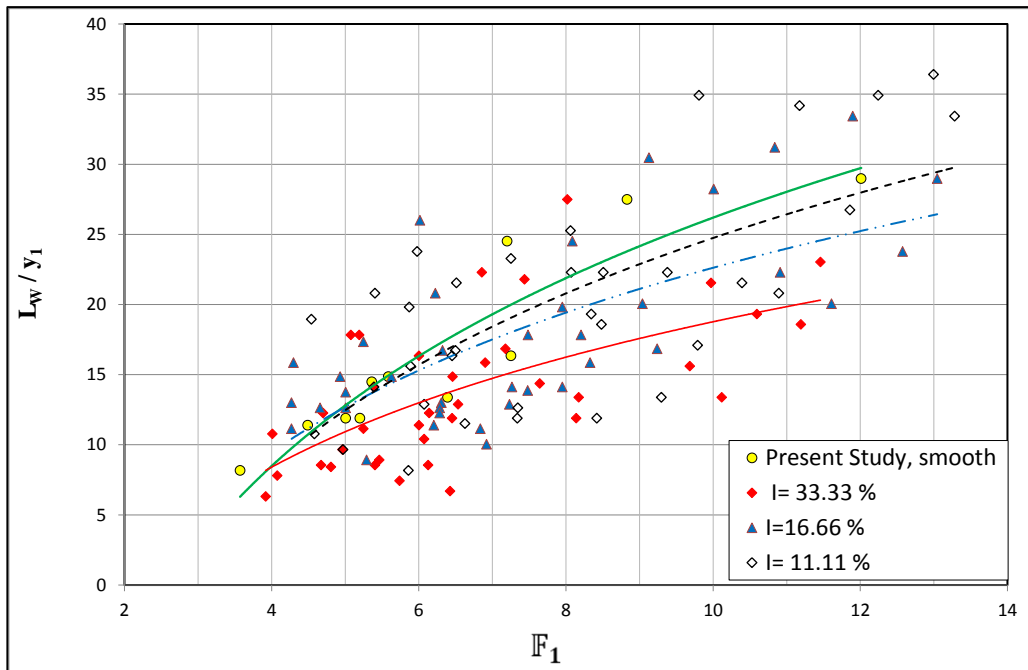


Figure 5-35: Normalized Wing Oscillations for Different Roughness Intensities

In Figure 5-36 the effect of different pitch ratios on normalized wing oscillations was investigated. Roughness patterns having pitch ratio greater than 4 was more efficient than roughness patterns having pitch ratio smaller than 4 at low Froude numbers. The experimental series of pitch ratio = 4 is irrelevant with other two series. Furthermore while roughness patterns $PR > 4$ and $PR < 4$ series are more effective than smooth channels, $PR = 4$ data series increase wing fluctuations when compared with smooth bed.

As mentioned in Section 5.2.5, flow structure inside the grooves is focus topic. The difference in geometry and flow structure should be effective on this behaviour of the wing oscillations. It was stated that wing oscillations are feed on with recirculations at downstream of oblique jump.

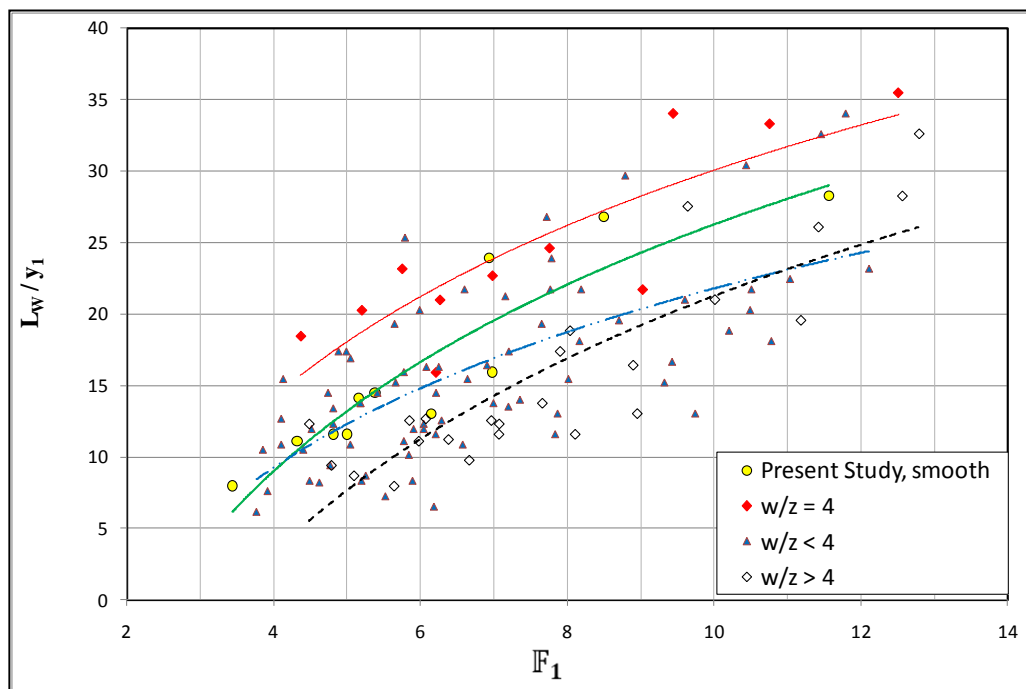


Figure 5-36: Normalized Wing Oscillations for Different Pitch Ratios

5.3 Experiments on Rough Side Walls

It was observed through experimental runs that, the effect of wall roughness on flow structure and jump characteristics is totally different than the effects of rough beds. As mentioned in Section 3.2, the triangular side areas at the downstream end, permit a certain degree of recirculation. This water is fed back into the jump and hence produces greater energy dissipation. In Section 5.1.2 it was understood that the difference in energy dissipation depends on both width of channel and side slopes.

The circulations close to the side walls form rollers between successive elements of the roughness pattern. Circulations on top of oblique jump usually splash to wall at angle, and sometimes they may hit the side walls perpendicularly. By the help of rollers and impact effect a part of kinetic energy of back circulation was dissipated (Figure 5-37).



Figure 5-37: The Effect of Side Roughness on Hydraulic Jump

5.3.1 The Sequent Depths

Figure 5-38 shows that the increasing wall roughness has approximately no effect on reduction of the required tailwater depth for given upstream conditions, y_1 and F_1 . The line represents best fit of smooth bed results and dots represents experiments on rough channel walls.

Figure 5-39, Figure 5-40, and Figure 5-41 show that there is a slight difference between normalised sequent depths of experiments conducted on smooth channel and channel with smooth walls, but it is negligible. The effect of different roughness intensities and different roughness pitch ratios on sequent depth ratio is also negligible.

These results prove that, for hydraulic jumps on rough beds, the main factor which decreases sequent depth ratio and increase energy dissipation efficiency is the friction on the bed of the channel.

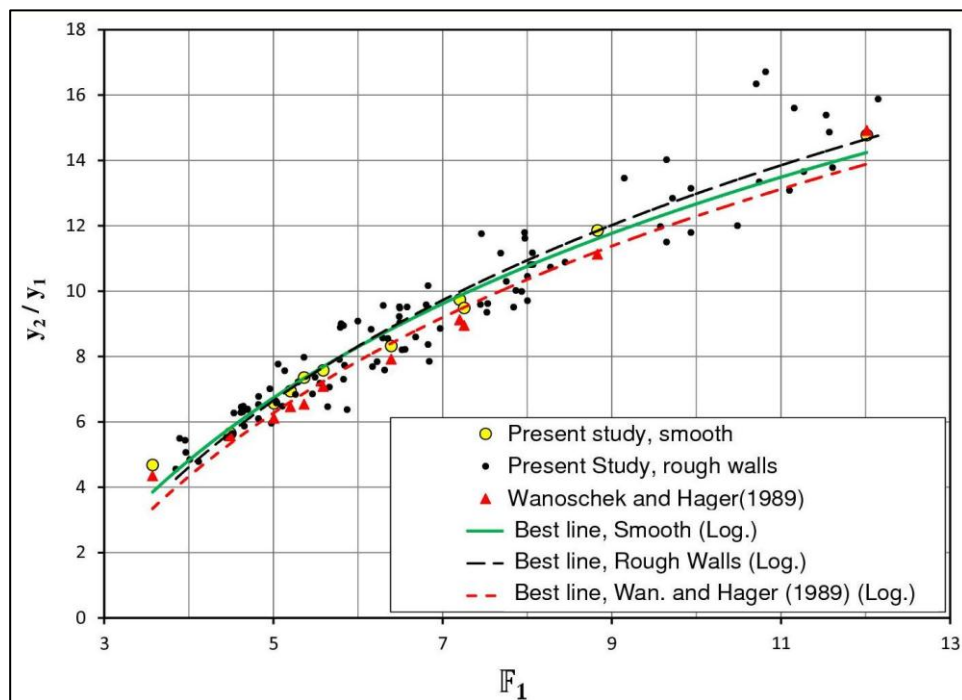


Figure 5-38: Comparison of Sequent Depth Ratio for Rough Walls

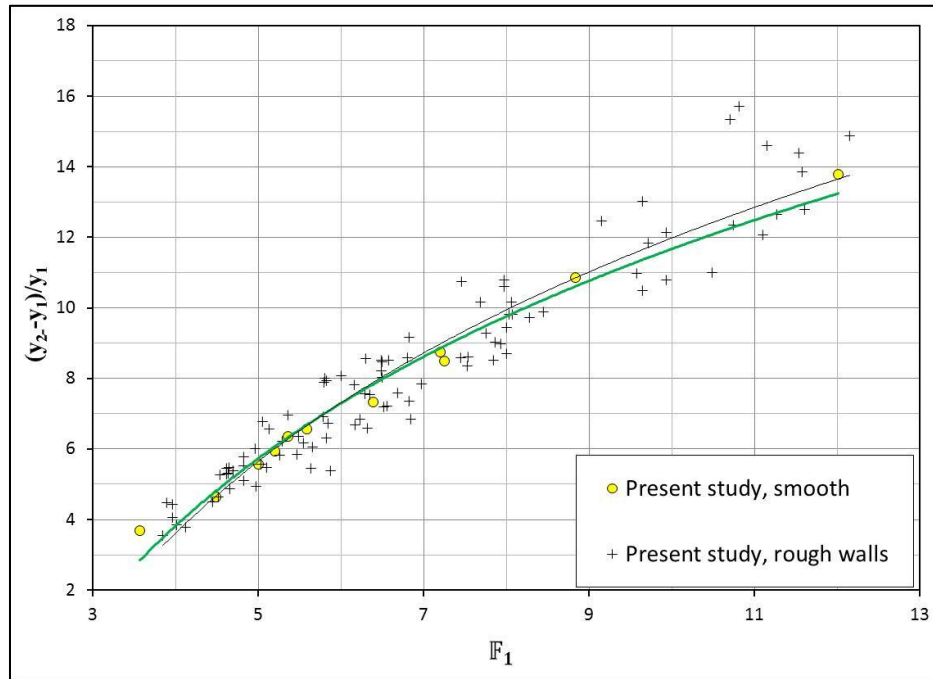


Figure 5-39: Normalized Sequent Depths for Rough Walls

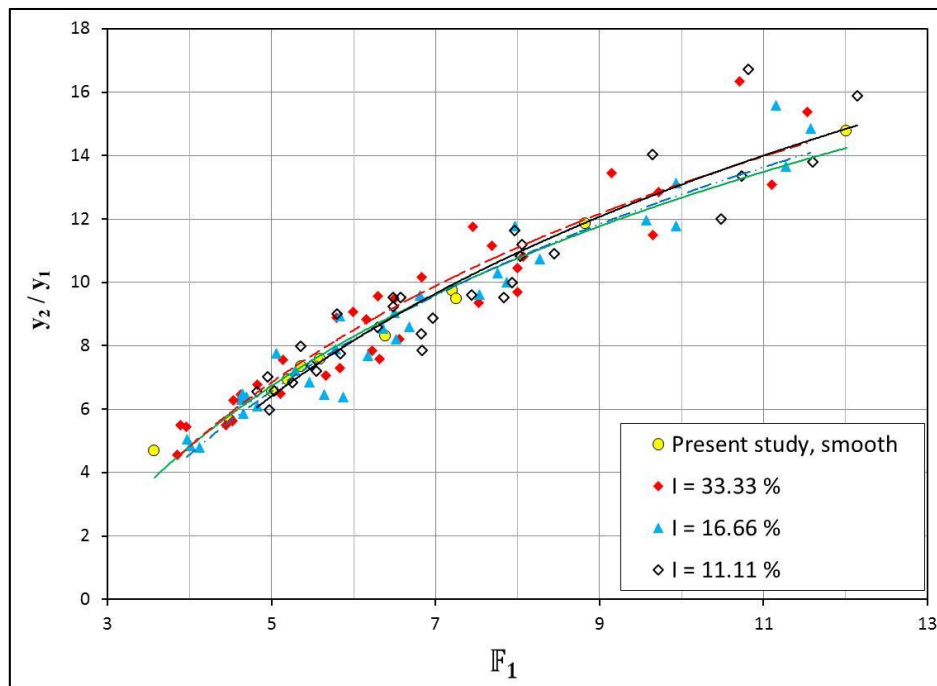


Figure 5-40: Sequent Depth Ratio of Different Wall Roughness Intensities

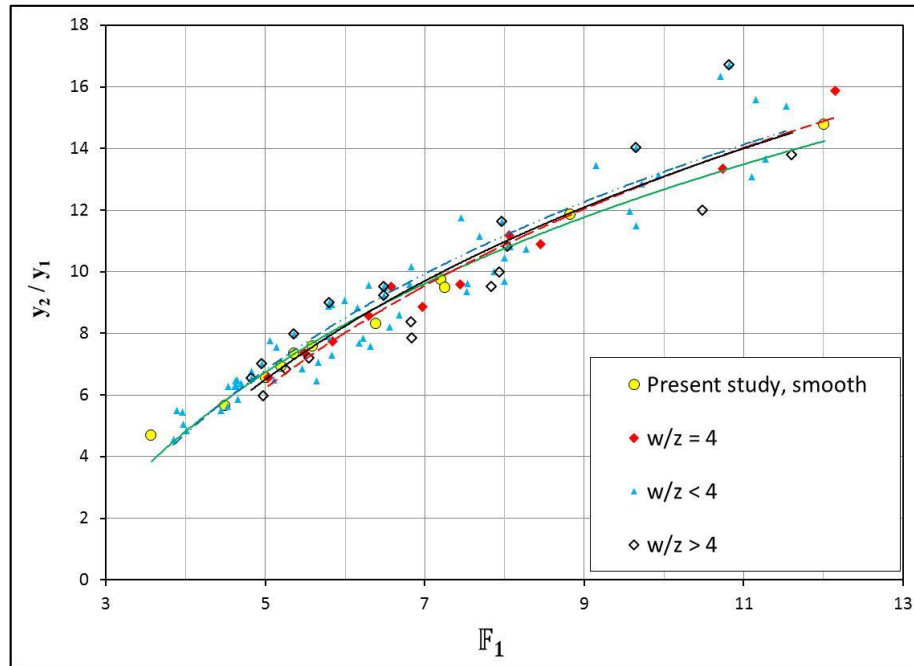


Figure 5-41: Sequent Depth Ratio of Different Wall Roughness Pitch Ratios

Therefore, it can be concluded that the rough walls are less effective and only a small part of the secondary flows are dissipated at the side areas, which are generally of triangular shape and which are not directly influenced by the jet.

5.3.2 Efficiency of Energy Dissipation

Figure 5-42 shows the efficiency of energy dissipation of a jump on rough side walls and its comparison with smooth channel and past studies. In Figure 5-42, while green line represents experiments conducted on smooth channel, dashed line represents the best fit of the data obtained in the present study. As can be seen from the figure, efficiency of energy dissipation of rough side walls are similar with jumps on smooth beds, proposed formula of Ohtsu (1976) for trapezoidal channels (Eq. 3.15), and formula of Hager (1995) (Eq. 2.13) are also given in Figure 5-42.

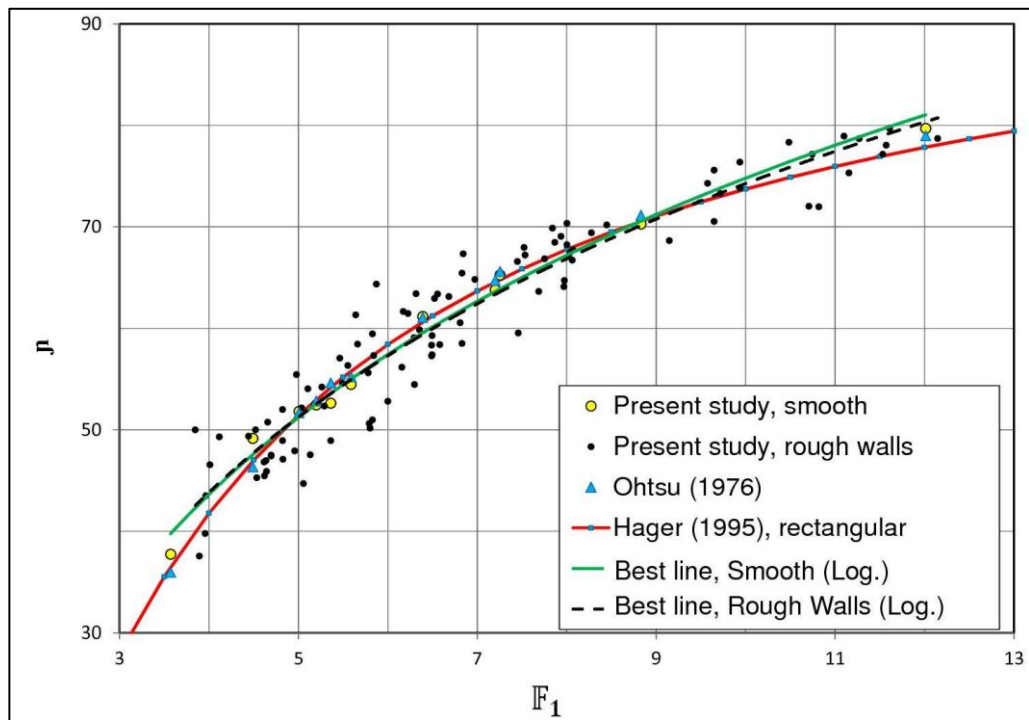


Figure 5-42: Comparison of Efficiency with Previous Studies on Rough Side Walls

Application of roughness pattern on side walls of a trapezoidal channel has negligible effect on efficiency of energy dissipation as shown in Figure 5-42. Due to negligible effect on energy dissipation, the gain in energy dissipation is also negligible.

While as F_1 increases, efficiency of energy dissipation increases (Figure 5-12) not only for of rough walls, but also for smooth channels. Ohtsu's proposed formula (Eq. 3.16), conducted on trapezoidal channels, and equation of Hager (1995) (Eq. 3.13), for rectangular channels are well corresponding.

Sharp (1977) pointed out that for $F_1, > 9$, the oblique jump always formed and in the range of $4 < F_1 < 9$ oblique jump forms but it is developing. The same F_1 range also observed in the analysis.

It was claimed the efficiency of tailwater reduction was related with unstable characteristics and oblique structure of jump, due to (Figure 5-12) higher depth reduction in the range of $4 < F_1 < 9$ than rectangular channels.

The splashing direction of an oblique jump changes often in the range of $4 < F_1 < 9$ and, this action results in more energy dissipation due to secondary flows. Secondary flows was also divided into three parts; intersecting, downstream and upstream flows.

While F_1 is increasing linearly for the same depth of flow, velocity increases quadratically. It can be claimed that the splashing velocity of water increases quadratically also. The dissipated energy is related with kinetic energy converted to turbulence, hence roughness elements increases turbulence intensity at the walls.

5.3.3 Length of Jump

Figure 5-43 represents the effect of incoming Froude number on normalized aeration length of hydraulic jump on rough side walls with the data series of present study on smooth channel section. The dots illustrate the experimental series of rough wall combinations.

Figure 5-43 shows there is almost no difference between smooth channel and rough side walls.

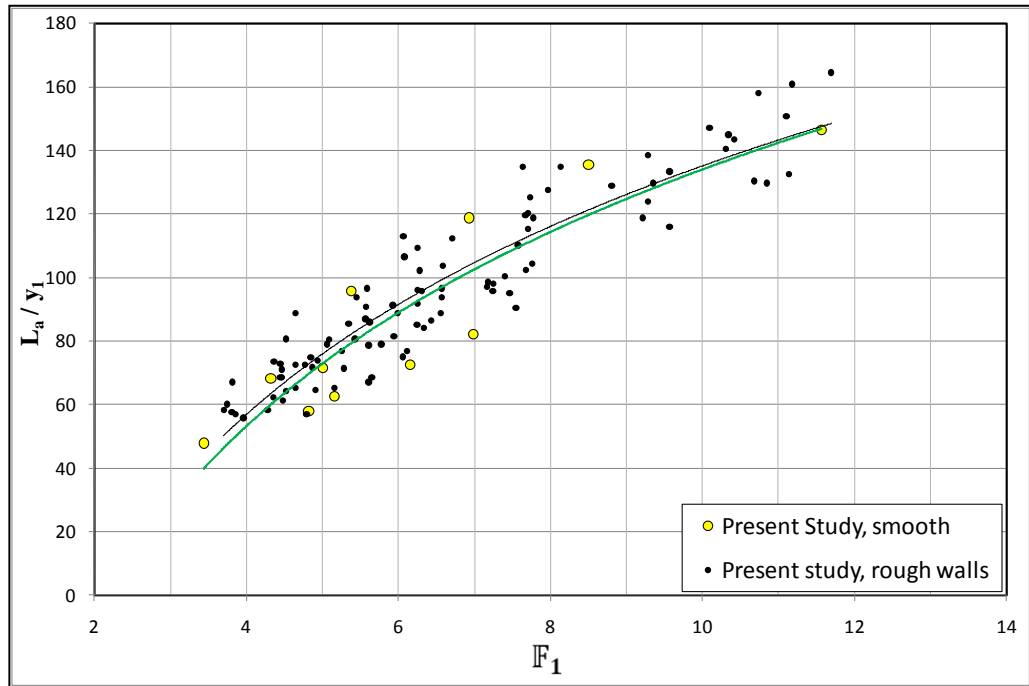


Figure 5-43: Normalized Aeration Length on Rough Side Walls

5.3.4 Wing Oscillations

As mentioned in Section 5.2.6, only a small part of the secondary flows dissipated at the side areas, which are generally of triangular shape and which are not directly influenced by the jet.

Figure 5-44 indicates that the increasing wall roughness reduces the normalized wing oscillations for given upstream conditions, y_1 and F_1 . The green line represents best fit of smooth bed results and, dots represent the data on rough walls. Black line is the best fit for rough walls.

Figure 5-44 shows that as Froude Number increases, the wing oscillation becomes smaller than that on smooth walls. This indicates while Froude Number, F_1 , increases, flow inside the grooves increase their effects on wing oscillations.

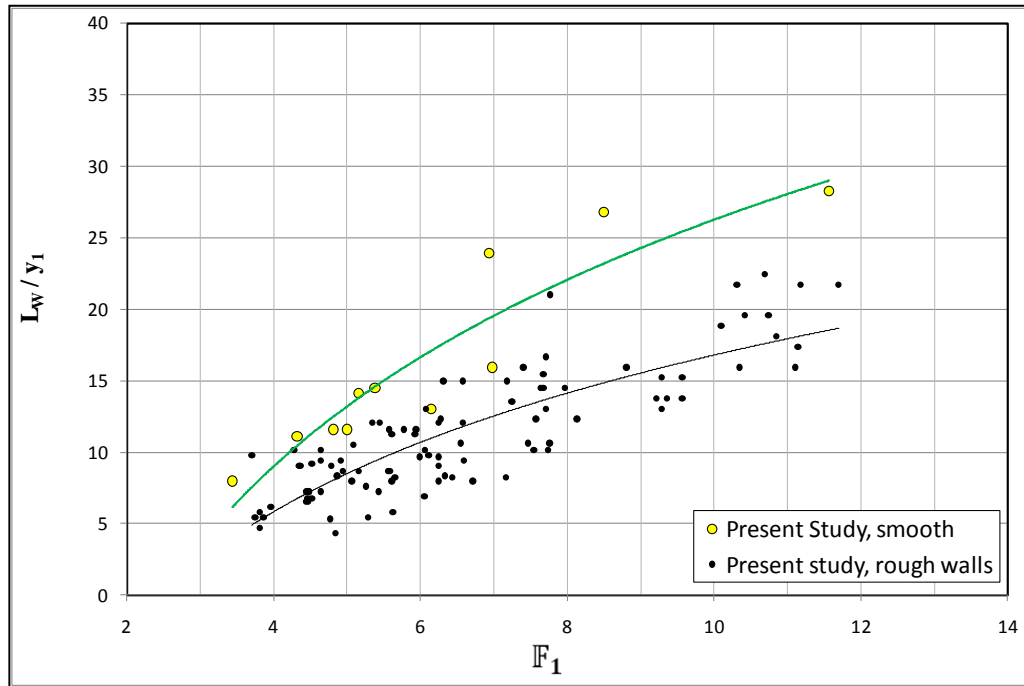


Figure 5-44: Normalized Wing Oscillations on Rough Side Walls

This behaviour of the wing oscillations should be the result of the difference in geometry and hence flow structure, in which the wing oscillations are fed by the recirculations at downstream of an oblique jump.

Figure 5-45 illustrates that the effect of different roughness intensities on normalized wing oscillations. As seen from figure that, increasing wall roughness reduces the normalized wing oscillations for given upstream conditions, y_1 and F_1 . While the most efficient roughness intensity is 11.11%, the least effective intensity is 33.33%. Whatever the value of Froude Number F_1 , wing oscillations are shorter considerably than that on smooth channels.

The wing oscillations for the roughness intensity of 16.66% series approaches to the wing oscillations for the roughness intensity 11.11% series at high incoming Froude numbers. As Froude number increases, flow structure might be changing inside and just outside the groove for $I=16.66\%$. This may cause more reduction in wing oscillation length.

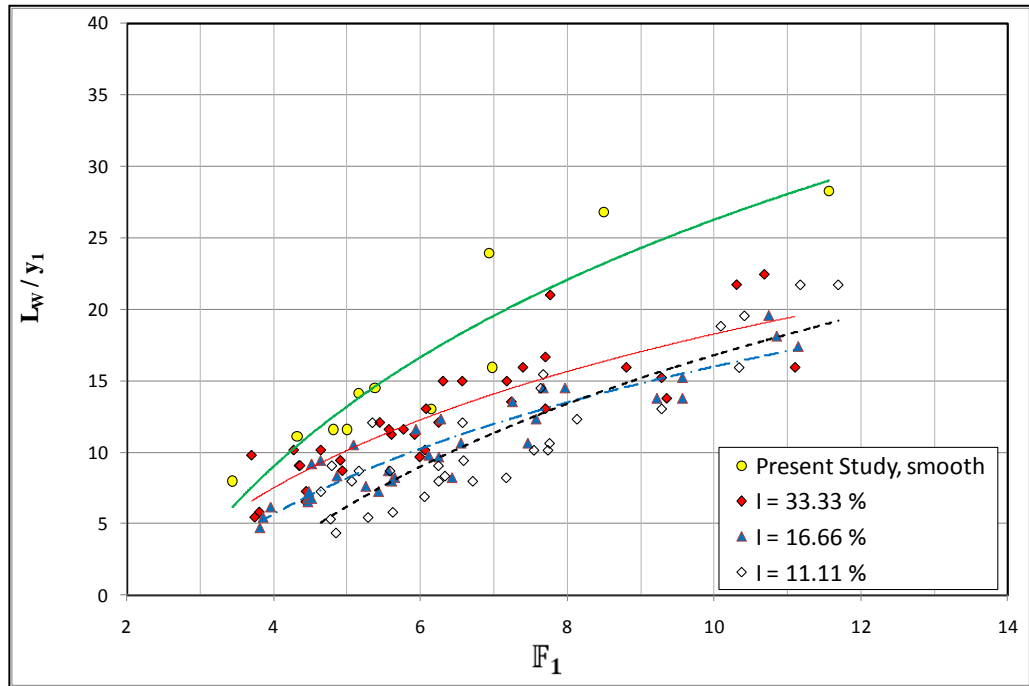


Figure 5-45: Dimensionless Wing Oscillations on Rough Side Walls for Different Roughness Intensities

Figure 5-46 shows normalized wing oscillations on rough side walls for different pitch ratios and its comparison with that on smooth channel. The green line represents experiments conducted on smooth channel, other lines represents the best fits of PR=4, PR>4 and, PR<4 series. As can be seen from the figure, the normalized wing oscillations of rough side walls are approaching to a limit of $L_w/y_1 \approx 20$ as the Froude Number increases. This corresponds to 40% reduction in wing oscillation compared to that on smooth walls.

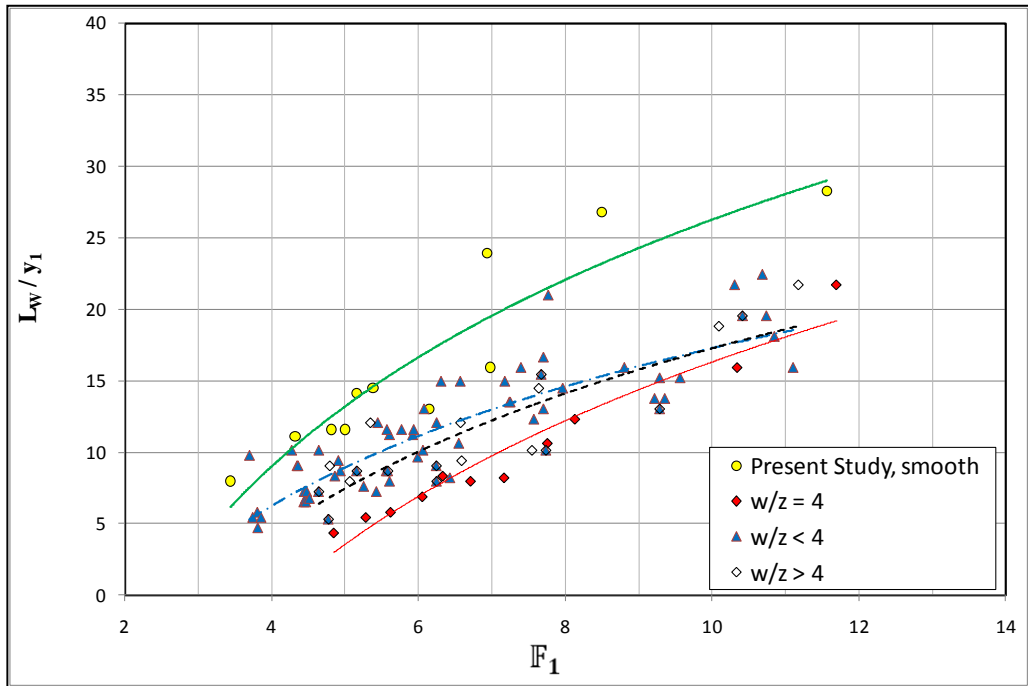


Figure 5-46: Normalized Wing Oscillations on Rough Side Walls for Different Pitch Ratios

CHAPTER 6

CONCLUSION AND RECOMMENDATIONS

The present study was conducted with the purpose of identifying the effects of roughened bed and side walls in trapezoidal channels upon the characteristics of hydraulic jumps. The characteristics of the hydraulic jump were investigated experimentally for a range of Froude numbers 4.61 to 14.68. The hydraulic jump in a trapezoidal channel of 60° side slopes was analyzed. Total of 217 tests were conducted. Nine different roughness patterns were installed separately on channel bottom and side walls throughout the experiments.

From the results and discussions, the following conclusions can be drawn:

Flow features

- The observed sequent depth ratios conducted on smooth trapezoidal channels with the prediction based on the conventional momentum approach compared well.
- It was observed that oblique jump did not always slew to the same side.
- Pitch ratio limit to define intermediate roughness is smaller than 4, for trapezoidal channels.

Sequent depths

- The observed sequent depth ratios with the experimental data of other studies conducted on smooth trapezoidal and rectangular channels are comparing well.

- The most efficient roughness intensity is 11.11%; it reduces the sequent depth ratio by 10-33% depending on the incoming Froude number, F_1 . The least effective intensity was 33.33%, having a reduction capacity in sequent depth ratio of 7-20%.
- The roughness pattern of rough bed having PR=4 series shows behaviour of intermediate roughness, having reduction capacity of 24-13%. At low Froude numbers the effect of PR=4 was intermediate, having 24% reduction capacity, at higher Froude numbers have similar flow field with PR>4, having 15% of sequent depth reduction capacity. PR<4 series have sequent depth reduction capacity of % 15 to 8%.

Depth reduction factor

- Rough side walls do not have any effect on depth reduction.

Efficiency of energy dissipation

- The most efficient roughness intensity is 11.11%, and the roughness intensity 16.66% is intermediate for efficiency of energy dissipation. Although the least effective intensity was 33.33%, it's 19% to 2% more efficient than that on smooth beds,
- PR = 4 series reach the same maximum energy dissipation efficiency of series PR<4 and PR>4 at %30 shorter aeration length.
- Non-protruding roughness elements are getting less “felt” by the flow with increasing F_1 , and all rough patterns converge to energy dissipation efficiency of smooth bed.
- While the pitch ratio increases and intensity decreases, the gain in energy dissipation increases at low and moderate Froude numbers.

- Application of roughness pattern on side roughness of a trapezoidal channel has no effect on efficiency of energy dissipation and gain in energy dissipation.

Length of Jump

- Aeration length of a hydraulic jump, L_a , can be used as a scaling parameter for hydraulic jumps in trapezoidal channels. Aeration length is longer than the length of jump.
- The bed roughness reduces the normalized aeration length for given upstream conditions, y_1 and F_1 .
- The most efficient roughness intensity in reducing length of jump was 11.11%, the effect of intensities 16.66% and 33.33% was similar and smaller.
- While at relatively low incoming Froude Numbers all pitch ratio patterns have similar effect on normalized aeration length, roughness pattern having $PR=4$ was more efficient in reducing length of jump than other roughness patterns at high Froude numbers. $PR=4$ data series dissipates more energy in shorter region when compared with $PR>4$ and $PR<4$ series. It might be due to the flow structure between roughness elements.
- $PR = 4$ series reach the same maximum energy dissipation efficiency of series $PR<4$ and $PR>4$ at %30 shorter aeration length.
- For the rough side walls, at relatively high Froude numbers, there is no difference with aeration length of jumps on smooth channel.

Wing Oscillations

- The bed roughness intensities reduces the normalized wing oscillations for given upstream conditions, y_1 and F_1 .
- The most efficient roughness intensity in reducing wing oscillations is 11.11%, while the least effective intensity is 33.33%.
- Roughness patterns having $PR > 4$ is more efficient than, roughness patterns having $PR < 4$ at low Froude numbers. Roughness patterns having $PR = 4$ data series increase wing fluctuations when compared with smooth bed.
- Both for rough beds and side walls, hydraulic jump wing oscillations are about 40% smaller than that on smooth bed conditions.

Considering the favourable changes in the jump parameters such as decrease in depth ratio, reduction in required tailwater depth, decrease in wing length and, increase in energy dissipation along jump on rough beds, the results of these experiments indicate that forming jumps on rough trapezoidal channels may become an attractive design approach which can be applied to energy dissipation structures.

Further work should be done in the case of jumps having $PR = 4$ with alternative rough wall and bed combinations and, especially concentrate on aeration distribution and 3D velocity recordings for investigation of flow structure through jump.

REFERENCES

- Afzal, N., & Bushra, A. (2002). Structure of the turbulent hydraulic jump in a trapezoidal channel. *Journal of Hydraulic Research*, 40(2), 205-213.
- Ali, K., & Ridgway, A. (1977). Hydraulic Jumps in Trapezoidal and triangular Channel. *Proc. Instn Civ. Engrs.*(63(3)), 203-214.
- Ayanlar, K. (2004). *Hydraulic Jump On Corrugated Beds*,. Ankara: Ms. Thesis, Middle East Technical University, Department of Civil Engineering.
- Bakhmateff, B. A. (1932). *Hydraulics of Open Channels*. New York and London: McGraw-Hill.
- Bakhmeteff, & Matzke. (1936). The Hydraulic Jump in Terms of Hydraulic Similarity. *Trans. Am. Soc. C.E.*, No. 101, 639.
- Carollo, F., Ferro, V., & Pampalone, V. (2007). Hydraulic Jumps on Rough Beds. *Journal of Hydraulic Engineering*(133-9), 989-999.
- Chanson, H. (1996). *Air bubble entrainment in free-surface turbulent shear flows*. London: Academic Press.
- Chanson, H. (2004). *The Hydraulics of Open Channel Flow:An Introduction*. London: Elsevier Butterworth-Heinemann.
- Chaudry, M. H. (2008). *Open-Channel Flow*. Columbia: Springer.
- Chow, V. t. (1959). *Open Channel Hydraulics*. McGraw-Hill.
- Cui, J., Patel, V., & Ching-Long, L. (2003). Large-eddy Simulation of Turbulent flow in a Channel with Rib Roughness. *International Journal of Heat and Fluid Flow*, (24) 372-388.
- Çelik, H., Birol, B., & Göğüş, M. (2003). Effect of Roughness on Hydraulic Jump Properties,. *I. National Hydraulic Engineering Symposium*. İzmir.

- Ead, S., & Rajaratnam, N. (2002). Hydraulic Jump on Corrugated Beds. *Journal of Hydraulic Engineering*, Vol.128, No.7, pp. 656-662.
- Ead S., Rajaratnam N., Katapodis, C., & ADE, F. (2000). Turbulent Open-Channel Flow in Circular Corrugated Culverts. *Journal of Hydraulic Engineering*, Vol.126, No.10, pp. 750-757.
- Ead, S., I. H. Elsebaie “Effect of bed corrugations on the characteristics of a hydraulic jump ” *Journal of Faculty of Engineering*, Al-Azhar University, CERM, 2009, Vol. 31, No. 1, pp. 238-251.
- Evcimen, T. U. (2005). *The Effect of Prismatic Roughness Elements on Hydraulic Jump*. Ankara: Ms. Thesis, Middle East Technical University, Department of Civil Engineering.
- Ezizah, G., Yousif, N., & Mostafa, S. (2012). Hydraulic Jumps on New Roughened Beds. *Asian Journal of Applied Sciences*.
- Falvey, H. T. (1990). *Cavitation in Chute and Spillways, Engineering Monograph No:42*. Denver: United State Bureau of Reclamation.
- French, R. H. (1987). *Open-Channel Hydraulics*. McGraw-Hill.
- Hager, W. (1991). Experiments on standard spillway flow. *Proc. Institution Civil Engineers*, 91, 399-416.
- Hager, W. (1995). Hydraulic Jump. In D. Vischer, & W. Hager, *Energy Dissipators* (pp. 43-60). Rotterdam: Balkema.
- Hager, W. H., & Bremen, R. (1989). *Classical Hydraulic Jump: Sequent Depths*. *Journal of Hydraulic Research*, Vol.27(5), pp. 565-585.
- Hager, W., Bremen, R., & Kawagoshi, N. (1990). Classical hydraulic jump: length of roller. *Journal of Hydraulic Research, IAHR*, 28(5), 591–608.
- Handerson, F. M. (1966). *Open Channel Flow*. New York: The Macmillian Company.
- Hsing, P. S. (1937). *The Hydraulic Jump in a Trapezoidal Channel*. Iowa City,: Thesis presented to the State University of Iowa, in partial fulfillment of the requirements; from French (1987).

- Hughes, W., & Flack, J. (1984). *Hydraulic Jump Properties Over a Rough Bed*. *Journal of Hydraulic Engineering*, Vol. 110, No.12, pp. 1755-1771.
- Izadjoo, F., & Bejestan, M. (2007). Corrugated Bed Hydraulic Jump Stilling Basin. *Journal of Applied Sciences* 7, 1164-1169.
- Khatsuria, R. (2005). *Hydraulics of Spillways and Energy Dissipators*. New York: Marcel Dekker.
- Khatsuria, R. (2009). *Hydraulic jump stilling basins on rough beds: A state of science summary*. Retrieved 03 25, 2012, from hydrotopics: <http://hydrotopics.wordpress.com/2009/05/20/hydraulic-jump-stilling-basins-on-rough-beds-a-state-of-science-summary/>
- Küçükali, S., & Chanson, H. (2008). Turbulence measurements in the bubbly flow region of hydraulic jumps. *Experimental Thermal and Fluid Science* 2008, 33, 41-53.
- Küçükali, S., & Çokgör, Ş. (2006). Investigation of hydraulic jump self aeration process. *İtü dergisi/d*, 5(5), 56-66.
- Leliavsky, S. (1959). Standing Wave. In S. Leliavsky, *Irrigation and Hydraulic Design-Vol.1- General Principles of Hydraulic Design* (pp. 273-316). London: Chapman&Hall.
- Leutheusser, H. J., & Schiller, E. (1975). Hydraulic Jump in a Rough Channel. *Int. Water Power and Dam Construction*, Vol.27, No. 5, May, 186-191.
- Leutheusser, H., Resch, F., & Solomon, A. (1972). Water Quality Enhancement Through Hydraulic Aeration. In J. L. Blanche, *Le Ressaut Hydraulique: Mesure de turbulence dans la region diphasique (the hydraulic jump: turbulence measurements in the two-phase flow region)* (pp. 279-293).
- Mohamed Ali, H. (1991). *Effect of Roughened Bed Stilling Basin on Length of Rectangular Hydraulic Jump*. *Journal of Hydraulic Engineering*, Vol.117, No.1, pp. 83-93.
- Mohed, M. B. (1970). *Hydraulic jump in trapezoidal channels*, MSc thesis. Strathclyde University.

- Mohed, M., & Sharp, J. (1971) The hydraulic jump in trapezoidal channels. *Water and Water Engineering*, 8-11.
- Negm, A. (2002). *Optimal Roughened Length of Prismatic Stilling Basins*,. Retrieved from <http://kfki.baw.de/conferences/ICHE/2002-Warshaw/authors2002.htm>.
- Nikmehr, S., & Tabebordbar, A. (2010). Hydraulic Jumps on Adverse Slope in Two Cases of Rough and Smooth Bed. *Research Journal of Applied Sciences, Engineering and Technology* 2(1), 19-22.
- Ohtsu, I. (1976). Free hydraulic jump and submerged hydraulic jump in trapezoidal and rectangular channels. *Trans. JSCE*, 8, 122-125.
- Ohtsu, I., & Yasuda, Y. (1994). Characteristics of Supercritical Flow Below Sluice Gate. *Journal of Hydraulic Engineering, ASCE, Vol. 120, No. 3*, 332-346.
- Perry, A. E., & Joubert, P. N. (1969). Rough-wall Turbulent Boundary Layers,. *Journal of Fluid Mech*, Vol. 37, pp. 383-413,.
- Peterka, A. (1958). Hydraulic Design of Stilling Basins and Energy Dissipators, *A Water Resources Technical Publication Engineering Monograph No:25*. Denver, Colorado: USBR.
- Posey, C. J., Hsing, P. S. (1938). Hydraulic Jump in Trapezoidal Channels *Engineering News-Record*, Vol 121, No. 25, pp 797-798. in Silvester (1964)
- Press, M. J. (1961). *The Hydraulic Jump*. Nedlands, Australia, 1961: engineering honours thesis presented to the University of Western Australia in French (1987).
- Rajaratnam, N. (1962). An Experimental Study of Air Entrainment Characteristics of Hydraulic Jump. *J. institution of Engineers (India)*, 42(7), 247- 273.
- Rajaratnam , N. (1965). The Hydraulic Jump As A Wall Jet. *Journal Of The Hydraulics Division* , 107-132.

- Rajaratnam, N. (1995). Almanac of Energy Dissipation Mechanism. In D. Vischer, & W. Hager, *Energy Dissipators* (pp. 23-42). Rotterdam: Balkema.
- Rajaratnam, N. (1968). Hydraulic Jumps on Rough Beds. *Trans. Eng. Inst. of Canada*, (11), 1-8.
- Rajaratnam, N., & Subramanya, K. (1968). Profiles of the Hydraulic Jump. *Journal of Hydraulic Division*, Vol.94, No.3, 663-673.
- Salehian, S., Bajestan, M., Jahromi, H., Kashkooli, H., & Kashefipour, S. (2011). Hydraulic Jump Characteristics Due to Natural Roughness. *World Applied Sciences Journal*(13-5), 1005-1011.
- Sandover, J. A., & Holmes, P. (1962). "The Hydraulic Jump in Trapezoidal Channels,". *Water Poive*, vol. 14, p. 445. from French(1987).
- Sharp, J. J. (1970). Discussion on graphical solution to hydraulic jump. *J. Hydraul. Div. ASCE*(96), 1767.
- Sharp, J. J. (1977). Discussion: Hydraulic Jumps in Trapezoidal And Triangular Channels by K. H. M. Ali & A. Ridgway. *Proc. Instn Civ. Engrs*, , 63, 761-767.
- Silvester, R. (1964). Hydraulic Jump in All Shapes or Horizontal Channels,. *Proceedings of the American Society of Civil Engineers, Journal of the Hydraulics Division from .french (2005)*, Vol 90., 23-55.
- Smetana, J. (1943). *Experimental Study of the Expanded (Submerged) Hydraulic Jump*. Prague, Czechoslovakia: T. G. Masaryk national Hydrologic and Hydrotechnic Institute.
- Şimşek, Ç. (2006). *Forced hydraulic jump on artificially roughned beds*. Ankara, Turkey: M.Sc. thesis, Department of Civil Engineering, Middle East Technical University.
- Tani, I. (1987). Turbulent Boundary Layer Development over Rough Surface. *Perspective in Turbulence Studies* (pp. 223-249). Springer-Verlag.
- Tokayay, N. (2005). Effect of channel bed corrugations on hydraulic jumps. *Proceedings of the World Water and Environmental Resources*

Congress: Impacts of Global Climate Change, May 15-19. Anchorage, Alaska: Curran Associates Inc.

Tokyay, N., Evcimen, T., & Şimşek, Ç. (2011). Forced hydraulic jump on non-protruding rough beds. *Canadian Journal of Civil Engineers*, 38(10), 1136-1144.

U.S.B.R. (1955). *Research Studies on Stilling Basins, Energy Dissipators and Associated Appurtenances.* U.S. Bureau of Reclamation, Hydraulic Laboratory Report No. Hyd-399. .

U.S.B.R. (1978). *Design of Small Channel Structures.* Denver: United States Government Printing Office.

U.S.B.R. (1987). *Design of Small Dams.* Washington D.C.: United States Government Printing Office.

Wanoschek, R., & Hager, W. (1989). Hydraulic Jump in Trapezoidal Channel. *Journal of Hydraulic Research*, 429-445.

APPENDIX A

INLET GATE CALIBRATION

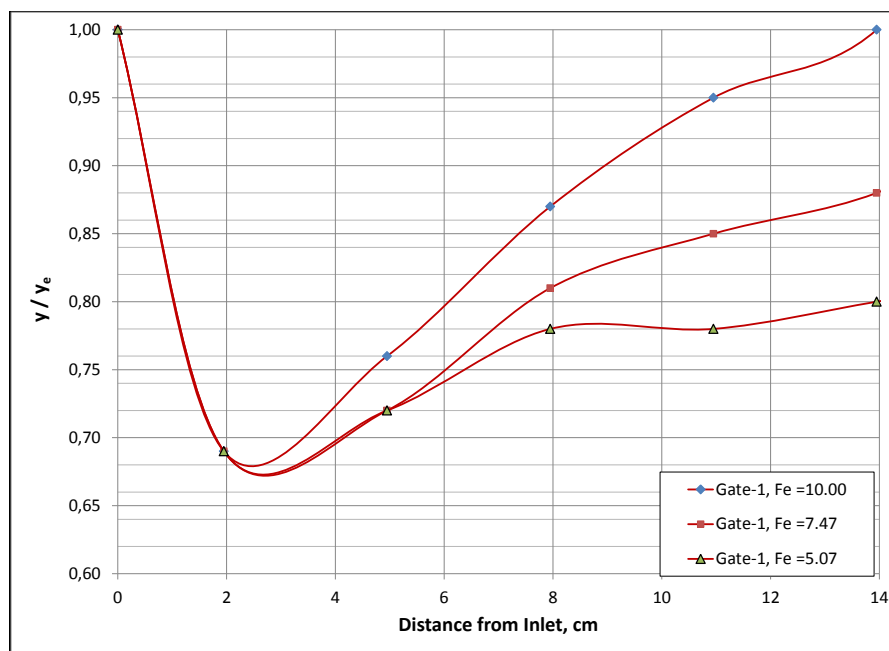


Figure A-1: Flow Surface Profile for G1

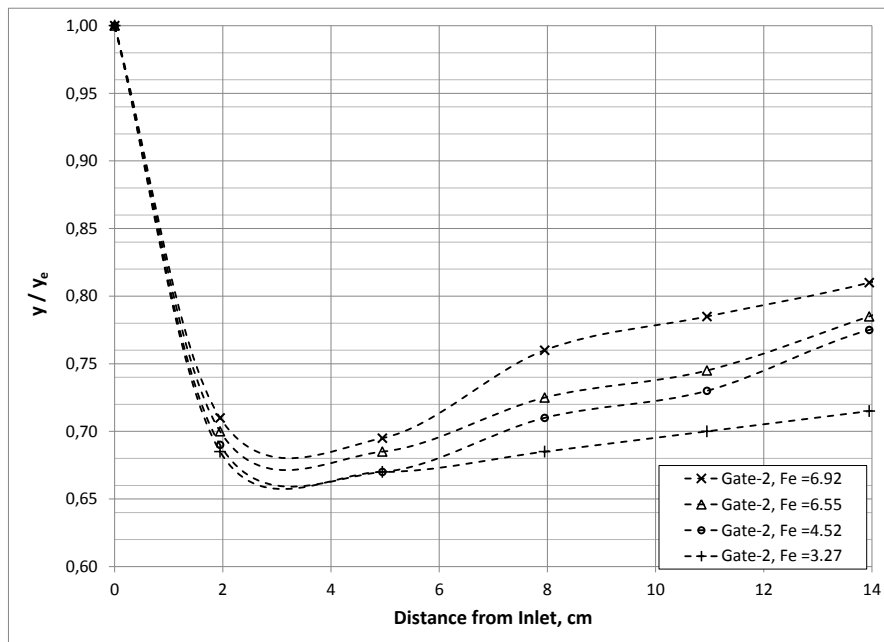


Figure A-2: Flow Surface Profile for G2

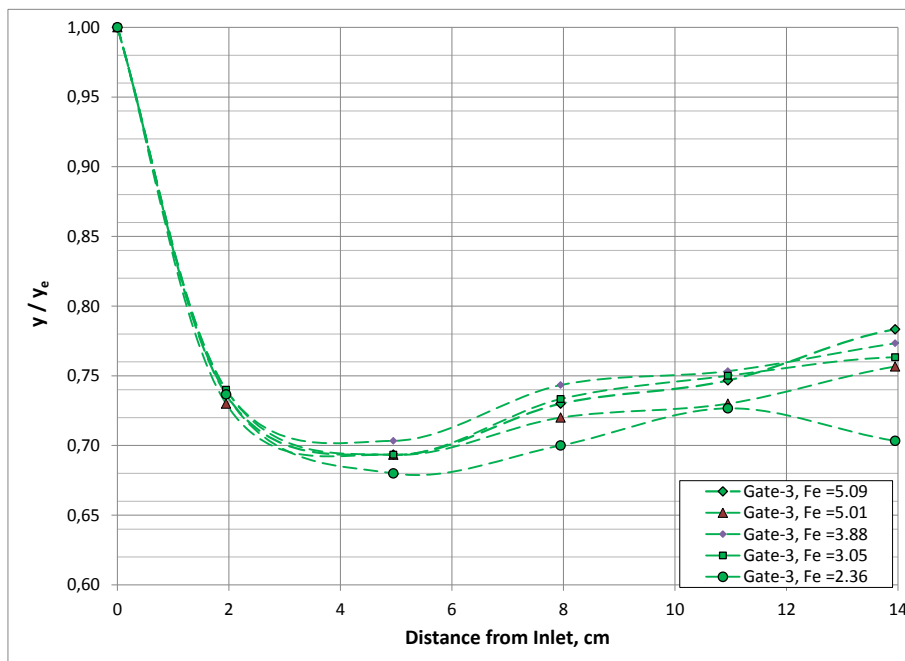


Figure A-3: Flow Surface Profile for G3

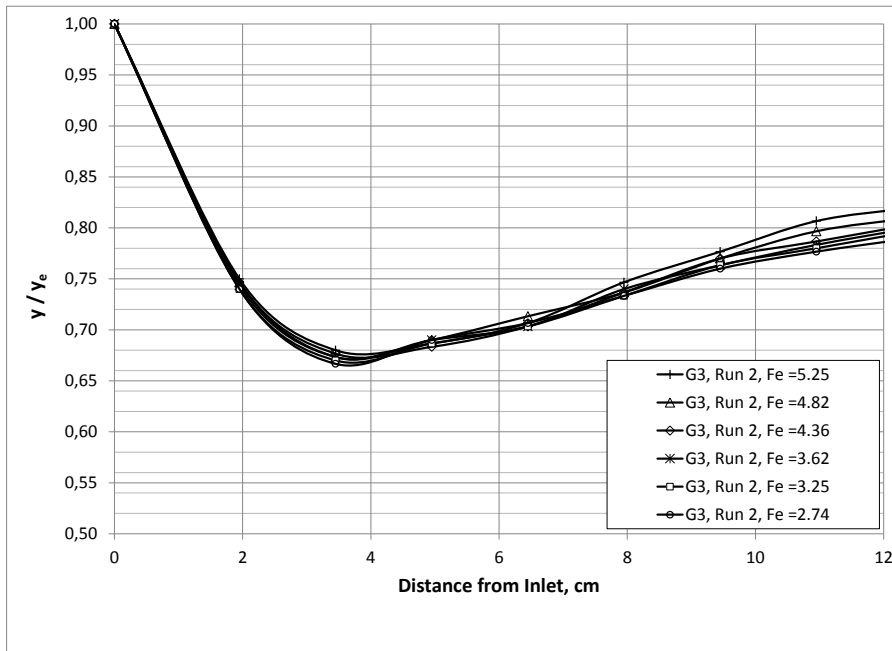


Figure A-4: Flow Surface Profile for G3

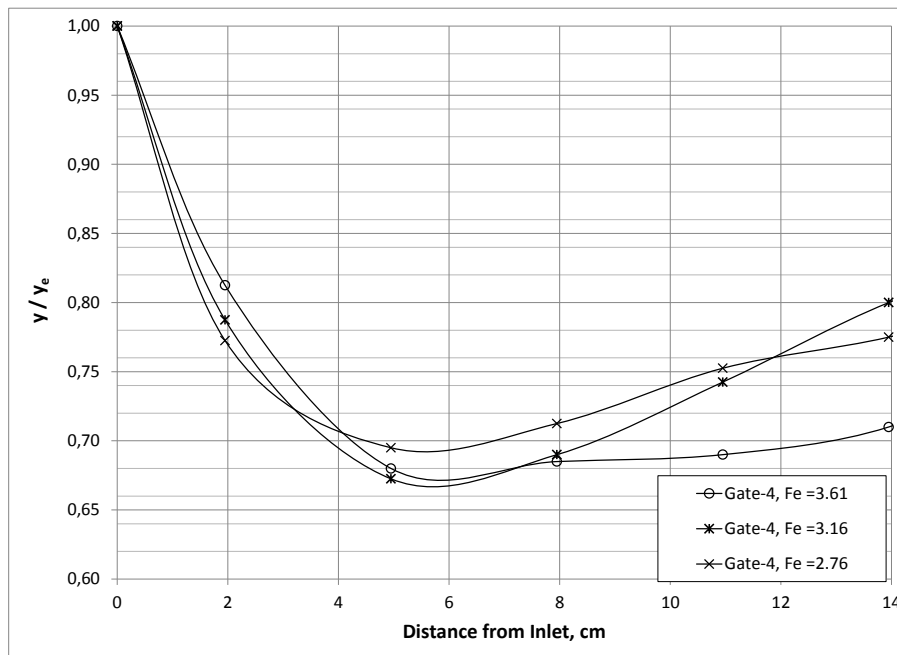


Figure A-5: Flow Surface Profile for G4

APPENDIX B

LABCARD MANAGEMENT

The following text is taken from the web page <http://www.churchill-controls.co.uk/downloads/wmman.pdf> in order to set up and use the Labcard in the Hydromechanics Laboratory at METU prior to experimental stage of this study. Since necessary documentation is not accessible in the Laboratory, the following text will certainly be helpful for prospective researchers and Labcard users and in new studies. As a final remark, it should be reminded to new researchers that the software “470.exe” should be run in DOS operating system on the computer in the Hydromechanics Laboratory at METU in order to take the digitalized output of the analog data sent by the Labcard.

There are two settings, one for the frequency and one for sensitivity made on the circuit card. For these the module must be withdrawn from the case.

Frequency Selection

The energisation frequency of the probe is selected by inserting a jumper into one of a series of 6 card mounted pins. Each pin is labeled with the approximate frequency. When probe are used in close proximity to each other there is some advantage in operating the probe at the highest frequency to reduce the ripple content of the output signal.

Sensitivity Switch

The small jumper mounted in the circuit board alters the amplitude of the energisation voltage which is applied to the SET DATUM control. For probes

up to 500mm in length the jumper should be set to position "S", i.e. with its jumper moved towards the front panel. For longer probes the jumper should be set to position "L", i.e. towards the rear plug connector to reduce the sensitivity of the SET DATUM control.

Connection of Probe

The probe may be connected either to the red 4 mm sockets on the front panel by means of the plugs provided, or by means of terminal connections at the back. The connecting cable should be a twisted pair or a flat "figure 8". No special characteristics are required and a suitable cable would be one consisting of 2 conductors each 7/0.25mm (2 amp). The energisation voltage is balanced about earth so it is important that neither of the conductors is earthed.

Lead Compensation

The instrument incorporates means for compensation for the resistance of the connecting cable to ensure that a high degree of linearity of measurements is maintained over a very wide dynamic range of probe conductivity. Disconnect the probe cable at the probe end and insert the plugs into the blue TEST sockets on the front panel. Depress the toggle switch into the TEST position, turn the SET OUTPUT control to its fully clockwise position, (i.e. maximum) and adjust the SET DATUM control until the pointer of the balance meter is in its central position (rotating the control clockwise raises the meter pointer). Depress the push button and rotate the COMP control with a screwdriver to restore the pointer to its balance position. Correct compensation is achieved when pressing and releasing the push-button results in no change in the position of the meter pointer. The plugs can then be removed from the TEST sockets and reconnected to the probe.

Output Signals

The instrument provides an output signal with a centre zero at earth potential and with maximum excursions of + and - 10 volts. Connections can be made either to the OUTPUT coaxial plug on the front panel or by terminal connections at the rear where the following signals are available:-

Terminal 1: 10V; 0; -10V

Terminal 2: 10mA; 0; - 10mA from a source impedance of 1 K ohm.

Terminal 3: 0.05 mA; -0.05 mA with a parallel resistance of 240 ohms for galvanometer recorder. (Galvo. SMI/S).

The frequency response of the output signals is limited by the smoothing filter in the rectifier circuit which has a 95% response at 10Hz.

Set Datum

This enables the output signal to be set to zero, i.e. to earth potential, for any initial depth of probe immersion. The instrument will then give its maximum full scale output of + and - 10 volts for waves which just reach the bottom of the probe in their troughs. To set up the control, fix the probe in position immersed to the required depth in still water, set the toggle switch on the front panel to the OPERATE position, set the SET OUTPUT control to its fully clockwise position, and then rotate the SET DATUM control to bring the indicating meter to its central position.

Set Output

This control attenuates the output signal and enables it to be set for a maximum voltage of any value between zero and 10 volts. Provided the datum has been adjusted as described in the previous paragraph the dial calibrations read directly in volts and/or milliamps. All that is required is to set the dial to

required output and to lock it. Note that in doing so, the sensitivity of the datum adjustment and the cable resistance compensation described above is reduced, and it is recommended that this control always be set to its maximum before carrying out these operations.

APPENDIX C

EXPERIMENTAL DATA

Table C-1: Experiments on Smooth Channel

Set	F_1	y_1 (cm)	y_2 (cm)	F_2	η (%)	L_w (cm)	L_A (cm)
<i>1</i>	12,01	1,346	19,89	0,11	79,68	39	202
<i>2</i>	8,83	1,346	15,96	0,14	70,27	37	187
<i>3</i>	7,20	1,346	13,11	0,17	63,78	33	164
<i>4</i>	5,59	1,346	10,20	0,23	54,48	20	132
<i>5</i>	7,25	2,019	19,15	0,14	65,25	33	170
<i>6</i>	6,39	2,019	16,80	0,17	61,16	27	150
<i>7</i>	5,20	2,019	14,01	0,20	52,45	24	148
<i>8</i>	4,49	2,019	11,40	0,27	49,15	23	141
<i>9</i>	5,36	2,692	19,81	0,15	52,61	39	173
<i>10</i>	5,01	2,692	17,68	0,18	51,81	32	160
<i>11</i>	3,57	2,692	12,61	0,27	37,73	22	132

Table C-2: Experiments on Rough Beds

PATTERN	W/Z	l (%)	F_1	y_1 (cm)	y_2 (cm)	F_2	η (%)	L_w (cm)	L_A (cm)
Rough Bed=1 ; Wave length=3 cm	2,00	33,30	11,19	1,35	19,07	0,12	77,63	25,00	178,00
	2,00	33,30	10,12	1,35	16,39	0,15	76,47	18,00	160,00
	2,00	33,30	8,17	1,35	13,57	0,18	70,47	18,00	152,00
	2,00	33,30	6,43	1,35	10,40	0,26	63,91	9,00	112,00
	2,00	33,30	6,13	2,69	21,20	0,15	60,25	23,00	153,00
	2,00	33,30	4,67	2,69	15,85	0,21	50,82	23,00	150,00
	2,00	33,30	5,41	2,69	18,65	0,17	55,78	23,00	156,00
	2,00	33,30	3,92	2,69	13,07	0,28	44,47	17,00	131,00
	2,00	33,30	7,64	2,02	19,75	0,14	67,54	29,00	163,00
	2,00	33,30	6,45	2,02	17,34	0,16	60,69	24,00	150,00
	2,00	33,30	6,00	2,02	14,71	0,21	61,47	23,00	147,00
	2,00	33,30	4,81	2,02	11,80	0,27	53,28	17,00	128,00
Rough Bed=2 ; Wave length=3 cm	1,00	33,30	10,60	1,35	17,57	0,13	76,99	26,00	149,00
	1,00	33,30	9,68	1,35	15,17	0,17	76,20	21,00	126,00
	1,00	33,30	8,14	1,35	13,67	0,18	70,01	16,00	112,00
	1,00	33,30	5,74	1,35	8,44	0,36	63,21	10,00	71,00
	1,00	33,30	6,90	2,02	17,10	0,17	65,71	32,00	178,00
	1,00	33,30	6,54	2,02	16,76	0,17	62,80	26,00	154,00
	1,00	33,30	6,07	2,02	14,24	0,23	63,33	21,00	136,00
	1,00	33,30	5,46	2,02	11,37	0,33	63,55	18,00	104,00
	1,00	33,30	6,14	2,69	20,41	0,16	61,78	33,00	157,00
	1,00	33,30	5,25	2,69	19,11	0,16	52,37	30,00	152,00
	1,00	33,30	4,96	2,69	15,91	0,23	55,50	26,00	149,00
	1,00	33,30	4,08	2,69	12,94	0,29	48,25	21,00	117,00
Rough Bed=3 ; Wave length=3 cm	0,66	33,30	5,08	1,35	7,42	0,42	59,24	24,00	76,00
	0,66	33,30	6,86	1,35	10,10	0,29	68,73	30,00	117,00
	0,66	33,30	8,02	1,35	12,43	0,22	71,76	37,00	136,00
	0,66	33,30	9,97	1,35	15,43	0,17	77,13	29,00	144,00
	0,66	33,30	11,46	1,35	17,91	0,14	79,84	31,00	151,00
	0,66	33,30	5,19	2,02	11,60	0,30	59,58	36,00	152,00
	0,66	33,30	6,00	2,02	14,03	0,23	63,05	33,00	160,00
	0,66	33,30	7,18	2,02	17,12	0,18	68,05	34,00	157,00
	0,66	33,30	7,44	2,02	19,25	0,14	66,66	44,00	164,00
	0,66	33,30	4,01	2,69	12,74	0,30	47,60	29,00	108,00
	0,66	33,30	4,70	2,69	15,33	0,23	52,70	33,00	133,00

Table C-2: Continued

PATTERN	W/Z	I (%)	IF ₁	y ₁ (cm)	y ₂ (cm)	IF ₂	η (%)	L _w (cm)	L _A (cm)
	0,66	33,30	5,39	2,69	17,83	0,19	57,33	38,00	139,00
	0,66	33,30	6,46	2,69	20,29	0,17	65,30	40,00	162,00
Rough Bed=1 ; Wave length=6 cm	5,00	16,60	9,24	2,02	20,86	0,15	76,10	34,00	213,00
	5,00	16,60	8,21	2,02	18,55	0,17	73,18	36,00	203,00
	5,00	16,60	7,23	2,02	15,83	0,21	70,63	26,00	172,00
	5,00	16,60	6,21	2,02	13,03	0,28	67,31	23,00	150,00
	5,00	16,60	6,92	2,69	21,55	0,16	67,69	27,00	175,00
	5,00	16,60	6,31	2,69	15,85	0,29	70,67	35,00	182,00
	5,00	16,60	5,29	2,69	18,65	0,17	54,08	24,00	178,00
	5,00	16,60	4,66	2,69	13,07	0,33	57,94	34,00	148,00
	5,00	16,60	13,05	1,35	19,75	0,13	82,79	39,00	205,00
	5,00	16,60	11,61	1,35	17,34	0,15	80,93	27,00	185,00
	5,00	16,60	10,01	1,35	14,71	0,19	78,28	38,00	162,00
	5,00	16,60	7,95	1,35	11,80	0,24	72,62	19,00	147,00
Rough Bed=2 ; Wave length=6 cm	2,50	16,60	6,02	1,35	8,49	0,37	65,96	35,00	114,00
	2,50	16,60	8,09	1,35	11,17	0,28	74,72	33,00	122,00
	2,50	16,60	9,13	1,35	13,66	0,20	75,86	41,00	126,00
	2,50	16,60	10,84	1,35	15,32	0,19	80,61	42,00	134,00
	2,50	16,60	11,90	1,35	17,10	0,16	82,05	45,00	152,00
	2,50	16,60	4,30	2,02	8,40	0,50	57,14	32,00	77,00
	2,50	16,60	5,25	2,02	11,16	0,33	61,56	35,00	96,00
	2,50	16,60	6,23	2,02	13,73	0,25	66,03	42,00	117,00
	2,50	16,60	7,49	2,02	14,69	0,26	74,13	36,00	144,00
	2,50	16,60	7,95	2,02	18,78	0,16	71,23	40,00	183,00
	2,50	16,60	4,27	2,69	12,21	0,35	54,12	35,00	111,00
	2,50	16,60	5,01	2,69	14,70	0,27	58,96	37,00	126,00
	2,50	16,60	5,63	2,69	17,51	0,21	61,10	40,00	145,00
	2,50	16,60	6,32	2,69	19,75	0,18	64,80	45,00	179,00
Rough Bed=3 ; Wave length=6 cm	1,66	16,60	4,27	2,69	12,49	0,33	53,30	30,00	139,00
	1,66	16,60	5,01	2,69	16,64	0,21	54,36	34,00	146,00
	1,66	16,60	6,28	2,69	21,66	0,14	61,29	34,00	163,00
	1,66	16,60	6,28	2,69	22,32	0,13	60,19	33,00	180,00
	1,66	16,60	6,84	2,69	23,10	0,13	64,77	30,00	196,00
	1,66	16,60	8,33	2,02	20,40	0,14	71,52	32,00	168,00
	1,66	16,60	7,48	2,02	15,16	0,24	73,39	28,00	151,00
	1,66	16,60	4,93	2,02	12,69	0,24	52,31	30,00	127,00

Table C-2: Continued

PATTERN	W/Z	I (%)	IF ₁	y ₁ (cm)	y ₂ (cm)	IF ₂	η (%)	LW(cm)	L _A (cm)
	1,66	16,60	12,57	1,35	18,78	0,14	82,38	32,00	177,00
	1,66	16,60	10,91	1,35	18,21	0,13	77,51	30,00	133,00
	1,66	16,60	9,04	1,35	14,70	0,17	73,68	27,00	129,00
	1,66	16,60	7,27	1,35	12,51	0,19	65,90	19,00	130,00
Rough Bed=1 ; Wave length=9 cm	8,00	11,10	13,28	1,35	18,10	0,16	84,68	45,00	194,00
	8,00	11,10	11,86	1,35	15,88	0,19	83,12	36,00	194,00
	8,00	11,10	10,39	1,35	13,88	0,22	80,80	29,00	161,00
	8,00	11,10	8,34	1,35	11,53	0,27	75,45	26,00	147,00
	8,00	11,10	9,30	2,02	19,54	0,17	77,74	27,00	204,00
	8,00	11,10	8,42	2,02	15,85	0,25	77,72	24,00	183,00
	8,00	11,10	7,34	2,02	18,65	0,15	66,83	24,00	170,00
	8,00	11,10	6,07	2,02	13,07	0,27	65,96	26,00	158,00
	8,00	11,10	7,35	2,69	19,75	0,21	73,17	34,00	193,00
	8,00	11,10	6,63	2,69	17,34	0,25	71,08	31,00	182,00
	8,00	11,10	5,86	2,69	14,71	0,32	68,58	22,00	162,00
	8,00	11,10	4,97	2,69	11,80	0,44	64,84	26,00	152,00
Rough Bed=2;Wave length=9 cm	4,00	11,10	4,54	2,69	13,73	0,29	54,38	51,00	150,00
	4,00	11,10	5,41	2,69	16,88	0,22	59,55	56,00	149,00
	4,00	11,10	5,98	2,69	19,52	0,17	61,45	64,00	157,00
	4,00	11,10	6,51	2,69	21,67	0,15	63,71	58,00	165,00
	4,00	11,10	9,38	1,35	12,12	0,27	79,35	30,00	105,00
	4,00	11,10	9,81	1,35	14,19	0,20	78,16	47,00	112,00
	4,00	11,10	11,17	1,35	16,85	0,15	80,03	46,00	133,00
	4,00	11,10	13,00	1,35	19,54	0,13	82,84	49,00	146,00
	4,00	11,10	6,45	2,02	13,30	0,28	68,96	33,00	116,00
	4,00	11,10	7,25	2,02	15,97	0,21	70,56	47,00	148,00
Rough Bed=3;Wave length=9 cm	2,66	11,10	5,87	2,02	12,87	0,27	64,34	40,00	129,00
	2,66	11,10	8,07	2,02	18,56	0,17	72,33	45,00	205,00
	2,66	11,10	8,51	2,02	20,39	0,14	72,65	45,00	158,00
	2,66	11,10	4,58	2,69	13,75	0,29	55,01	29,00	124,00
	2,66	11,10	5,39	2,69	16,55	0,22	60,04	38,00	148,00
	2,66	11,10	5,89	2,69	19,33	0,17	60,77	42,00	148,00
	2,66	11,10	6,50	2,69	21,80	0,15	63,34	45,00	157,00
	2,66	11,10	8,48	1,35	12,49	0,23	74,45	25,00	118,00
	2,66	11,10	9,79	1,35	15,25	0,17	76,59	23,00	121,00

Table C-2: Continued

PATTERN	W/Z	I (%)	IF ₁	y ₁ (cm)	y ₂ (cm)	IF ₂	η (%)	LW(cm)	L _A (cm)
	2,66	11,10	10,89	1,35	17,73	0,13	78,00	28,00	141,00
	2,66	11,10	12,24	1,35	20,14	0,11	80,18	47,00	148,00

Table C-3: Experiments on Rough Walls

PATTERN	W/Z	I (%)	F ₁	y ₁ (cm)	y ₂ (cm)	F ₂	η (%)	L _F (cm)	L _A (cm)
Rough Bed=1 ; Wave length=3 cm	2,00	33,30	7,52	2,02	18,88	0,15	67,96	28,00	198,00
	2,00	33,30	6,56	2,02	16,58	0,17	63,38	31,00	198,00
	2,00	33,30	5,66	2,02	14,25	0,21	58,44	25,00	194,00
	2,00	33,30	4,44	2,02	11,12	0,28	49,37	21,00	120,50
	2,00	33,30	11,10	1,35	17,60	0,14	78,92	31,00	180,00
	2,00	33,30	9,65	1,35	15,48	0,16	75,58	21,00	171,00
	2,00	33,30	8,00	1,35	13,06	0,19	70,34	23,00	159,00
	2,00	33,30	6,31	1,35	10,20	0,26	63,40	18,00	147,00
	2,00	33,30	5,83	2,69	19,65	0,17	59,44	31,00	185,00
	2,00	33,30	5,10	2,69	17,43	0,19	54,04	26,00	178,00
	2,00	33,30	4,52	2,69	15,16	0,23	49,99	25,00	172,00
	2,00	33,30	3,85	2,69	12,25	0,31	49,99	27,00	161,00
Rough Bed=2 ; Wave length=3 cm	1,00	33,30	6,16	2,69	23,76	0,11	56,16	31,00	252,00
	1,00	33,30	5,13	2,69	20,34	0,13	47,52	24,00	204,00
	1,00	33,30	4,62	2,69	16,91	0,18	46,82	18,00	189,00
	1,00	33,30	3,96	2,69	14,62	0,22	39,77	16,00	159,00
	1,00	33,30	7,69	2,02	22,53	0,10	63,63	33,00	208,00
	1,00	33,30	6,49	2,02	19,14	0,13	57,39	25,00	190,00
	1,00	33,30	6,23	2,02	15,82	0,18	61,46	20,00	184,00
	1,00	33,30	4,62	2,02	13,02	0,21	45,46	15,00	151,00
	1,00	33,30	11,53	1,35	20,70	0,10	77,15	22,00	208,00
	1,00	33,30	9,72	1,35	17,28	0,13	73,29	19,00	179,00
	1,00	33,30	8,00	1,35	14,06	0,17	68,23	18,00	166,00
	1,00	33,30	6,30	1,35	12,87	0,16	54,46	14,00	156,00

Table C-3: Continued

PATTERN	W/Z	I (%)	F ₁	y ₁ (cm)	y ₂ (cm)	F ₂	η (%)	L _F (cm)	L _A (cm)
<u>Rough Bed=3 ; Wave length=3 cm</u>	0,66	33,30	6,00	2,69	24,44	0,10	52,81	32,00	218,00
	0,66	33,30	4,53	2,69	16,87	0,18	45,28	25,00	203,00
	0,66	33,30	3,89	2,69	14,77	0,21	37,55	15,00	166,00
	0,66	33,30	7,46	2,02	23,73	0,09	59,53	31,00	204,00
	0,66	33,30	6,83	2,02	20,52	0,11	58,50	31,00	200,00
	0,66	33,30	5,79	2,02	17,93	0,13	50,61	24,00	188,00
	0,66	33,30	4,83	2,02	13,67	0,20	47,10	21,00	184,00
	0,66	33,30	10,71	1,35	21,99	0,08	72,02	30,00	194,00
	0,66	33,30	9,15	1,35	18,10	0,11	68,63	22,00	178,00
	0,66	33,30	8,07	1,35	14,55	0,15	67,72	29,00	164,00
<u>Rough Bed=1 ; Wave length=6 cm</u>	5,00	16,60	6,35	2,69	23,00	0,13	59,85	27,00	212,00
	5,00	16,60	5,29	2,69	19,42	0,15	52,34	29,00	222,00
	5,00	16,60	4,82	2,69	16,40	0,20	51,99	26,00	200,00
	5,00	16,60	4,12	2,69	12,87	0,30	49,30	17,00	154,00
	5,00	16,60	11,57	1,35	20,01	0,11	78,03	24,00	183,00
	5,00	16,60	9,94	1,35	15,87	0,16	76,37	19,00	160,00
	5,00	16,60	7,97	1,35	15,87	0,13	64,09	20,00	165,00
	5,00	16,60	6,52	1,35	11,04	0,23	62,94	17,00	141,00
	5,00	16,60	7,75	2,02	20,78	0,12	66,85	22,00	197,00
	5,00	16,60	6,49	2,02	18,24	0,14	59,28	20,00	199,00
	5,00	16,60	5,87	2,02	12,87	0,27	64,35	17,00	142,00
	5,00	16,60	4,69	2,02	12,87	0,22	47,50	19,00	133,00
<u>Rough Bed=2 ; Wave length=6 cm</u>	2,50	16,60	7,53	2,02	19,41	0,14	67,21	28,00	203,00
	2,50	16,60	6,68	2,02	17,35	0,16	63,12	17,00	179,00
	2,50	16,60	5,64	2,02	13,04	0,26	61,32	15,00	167,00
	2,50	16,60	4,64	2,02	12,72	0,22	46,96	14,00	147,00
	2,50	16,60	11,27	1,35	18,37	0,13	78,68	25,00	179,00
	2,50	16,60	9,57	1,35	16,12	0,15	74,27	19,00	164,00
	2,50	16,60	7,87	1,35	13,48	0,18	68,46	17,00	152,00
	2,50	16,60	6,17	2,69	20,68	0,16	61,65	32,00	225,00
	2,50	16,60	5,46	2,69	18,44	0,18	57,05	21,00	212,00
	2,50	16,60	4,66	2,69	15,78	0,22	50,74	20,00	169,00
	2,50	16,60	4,01	2,69	13,04	0,28	46,56	15,00	157,00

Table C-3: Continued

PATTERN	W/Z	I (%)	F ₁	y ₁ (cm)	y ₂ (cm)	F ₂	η (%)	L _F (cm)	L _A (cm)
<u>Rough Bed=3 ; Wave length=6 cm</u>	1,66	16,60	5,83	2,69	24,08	0,10	50,96	22,00	217,00
	1,66	16,60	5,06	2,69	20,91	0,12	44,69	23,00	198,00
	1,66	16,60	4,64	2,69	17,42	0,17	45,90	18,00	189,00
	1,66	16,60	3,96	2,69	13,63	0,25	43,51	13,00	185,00
	1,66	16,60	11,16	1,35	20,99	0,09	75,30	27,00	218,00
	1,66	16,60	9,94	1,35	17,69	0,12	73,82	21,00	184,00
	1,66	16,60	8,28	1,35	14,45	0,16	69,41	20,00	176,00
	1,66	16,60	6,81	2,02	19,34	0,13	60,55	22,00	184,00
	1,66	16,60	5,78	2,02	15,96	0,17	55,59	18,00	180,00
	1,66	16,60	4,69	2,02	12,89	0,22	47,41	14,00	167,00
<u>Rough Bed=1; Wave length=3 cm</u>	8,00	11,10	5,26	2,69	18,40	0,17	54,21	22,00	218,00
	8,00	11,10	4,98	2,69	16,02	0,22	55,43	25,00	157,00
	8,00	11,10	11,61	1,35	18,55	0,13	79,69	30,00	222,00
	8,00	11,10	10,49	1,35	16,15	0,16	78,32	26,00	203,00
	8,00	11,10	7,93	1,35	13,44	0,18	69,06	20,00	186,00
	8,00	11,10	6,84	1,35	10,56	0,26	67,34	13,00	143,00
	8,00	11,10	7,84	2,02	19,19	0,15	69,87	21,00	187,00
	8,00	11,10	6,83	2,02	16,89	0,17	65,42	25,00	194,00
	8,00	11,10	5,55	2,02	14,49	0,20	56,33	25,00	177,00
<u>Rough Bed=2; Wave length=9 cm</u>	4,00	11,10	12,15	1,35	21,37	0,10	78,70	30,00	227,00
	4,00	11,10	10,74	1,35	17,95	0,13	77,14	22,00	200,00
	4,00	11,10	8,45	1,35	14,65	0,16	70,18	17,00	186,00
	4,00	11,10	6,97	1,35	11,92	0,21	64,81	11,00	155,00
	4,00	11,10	8,06	2,02	22,55	0,11	66,71	22,00	216,00
	4,00	11,10	7,45	2,02	19,36	0,14	66,57	17,00	201,00
	4,00	11,10	5,84	2,02	15,60	0,18	57,31	12,00	178,00
	4,00	11,10	5,04	2,02	13,27	0,22	52,15	9,00	155,00
	4,00	11,10	6,58	2,69	25,60	0,10	58,38	23,00	232,00
	4,00	11,10	6,29	2,69	23,04	0,12	59,08	19,00	207,00
	4,00	11,10	5,49	2,69	19,81	0,15	54,57	15,00	197,00
<u>Rough Bed=3; Wave length=9 cm</u>	2,66	11,10	7,97	2,02	23,45	0,10	64,71	32,00	212,00
	2,66	11,10	5,80	2,02	18,17	0,13	50,15	18,00	200,00
	2,66	11,10	4,96	2,02	14,15	0,19	47,92	11,00	150,00
	2,66	11,10	10,82	1,35	22,49	0,08	71,97	27,00	198,00
	2,66	11,10	9,65	1,35	18,86	0,10	70,52	18,00	191,00
	2,66	11,10	8,04	1,35	14,54	0,15	67,47	14,00	173,00

Table C-3: Continued

PATTERN	W/Z	I (%)	F ₁	y ₁ (cm)	y ₂ (cm)	F ₂	η (%)	L _F (cm)	L _A (cm)
	2,66	11,10	6,49	1,35	12,41	0,18	58,33	11,00	151,00
	2,66	11,10	6,49	2,69	25,61	0,10	57,27	25,00	235,00
	2,66	11,10	5,36	2,69	21,46	0,12	48,93	24,00	180,00
	2,66	11,10	4,82	2,69	17,57	0,18	48,92	20,00	180,00

VITA

PERSONAL INFORMATION

Surname, Name: Evcimen, Taylan Ulaş
Nationality: Turkish (TC)
Date and Place of Birth: 20 September 1979, İzmir
Marital Status: Married
Phone: +90 536 870 72 58
Fax: +90 312 473 85 46
email: taylan.evcimen@gmail.com

EDUCATION

Degree	Institution	Year of Graduation
MS	METU Civil Engineering	2005
BS	METU Civil Engineering	2002
High School	Ödemiş High School, İzmir	1996

WORK EXPERIENCE

Year	Place	Enrollment
2010- Present	EnerjiSA Energy Generation Co.	Dam / Design Engineer
2007-2010	Sanko Energy Generation Co.	Dam Engineer
2005-2007	Birim Engineering and Consultancy Ltd,	Design Engineer
2003-2005	Chamber of Civil Engineers	Civil Engineer

FOREIGN LANGUAGES

Advanced English

PUBLICATIONS

1. Evcimen T.U., Tokyay N.D., Şimşek Ç. “Forced hydraulic jump on non-protruding rough beds” Canadian Journal of Civil Engineering, 2011, 38:(10) 1136-1144, 10.1139/111-072.(2011)
2. Evcimen T.U., UCOK M., KAYA S. “Case Studies of 6 Different Hydro Power Dams Under Construction” Proc., 8th ICOLD European Club Symposium , ATCOLD, Innsbruck, Austria, 105–110 (2010).

HOBBIES

Water Politics, Writing, Movies, Jogging, Swimming, Gourmet, Motorcycling